PGandE Letter No.: DCL-87-102

ENCLOSURE

DIABLO CANYON LONG TERM SEISMIC PROGRAM

METHODS AND PROCEDURES FOR THE PHASE IIIA SEISMIC FRAGILITIES OF STRUCTURES AND COMPONENTS AT THE DIABLO CANYON POWER PLANT

Pacific Gas and Electric Company
Diablo Canyon Power Plant
Docket Nos. 50-275 and 50-323
May 1987

1386S/0050K

TABLE OF CONTENTS

[illegible]

TABLE OF CONTENTS (Cont.)

[illegible]

TABLE OF CONTENTS (Continued)

TABLE OF CONTENTS (Cont.)

[illegible]

LIST OF FIGURES

[illegible]

LIST OF FIGURES (Continued)

[illegible]

LIST OF TABLES

[illegible]

1. INTRODUCTION

As part of the Long Term Seismic Program (LTSP) for the Diablo Canyon Power Plant, a seismic probabilistic risk assessment (SPRA) is being conducted by the Pacific Gas and Electric Company (PG&E). In this evaluation, event trees, and fault trees are utilized to assess the expected frequencies of plant damage states and core melt from both internal and external events including earthquakes. This report discusses the methodology for determining the seismic capacities of selected civil structures and equipment items included in the PRA risk models. The seismic capacities of the Diablo Canyon structures and equipment are being developed in several phases consistent with the Long Term Seismic Program (LTSP). Phase I consisted primarily of planning. In Phase II, preliminary seismic fragilities were developed in order to develop a preliminary ranking of the items which are expected to be the dominant contributors to the overall plant seismic risk. In Phase III A, the seismic capacities of several of the dominant contributors were refined, and several studies were completed to benchmark various aspects of the methods used to develop the seismic fragilities. In Phase III B, the capacities of several additional components will be refined and final fragilities for all the essential structures and equipment will be developed which will incorporate the results of several on-going LTSP programs such as geotechnical investigations and soil-structure interaction analysis.

The frequency of seismically-induced failure as a function of peak ground spectral acceleration for both safety-related civil structures and equipment is being developed for Diablo Canyon. Also included is the expected variability in the frequency of failure. The evaluation of the seismic hazard is being conducted as part of another element of the LTSP. The information for the frequency of failure for the safety-

related systems and components will then be incorporated into the risk models by PG & E to assess the frequency of seismic-induced radioactive release from the site.

In order to correctly interpret the fragilities discussed in this report, it is necessary to define the spectral ground acceleration to which these fragilities are anchored. It is recognized that the damage potential of an earthquake depends on many factors, among which are magnitude, peak acceleration, and duration. An ensemble of natural and numerically generated earthquake records which are considered representative of those which could be expected at the Diablo Canyon site has been assembled (see Appendix B). All actual ground response spectra have peaks and valleys which cannot be exactly predicted for the Diablo Canyon site at this time. However, a smoothed ground response spectrum was chosen as the basis of the fragilities discussed herein. The mean spectral amplification factors for 5% critical damping are listed below:

Frequency (Hz)	Spectral Amplification Factor
>33	1.0
15	1.65
8.5	2.35
3	2.35
2	1.7
1	0.95

All fragilities described here are keyed to 5% damped spectral accelerations in the 3 to 8.5 Hz range. This is true for both the civil structures and equipment items, irrespective of the expected damping or frequency of the structure or component.

[illegible]

Past experience in the development of probabilistic risk assessments for nuclear plants has indicated that the earthquake accelerations which dominate the risk are expected to exhibit peak ground accelerations of 0.4g or greater, even for east coast plants. For a plant such as Diablo Canyon which was designed for even higher accelerations and which has subsequently been evaluated for a Hosgri event in the 0.75g effective PGA range, it is expected that the majority of seismic risk could be expected from earthquakes in the magnitude 7 range or greater. At lower magnitudes, the seismic excitation is not strong enough that significant probabilities of failure exist, and there is a low probability of higher magnitude earthquakes affecting the site. Magnitude effects including duration and effective ductility for the various seismic modes of failure were evaluated assuming that the majority of risk results from earthquakes in the M_b 7.0 or somewhat higher range. Using this approach, the fragility descriptions are anchored to the 5% damped spectral accelerations in the 3 to 8.5 Hz range. At higher magnitudes with corresponding higher peak ground accelerations, lower spectral amplification in the amplified frequency range is expected. However, for the fragilities described in this report, a constant amplification of 2.35 for the 5% damped response in the 3 to 8.5 Hz range is used. This is expected to introduce some slight conservatism for some structures and equipment items depending on the frequency range of primary response of the structure and the expected capacity of the structure. However, this conservatism primarily affects the higher capacity structures and equipment which are not the dominant contributors to the plant seismic risk.

Diablo Canyon was designed in the 1960's in accordance with criteria and codes in effect at that time. The Diablo Canyon systems and components which are essential to the prevention or mitigation of consequences of

[illegible]

accidents which could affect the public health and safety were designed to enable the facility to withstand the effects of natural forces including earthquakes. The design criteria included the effects of simultaneous earthquake and loss-of-coolant-accident (LOCA) conditions. The plant was originally designed to withstand both a Design Earthquake (DE) corresponding to an Operating Basis Earthquake (OBE) and a Double Design Earthquake (DDE) corresponding to a Safe Shutdown Earthquake (SSE). The original design earthquakes were 0.2g peak ground accelerations for the DE and 0.4g for the DDE.

Subsequent to the design and construction of the plant, additional analyses and evaluations were conducted for a postulated seismic event on the Hosgri fault. The effective peak ground acceleration for this event was established at 0.75g. However, Newmark tau filtering effects were included which resulted in decreased accelerations of various amounts at the base slabs of the individual structures. Various structural modifications have been implemented to account for the increased seismic loads resulting from the Hosgri event. Also, acceptance criteria for civil structures for the Hosgri event were based on average plant specific material properties rather than code design allowables and limited inelastic response was permitted.

The civil structure covered in this report include:

- Containment Building
- Containment Building Internal Structure
- Intake Structure
- Turbine Building
- Turbine Building Block Wall
- Refueling Water Storage Tank
- Condensate Storage Tank

Diesel Generator Fuel Oil Tank (Buried)
Auxiliary Saltwater Piping (Buried)

The fragility evaluation of the auxiliary building is not included in this report.

The equipment items evaluated for the seismic PRA are developed from systems consideration and contain both Seismic Category I and Non-Seismic Category I components. Non-Seismic Category I components have been included in this study where it can be shown that they could help mitigate a postulated accident sequence, or alternatively, if their failure could initiate an accident sequence.

All Diablo Canyon structures are supported on competent bedrock foundation media with a shear wave velocity of about 3500 fps. Most of the design analysis for the plant were conducted using fixed base analytical models as was the more recent Hosgri evaluation. Soil-structure interaction analyses accounting for embedment and other effects are currently underway. Preliminary results indicate that the fixed base models are conservative over at least some ranges of frequency. While it is expected that these results will be incorporated in the final seismic PRA results, all results reported herein are based on fixed-base models with a conservative estimation of the statistical incoherence from the ground motion.

Over the course of the design and subsequent reanalyses for Diablo Canyon both response spectrum and time history analyses have been conducted. In general, both time history and the response spectrum analysis results were used for evaluation of the civil structure loads, while the time history results were used to generate in-structure response spectra for the design and evaluation of piping and equipment. Different ground

[illegible]

response spectra, different structure damping, and different structure models have also been used at different times and numerous details such as the degree of accidental torsion, use of Newmark tau filtering, and changes in acceptance criteria have been incorporated. A detailed chronology of these variations is not repeated here but can be found elsewhere (Ref. 1,2).

For the most part, results of existing analyses and evaluations of structures and equipment for the Diablo Canyon plant were utilized in this study. The results of the existing analyses were supplemented by specialized analyses for this study where it was necessary to investigate important effects which could result at higher accelerations than those previously considered in either design or the Hosgri evaluation. As part of this evaluation, some limited ultimate load analyses based on the existing analyses load distributions were conducted to assess the expected seismic capacities of the important structures. Also, some additional analysis was conducted using a simplified structural model representative of the auxiliary building and simplified equipment models. This additional analysis was conducted in order to verify that the separation of variables approach used to evaluate the overall factor of safety is appropriate and to attempt to identify cut-offs of the tails of the fragility curves.

Simplified models of several components qualified by test were developed in order to obtain a better estimate of the seismic loads in these components. Also, a simple nonlinear model of the turbine building was developed and used to establish the nonlinear load distribution in the structure and assess the effect of impact of the turbine pedestal with the operating floor at high accelerations. However, for the majority of structures and components, the approach adopted in this study was to assess the median factor of safety and its statistical variability which

[illegible]

exists based on existing analysis. For the most part, the existing analyses used were the Hosgri evaluations of the structures and equipment components since this work tended to be the most recent and at acceleration levels which generally produced higher response than the DDE analyses.

An evaluation of the individual important structures and most of the equipment was conducted for specific items and failure modes. However, some piping and equipment components were evaluated on the basis of generic categories using the experience data base or a limited number of plant specific samples. Although inelastic energy dissipation is included in evaluating the factors of safety, the only nonlinear analysis conducted for either the structures or equipment was the turbine building analysis discussed in Appendix C. All other evaluations were based on elastic analysis and load distributions. Emphasis was devoted to equipment and structures with median seismic capacities below spectral acceleration of 7g for the structures or 10g for equipment. Once the median capacity of an item could be shown to be above 7 or 10g, further effort to develop more accurate capacities as well as detailed evaluations of the variability were normally discontinued.

The final fragilities can be used together with the estimated annual frequency of occurrence of various ground spectral acceleration levels to assess the frequency of seismic-induced failure for each safety-related structure or component in the plant. In the total study, these conditional component failure frequencies are used with systems models to assess the expected frequencies of plant damage states and core melt from both internal and external events including earthquakes.

[illegible]

2. GENERAL CRITERIA FOR DEVELOPMENT OF MEDIAN SEISMIC SAFETY FACTORS

The factor of safety of a structure or component is defined herein as the resistance capacity divided by the response associated with an existing earthquake; in most cases the Hosgri event. The development of seismic safety factors associated with the Hosgri event is based on consideration of several variables. The variability of dynamic response to the specified acceleration and the strength capacity of the structure or equipment component are the two basic considerations in evaluating the variability in the factor of safety. Several variables are involved in assessing both the structural response and the structural capacity, and each such variable, in turn, has a median factor of safety and variability associated with it. The overall factor of safety is the product of the factors of safety for each variable. The median of the overall factor of safety is the product of the median safety factors of all the variables. The variabilities of the individual factors also combine to assess the variability of the overall safety factor.

Variables influencing the factor of safety on structural capacity to withstand seismic-induced vibration include the strength of the equipment or structure compared to the Hosgri stress level and the inelastic energy absorption capacity (ductility) of the structure or component defined as its ability to carry load beyond yield. The variability in computed structural response for a given free-field spectral ground acceleration is made up of many factors. The more significant factors include variability in (1) ground motion and the associated ground response spectra for a given free-field median spectral ground acceleration, (2) energy dissipation (damping), (3) structural modeling, (4) method of analysis, (5) combination of modes, (6) combination of earthquake components, and (7) soil-structure

interaction. No structures at Diablo Canyon were identified which are considered to be susceptible to sliding. Equipment located inside a building acts as a secondary system and requires the incorporation of the previously mentioned structural response factors together with a similar set of equipment response factors which are specific to the equipment itself (see Chapter 5). The ratio between the median and Hosgri values of each parameter affecting seismic capacity and response and their variabilities must then be quantitatively estimated for the various important Diablo Canyon structures and components. These estimates are based on available test data, limited analysis, and engineering judgment and experience in the analysis of nuclear power plants and components.

2.1 Definition of Failure

In order to estimate the median factor of safety for the structure or component failure for the Hosgri event, it is necessary to define what constitutes failure.

2.1.1 Seismic Category I Structures

For purposes of this study, Category I structures are considered to fail functionally when inelastic deformations of the structure under seismic load are estimated to be sufficient to potentially interfere with the operability of safety-related equipment attached to the structure. The limits on inelastic energy absorption capability (ductility limits) chosen for Category I structures are estimated to correspond to the onset of significant structural damage. For many potential modes of failure, this is believed to represent a conservative bound on the level of inelastic structural deformation which might interfere with the operability of components housed within the structure. It is important

[illegible]

to note that considerably greater margins of safety against structural collapse are believed to exist for these structures than many cases reported within this study. Thus, the conditional probabilities of failure for a given free-field ground spectral acceleration for Category I structures are considered appropriate for equipment operability limits and should not necessarily be inferred as corresponding to structure collapse.

2.1.2 Seismic Category I Equipment and Piping

Piping, electrical, mechanical, and eletro-mechanical equipment vital to safe shutdown of the plant or mitigation of an accident are considered to fail when they will no longer perform their designated functions. Therefore, for mechanical equipment, the fragility definition may represent failure to function, loss of anchorage, or rupture of the pressure boundary. Depending upon the type of equipment being considered, one of these definitions will generally govern. For active equipment, either functional failure or loss of anchorage usually defines the fragility since equipment pressure boundaries are generally conservatively designed for active equipment such as pumps and valves. For piping, failure of the support system or plastic collapse of the pressure boundary are considered to represent failure. The inelastic energy absorption capability (ductility limits) associated with these failure modes have been conservatively estimated in defining the margins of safety.

2.1.3 Non-Category I Structures

In the Diablo Canyon power plant, the non-Category I structures are separated from Category I structures by seismic gaps or "rattle spaces". The only non-seismic Category I structures of interest are the

turbine buildings and the intake structure. The turbine buildings and the intake structure were originally designed as a Non-Category I (Design Class II) structure although the standby diesel generator sets and the CCW heat exchangers are housed in the turbine buildings and the auxiliary salt water pumps are located in the intake structure. Extensive analyses have been conducted for these structures for the Hosgri event, and structural modifications including strengthened connections and new braces in some locations in the turbine buildings were incorporated. Thus, the level of seismic analysis information for the turbine buildings and intake structure is not significantly different from the seismic Category I structures for Diablo Canyon. In addition, as part of this study (Appendix C) nonlinear time history analyses were conducted on a simple two dimensional model of the turbine building. Therefore, for this study, the treatment of the fragilities for the non-seismic Category I structures is essentially the same as the treatment of the Category I structures.

2.1.4 Non-Seismic Category I Equipment and Piping

Failure of Non-Seismic Category I piping, electrical, mechanical and electro-mechanical equipment is defined the same as for Category I equipment; i.e., failure to perform its intended function or failure of the pressure boundary. There were no obvious non-Seismic Category I equipment items identified during the plant visit whose failure could cause damage to the safety-related equipment investigated in the fragility studies.

2.2 Basis for Safety Factors Derived in Study

There was a general lack of detailed information available for this study on the ultimate seismic capacities of specific Diablo Canyon

structures and equipment. This condition exists for all plants and occurs because existing codes and standards do not require assessment of ultimate seismic capacities, either for structures or equipment qualified by analysis, or for equipment or components qualified by testing. Therefore, most median safety factors, estimates of variability, and conditional frequencies of failure estimated in this study are based on existing analyses and qualified engineering judgment and assumptions. Limited additional analyses were conducted to evaluate the expected failure capacities of selected civil structures and equipment items. Included was some nonlinear time-history analysis of the turbine building. All other analyses were limited to linear elastic models, and for the most part, were based on the available design or Hosgri analysis models.

2.2.1 Structural Response and Capacities

The results from dynamic analyses which were used in the design and Hosgri evaluation of the important structures were extensively used in this study. These were supplemented as required to provide estimates of load redistributions resulting from localized distress and the nonlinear load distribution in the turbine building. Levels of conservatism associated with the method of analysis used in design and Hosgri event were estimated such that safety factors reflecting this analysis could be estimated for the building structures and for the seismic excitation of equipment mounted within the building.

Detailed structural design calculations were not reviewed, but the acceptance criteria used in design as defined in the FSAR (Reference 1) and Hosgri evaluation (Reference 2) were reviewed. Some ultimate load capacity analyses were conducted which served as a basis for estimating the median factor of safety on structural resistance to the Hosgri event.

[illegible]

2.2.2 Seismic Category I Piping and Equipment Response and Capacity

For most of the safety equipment, information on analysis methods was available in the design analyses and in summary form in the FSAR. Seismic response information for the selected sample of safety-related equipment evaluated in this study was obtained from available vendor seismic qualification reports or design calculations for specific components. In some cases, only the seismic analysis requirements and stress acceptance criteria were considered. Safety factors for response and structural or functional capacity were primarily estimated from existing information.

In-structure response spectra for all Category I structures were generated during the design process. From these typical floor response spectra and knowledge or estimates of equipment fundamental frequencies, an estimate was made of the median peak equipment response. The median peak equipment response estimate was then compared to the dynamic response or equivalent static coefficient used in design to establish a median safety factor on response.

Capacity factors are derived from several sources of information; plant-specific design reports, test reports, generic earthquake experience data and generic analytical derivations of capacity based on governing codes and standards. Two failure modes were considered in developing capacity factors for piping and equipment: structural and functional. Equipment and piping design reports delineate stress levels for the specified seismic loading plus normal operating conditions. Where the equipment fails in a structural mode (i.e., pressure boundary rupture or loss of support), the median capacity factor and its variability were derived in the same manner as for structures considering strength and energy absorption capability (ductility). In

[illegible]

cases where equipment function controls, the capacity factor is assessed by comparing the equipment functional failure (or fragility) level to the design level of seismic loading. Functional or structural fragility levels are not normally determinable from equipment qualification reports, but the achieved test levels can be utilized to update generic fragilities derived from experience data.

2.3 Formulation Used for Fragility Curves

Seismic-induced fragility data are generally unavailable for most of the specific plant components and are certainly unavailable for the specific Diablo Canyon structures. Thus, fragility curves must be developed primarily from analysis combined heavily with engineering judgment supported by limited test data. Fragility curves developed in this manner contain a relatively large uncertainty, and it is imperative that this uncertainty be recognized in all subsequent analyses. Because of the inherent uncertainties, great precision in defining the shape of these curves is unwarranted. Thus, the procedure used in this study requires a minimum amount of information, incorporates uncertainty into the fragility curves, and easily enables the use of engineering judgment.

The entire fragility curve for any mode of failure and its uncertainty can be expressed in terms of the best estimate of the median ground spectral acceleration capacity, $\check{A}_{SA}$, times the product of random variables. Thus, the ground acceleration, A_{SA}, corresponding to failure is given by:

$$A_{SA} = \check{A}_{SA} \, \varepsilon_R \, \varepsilon_U \qquad (2\text{-}1)$$

where ε_R and ε_U are random variables with unit median representing the inherent randomness (failure fraction) about the median and the uncertainty (probability) in the median value, respectively. The median ground spectral acceleration is keyed to the 5% damped, amplified spectral acceleration in the 3 to 8 1/2 Hz range with the amplification factors as defined in Section 1. Equation 2-1 enables the fragility curve and its uncertainty to be represented as shown in Figure 2-1; i.e., as a set of shifted curves with attached uncertainty levels. Thus, it is assumed that all uncertainty in the fragility curves can be expressed through uncertainty in the median alone.

Next, it is assumed that both ε_R and ε_U are lognormally distributed with logarithmic standard deviations of β_R and β_U, respectively. The advantages of this formulation are:

1. The entire fragility curve and its uncertainty can be expressed by three parameters - A_{SA}, ε_R, and ε_U. With the limited available data on fragility, it is much easier to only estimate three parameters rather than the entire shape of the fragility curve and its uncertainty.

2. The formulation in Equation 2-1 and the lognormal distribution are very tractable mathematically.

In this study, the guidelines used to estimate the values of β_R and β_U for each variable affecting A_{SA} were based on considering the inherent randomness, β_R, to be associated primarily with the earthquake characteristics themselves, and β_U to be associated with other lack of knowledge. Thus, such variability as resulting from earthquake response spectra shapes and amplification, earthquake duration, numbers and phasing of peak excitation cycles, etc., together

with their contributions to structure ductility and response characteristics was attributed to randomness. In general, it is not considered possible to significantly reduce randomness by additional analysis or test based on current state-of-the-art techniques. Uncertainty, on the other hand, is considered to result primarily from analytical modeling assumptions and other lack of knowledge concerning variables such as material strength, damping, etc., which could in many cases be reduced by additional study or test.

The lognormal distribution can be justified as a reasonable distribution since the statistical variation of many material properties (References 3 and 4) and seismic response (Reference 5) variables may reasonably be represented by this distribution. In addition, the central limit theorem states that a distribution consisting of products and quotients of distributions of several variables tends to be lognormal even if the individual distributions are not lognormal. Some characteristics of the lognormal distribution as applied to seismic capacities are discussed in Appendix A of this report.

It should be noted that the use of the lognormal distribution for estimating failure fractions on the order of five percent or greater is considered to be quite reasonable. However, lower fraction estimates which are associated with the extreme tails of the distributions must be considered less accurate. Use of the lognormal distribution in these regions is conservative since the low frequency tails of the lognormal distribution generally extend farther from the median than actual structural resistance or response data might indicate. The degree of conservatism introduced into the probability of release is dependent not only on the conservatism in the fragility description, but also on the seismic hazard description at low seismic levels. If the seismic hazard for low seismic input levels is large enough, it is apparent that very

low level earthquakes can govern the seismic-induced release. This is considered unrealistic for engineered structures and equipment found in nuclear power plants since such structures and equipment are subjected to various low level dynamic loads on a repetitive basis from a number of sources (i.e., wind and low level earthquakes) which have never been known to produce nuclear power plant failures.

2.4 Correlation Between Failure Modes

Many of the potential failure modes of safety related equipment are not considered to be completely independent. For instance, the collapse of a structure is also expected to result in failure of the equipment and piping located in that structure. Similarly, failure of a relatively heavy component may often be expected to fail lighter equipment in the immediate vicinity. Some degree of correlation exists for all items and for all modes of failure since they are all excited by the same earthquake. An example of very high dependency of failure is the case where two identical items are located very close to each other in the same structure. Where two components which are identical are located in different structures or different locations in the same structure, some degree of correlation is expected but less than 100%.

For different modes of failure in a given structure, or in similar structures, some degree of correlation between modes is also expected. For instance, if the capacity of a lateral force resisting system (i.e., the shear walls) is actually higher or lower than the value determined in the fragility analysis, the acceleration capacities of all failure modes governed by shear walls is expected to be proportionately higher or lower. The actual capacity of the force resisting system may be different from that developed in the fragility evaluation due to differences in strength or modeling assumptions. The effects of these assumptions are of course included in the variabilities associated with

[illegible]

each mode of failure for a given structure or component. However, different degrees of correlation may exist from mode-to-mode. For instance, for a given structure with given concrete and reinforcing steel strengths, the variability on strength from mode-to-mode may be strongly correlated, while different modeling assumptions may result in little correlation for different failure modes.

As part of the Phase IIIA investigation a limited study to investigate the expected correlation between failure modes of different equipment items located in one structure was conducted. This study was based on the same structure model, equipment frequencies, and time history ensemble as was used in the cut-off study. Correlation between failure modes ranged from slightly above 90% to essentially no correlation depending on equipment frequency and location in the structure. The details of this study are contained in Appendix D of this report. For failure modes with little contribution to risk, consideration of correlations between modes is probably unimportant. However, considerations should be given to possible correlation between controlling seismically-induced failure modes.

2.5 Redundancy and Recovery Consideration

The benefit of multiple or redundant components and the time for failure recovery must be considered differently for a seismic PRA than for an internal events PRA. For example, both Diablo Canyon Units are equipped with three (3) Component Cooling Water (CCW) Pumps. Should the motor for one CCW Pump randomly fail for some unexpected reason while in operation, the remaining pumps can safely maintain the necessary component cooling water flow and thus, the consequences of the loss of one CCW Pump is small. However, in a seismic event, the fragility of the CCW Pump (i.e., due to anchorage failure) indicates the probable

[illegible]

[illegible]

simultaneous loss of all three pumps and therefore, the consequences are much more significant. In such a case, the redundant pumps are of little benefit.

Similarly, for an internal events PRA, the mission time for the Emergency Diesel Generators is typically set to be some relatively short period of time (i.e., 3 hours), based upon the judgement that recovery of a random failure of off-site power could take place within that time frame. In contrast, the mission time for the Emergency Diesel Generators may be much longer for a seismic PRA since the damage to the transmission lines, switchyard components, or ceramic insulators from a seismic event is expected to be sufficiently extensive that off-site power should be considered unrecoverable within a meaningful period of time.

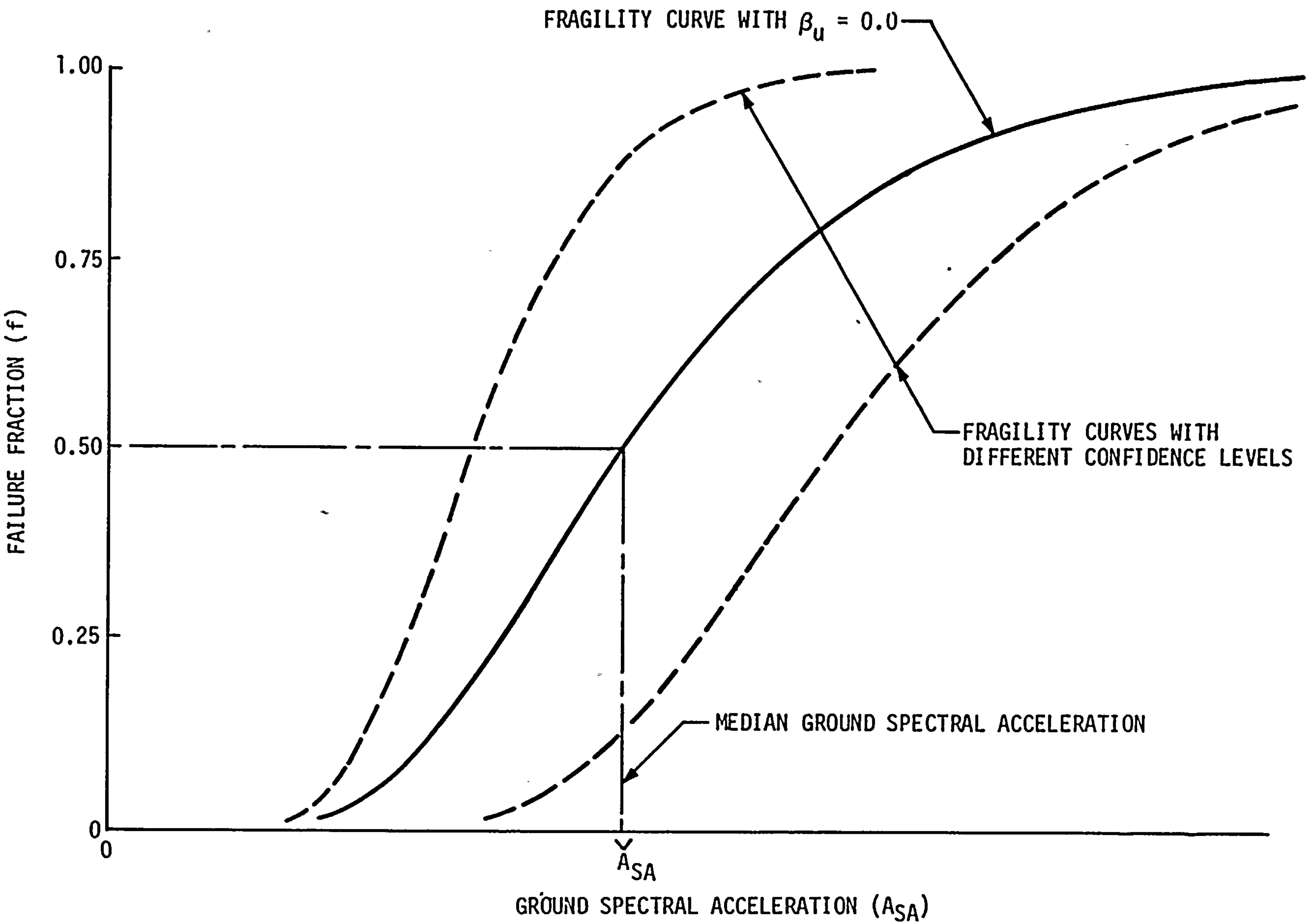

Figure 2-1. Fragility Curve Representations

1611-A

[illegible]

3. DIFFERENCES BETWEEN CRITERIA USED FOR PREVIOUS EVALUATIONS OF DIABLO CANYON AND PARAMETERS USED IN THE EVALUATION OF THE SEISMIC FRAGILITY

The seismic design of the Diablo Canyon structures and equipment was based for the most part on accepted methodology and criteria in conformance with USNRC licensing requirements at the time of the plant design. These criteria and methods together with the design codes (c.f. References 6 and 7) in use at the time of the design formed a conservative design basis and ensured that substantial factors of safety were introduced at various stages in the design procedure. In a number of instances, less stringent acceptance criteria were adopted for the subsequent Hosgri evaluation. Nevertheless, modifications were implemented in many areas which further enhanced the seismic safety of the plant, although the factor of safety based on the Hosgri event is normally lower than the corresponding factor of safety would be if based on the DDE.

The exact magnitude of many of these safety factors is still a matter of considerable discussion. Nevertheless, in order to establish a realistic value of the actual seismic capacity of a structure or equipment component, the amount of conservatism along with its variability must be established as accurately as possible. In this chapter, the design bases for the most important parameters affecting seismic capacity are identified, and the general methods used in obtaining more realistic values associated with very high seismic response levels are discussed. The methods of assessing these parameters is described in Chapters 4 and 5 for structures and equipment, respectively.

[illegible]

The general approach used in the evaluation of the Diablo Canyon seismic capacities is to develop the overall factor of safety associated with each important potential failure mode. Based on the governing Hosgri evaluation parameters, a median seismic capacity is then obtained in terms of a representative seismic input characteristic. The overall factor of safety is typically composed of several important contributions such as strength, allowance for inelastic energy absorption (ductility), and differences in median response compared to the Hosgri evaluation values resulting from such parameters as earthquake characteristics, damping, and directional load components.

3.1 Strength

The design strength of a structure or an equipment component is typically determined from applicable codes and standards such as the ACI building codes for concrete or the ASME boiler and pressure vessel code for mechanical equipment. Inherent in these design codes is a factor of safety on material strength. Sometimes this factor is known reasonably accurately, such as the design allowable being one-half the minimum yield strength or some similar relationship. At other times, it is less well defined or may be a function of the geometry or other physical characteristics of the component such as for reinforced concrete shear walls. For metal structures and components, the safety factor included in the codes is usually fairly accurately known as are the relationships between minimum and mean or median strengths.

For concrete structures, the factor of safety is normally less accurately known. In this case, the strength of the element is a function of the concrete strength, the amount and strength of the reinforcing steel, and the configuration of the element including the element geometry and reinforcing steel details. In establishing the

[illegible]

strength and seismic capacity of concrete components, the results of concrete compression tests and reinforcing steel strength and elongation tests provide a valuable basis for establishing the element strength capacity. However, the increase in concrete strength with age together with the specific geometric details of the element must also be considered. These effects are discussed in more detail in Chapter 4 for structures and Chapter 5 for the piping and equipment.

3.2 Ductility

In order to establish realistic seismic capacity levels for most structures and components, an assessment of the inelastic energy absorption must usually be considered. Exceptions to this are some modes involving brittle failure, functional electrical failure or elastic buckling. However, most failures due to seismic response involve at least some degree of yielding. This is true of reinforced concrete as well as the somewhat more ductile metal structures and components.

Consideration of structure ductility typically results in the ability of the structure to withstand greater seismic excitation than would be predicted using linear elastic techniques. In the design analysis of the Diablo Canyon structures, all design and Hosgri analyses were based on linear elastic analyses. Although no nonlinear analyses of the structures were conducted for either of these analyses, the Hosgri acceptance criteria permitted seismic stresses above yield in a number of instances. As part of the Phase IIIA fragilities investigation, a series of time history analyses were conducted on a simplified, two dimensional nonlinear model of the turbine building. This structure was selected since it is expected to have lower seismic capacity than the other civil structures and also since there was a greater uncertainty in

the expected nonlinear load distribution compared to the elastic loads. This was the only structure or equipment item for which nonlinear analyses were conducted. The results of this investigation formed the basis of the turbine building fragility reported herein. A description of the analysis model and results is provided in Appendix C.

Although inelastic analyses would be desirable in order to more accurately quantify the inelastic effects for the remaining structures, the dissipation of inelastic energy may be adequately accounted for without the time and expense of performing nonlinear analyses. This can be accomplished by the use of the ductility-modified response spectrum approach (References 8 and 9) together with a knowledge of the elastic model results and the expected ductility ratios of the critical elements of the structure or component. This approach is based on a series of nonlinear time-history analyses using single-degree-of-freedom models with various nonlinear resistance functions and levels of damping. For different levels of ductility, the reduction in seismic response for the nonlinear system compared to the equivalent elastic system response is calculated. This reduction has been shown to be a function of the frequency and damping of the system as well as the ductility. However, a reasonably accurate assessment of the reduction in response of a structure or component can be made provided the results of the elastic analysis are available and a realistic evaluation of the system ductility for multi-degree-of-freedom structures can be made.

For Phase IIIA for example, for reinforced shear wall structures, the overall system ductility and the corresponding ductility factor of safety was determined using both a story ductility and story drift approach. Using the ductility approach

[illegible]

[illegible]

[illegible]

[illegible]

$$\mu_{system} = \frac{\mu_{story}-1}{F} + 1 \tag{3-1}$$

where 1.2 < F < 2 for fixed base structures on a case by case basis depending on the expected inelastic response throughout the structure, and μ_{story} is approximately 5 for well-detailed reinforced concrete shear walls.

Using the story drift approach

$$\mu_{system} = \frac{\sum_i W_i \, \Delta_{\mu,i}}{\sum_i W_i \, \Delta_{e,i}} \tag{3-2}$$

where W_i is the story weight, $\Delta_{\mu,i}$ is the total story drift at failure (limited by approximately 0.005 times the story height) and $\Delta_{e,i}$ is the elastic story drift at yield.

Once the systems ductility, μ_{syst}, was obtained from either the ductility or story drift approach, an effective system ductility was obtained which accounts for type of inelastic response (i.e. pinched concrete shear wall, moment resisting steel frame, etc.), and the duration of the earthquake:

$$\mu_{eff} = C_D(\mu_{syst} - 1) + 1 \tag{3-3}$$

where C_D is approximately 0.7 for long duration earthquakes and reinforced concrete shear wall structures. The factor of safety resulting from consideration of inelastic energy dissipation was then obtained using the Riddell-Newmark approach.

3.3 System Response

A number of parameters must be evaluated when considering the expected

[illegible]

system response near failure compared to either the design or Hosgri conditions. Among these are the expected compared to the design or Hosgri earthquake characteristics, directional combinations, system damping, load combinations, and system modeling approaches and assumptions. Some of these parameters may be essentially median centered and introduce little change in the expected seismic capacity while other design criteria may be quite conservative. Several of the more important parameters required in evaluating the system seismic response are discussed below.

3.3.1 Earthquake Characteristics

The important Diablo Canyon civil structures are founded on competent bedrock. The seismic Category I structures and most essential equipment within the structures were designed for a DDE of 0.40g free-field ground response spectra. For the Hosgri evaluation, both Blume and Newmark type ground response spectra were used for the horizontal response analyses with Newmark spectra used for the vertical analysis. These spectra were developed from a number of earthquakes that occurred on both soil and rock sites. They were developed for design purposes and are smoothed envelopes of the actual earthquake spectra from which they were developed. A smoothed ground response spectrum was also selected as the mean spectrum for the Phase IIIA fragilities evaluation. The spectral amplification factors for the 5% damped spectrum are listed in Section 1. Amplification factors for other damping ratios were developed using the recommendations in Reference 5. The same shape spectra were used for both vertical and horizontal directions. It was assumed the median vertical acceleration was two thirds of the median horizontal acceleration, but that there was approximately a 2 percent probability that the vertical acceleration could be as much as 1.5 times the horizontal. Figure 3-1 shows a comparison of the 7% damped Blume

and Newmark spectra together with the corresponding 7% damped mean spectrum used for the fragilities evaluation. Both the Blume and Newmark spectra are seen to be conservative over much of the frequency range.

It should be noted, however, that foundation filtering was used for the Hosgri evaluation for horizontal response. The effects of the foundation filtering are dependent on the plan dimensions of the structures so that different reductions in base slab input were developed for the various Diablo Canyon structures. For the turbine building, different foundation filtering was used depending on whether the Blume or the Newmark spectra were used. Table 3-1 shows a comparison of the foundation filtering coefficients used for the Hosgri evaluation. Foundation filtering was not used for fragility evaluation for Phase IIIA except to account for the statistical incoherence from the ground wave motion. This effect is described in Section 3.3.3.

3.3.2 System Damping

Damping values used for the DDE design analysis, Hosgri evaluation, and the Phase IIIA fragility evaluation are shown in Table 3-2. The DDE design damping values are lower than those currently recommended for use in design (Reference 10), while those used for the Hosgri evaluation are generally in agreement with the SSE values in Reference 10.

At response levels of structures and equipment near failure levels, the damping ratios based on stress levels used for both the design and Hosgri evaluations are considered conservative when used in conjunction with the ductility factors used in this evaluation. Very little actual test data for damping ratios exist at failure levels, particularly for structures. However, the damping values used for design, even at the

[illegible]

higher stress levels, are generally lower compared with median centered values recommended in References 8, 11 and 12. These damping values for structures and equipment at or near yield are shown in Tables 3-2 in comparison with those used for the DDE design and Hosgri analysis. In accordance with the recommendations in Reference 11, the lower levels of the pairs of values shown in Table 3-2 for the fragility are considered to be lower bounds while the upper levels are considered to be essentially average values. The values of damping used for the fragility evaluation were taken from Table 3-2 assuming the upper level to be a median value. Review of piping damping values derived from experiments support the use of 5% of critical (Reference 12).

Damping values used in the Diablo Canyon fragility evaluation are considered appropriate for structures, equipment, and piping at seismic stress levels at or just below the yield point. For the turbine building E-W response, a somewhat lower (7%) median damping was assumed in order to avoid a possibly unconservative combination with the ductility effects since a higher median story drift was permitted for the turbine building shear walls. Higher drift was allowed in the turbine building since no essential equipment is anchored to the controlling shear walls and therefore somewhat increased cracking in the walls was permitted without concern for loss of equipment anchorage compared to the other structures.

3.3.3 Soil Structure Interaction

The Diablo Canyon structures are founded on competent bedrock with a shear wave velocity of about 3500 fps. The Hosgri evaluation seismic analyses utilized fixed base models of the structures. Preliminary results from the LTSP indicate that the seismic response from fixed base models is likely to be conservative over some frequency ranges. These

results were not available for the Phase IIIA fragilities, however. Therefore the factor of safety used for soil structure interaction effects was considered to result only from statistical incoherence from the ground motion wave. For a structure with 150 foot plan dimension, the following reduction factors were used (Ref. 13).

Frequency (Hz)	Reduction
5	1.0
10	0.9
25	0.8

For structures with different plan dimensions, a linear reduction proportional to the plan dimension was used (i.e. 0.95 at 10 Hz for a 75' dimension and 0.8 at 10 Hz for a 300' dimension).

3.3.4 Load Combinations

The load combinations on which the design of the Diablo Canyon containment and concrete internal structures were based are shown in Table 3-3 (Reference 1). These load combination criteria define a large number of load combinations that must be considered in design. In addition, the standard ACI capacity reduction (ϕ) factors were used for the design of concrete structures. For the containment building structure, these load combinations include a combination of a loss of coolant accident (LOCA) and the DDE or Hosgri loads. Random LOCA events have an extremely low frequency of occurrence as do seismic events such that the frequency of both events occurring simultaneously is so small that their inclusion is judged to not be important to the risk analysis results. Therefore, for the Diablo Canyon fragility evaluation, LOCA was not combined with earthquake loads.

[illegible]
[illegible]
[illegible]
[illegible]

[illegible]

[illegible]
[illegible]
[illegible]
[illegible]
[illegible]
[illegible]
[illegible]
[illegible]

[illegible]

[illegible]
[illegible]
[illegible]
[illegible]

3.3.5 Modal Combination

The Diablo Canyon seismic design and Hosgri evaluation analyses were conducted on the basis of loads determined by the square-root-of-the-sum-of-the-squares (SRSS) method for both the NSSS and non-NSSS structures and equipment. SRSS methods are considered to give approximately median centered results. Although some frequency shifts are expected as structures approach failure, these shifts in frequency are normally not large unless very high ductility ratios exist. Also, the relationship between loads developed from individual modes may be expected to change once nonlinear response levels are reached. In the absence of a nonlinear analysis, the changes in the modal ratios are unknown. For the seismic evaluation of most of the Diablo Canyon structures, it is assumed that the load response relationships between modes do not change significantly once the structures reach the yield point. For systems where most of the response results from one mode, this assumption introduces negligible possibility for error. For systems with a large number of modes with significant response levels, some additional uncertainty is introduced. The resulting assumed dispersion is discussed in Chapter 4 for structures.

For turbine building in the E-W response direction, the nonlinear analysis accounted for the shift in frequency at ductilities approaching failure. In addition, the variation in time phasing is included in the structure variability as a result of the multiple time history analyses conducted. One other difference in the turbine building fragilities analysis is that the seismic loads used to evaluate the

localized failure of the strut and subsequent increased seismic input to the switchgear at El. 119' were based on the double algebraic sum method for closely spaced modes. This method results in increased loads compared to the SRSS method but is considered more realistic for a structure such as the turbine building where a great many modes contribute to the response.

3.3.6 Combination of Responses for Earthquake Directional Components

The design of the Diablo Canyon structures was based on loads developed from the absolute sum of one horizontal and the vertical direction. For the Hosgri evaluation, however, the seismic loads were developed from the square-root-of-the-sum-of-the-squares (SRSS) of all three directions. For the Hosgri evaluation, accidental torsion in various amounts was added depending on the structure configuration. Another method of combining directional components such as delineated in Newmark and Hall (Reference 11) also yields realistic results. This approach recommends adding 100% of one directional component to 40% of the remaining components. This method has the advantage of being easy to use and retains a consistent relationship between loads and stresses. Both the SRSS and the 100%, 40%, 40% methods yield similar results and are considered to be essentially median centered. Therefore, no increase in the factor of safety to account for earthquake directional components was included for the structures. Generic earthquake component response factors were developed for components of different geometries by comparing resulting acceleration vectors for the applicable design criteria to median response vectors as defined by either the SRSS methodology or the 100%, 40%, 40% methodology.

3.3.7 Structure Modeling Considerations

In the seismic analysis of Diablo Canyon structures, both finite element and lumped-mass models were developed for the various buildings. Some aspects of the analysis procedure yield variations which can be quantifiably assessed and compared to the design results. For instance, the increase in the actual concrete strength compared to the design values may be used to evaluate the change in stiffness and, hence, the change in frequencies of the concrete structures compared to the design values. The modified frequencies may, in turn, be used to reevaluate the modal responses. More than offsetting this rather small frequency increase, however, is the fact that tests of stiff concrete structures have indicated lower frequencies than are calculated using conventional analysis procedures.

These expected reductions in structure stiffness were accounted for in several areas for the Phase IIIA fragilities. For the investigations into the correlation between failures of equipment items and cut-offs in the tails of the fragilities, a simplified analytical model representative of the auxiliary building was developed. The fundamental frequency of the simplified model was selected to be approximately 8.1 Hz. This includes some frequency shift resulting from softening of the building at higher shaking levels. Median and plus one standard deviation in-structure response spectra were developed using the simplified (8.1 Hz) model, and these spectra were used to obtain the seismic fragilities of the dominant contributors to risk for components which are located in the auxiliary building.

A similar approach was used for the N-S direction response of the turbine building. In the E-W direction, in-structure response spectra were developed using the nonlinear model described in Appendix C.

However, at response accelerations below those at which failure of the structure in the E-W direction is expected, a localized failure of a strut at El. 119' is expected to occur. Failure of this strut is not expected to result in failure of the equipment located at El. 119'. However, failure of the strut is expected to lead to increased seismic input to the equipment. Therefore, the fragilities of these items of equipment for acceleration levels above the strut failure level were based on in-structure response spectra which had been developed prior to the addition of the strut. However, the peaks of these in-structure response spectra were shifted to account for the expected frequency shift resulting from softening of the building at higher shaking levels.

Table 3-1. Foundation Filtering Used in the Hosgri Evaluation

Structure	Tau
Containment and Internal Structure	0.040
Intake Structure	0.040
Auxiliary Building	0.052
Turbine Building	0.080 Blume
	0.067 Newmark
Storage Tanks	0

Note: No foundation filtering was used for the vertical direction for any structure

Table 3-2. Comparison of Damping Values for Structures

Structure	Item	Damping (% of Critical)		
		DDE (Ref. 1,2)	Hosgri (Ref. 1,2)	Fragility (Ref. 8,11,12)
Containment and Internal Structure	Concrete	5	7	7-10
	Steel	2	7	7-10
Intake Structure	Concrete	5	7	7-10
Turbine Building	Concrete	5	7	7-10*
	Bolted Steel	2	7	7-10
	Welded Steel	1	4	N.A.

*For the E-W response of the turbine building, a median damping of 7% of critical with a lognormal standard deviation of 0.35 was used consistent with the ductility (story drift) limit at failure.

Table 3-3. Containment and Internal Structure Accident Design Load Combinations (Ref. 1)

(1) Exterior Shell and Base Slab

1) $U = 1.0D \pm 0.05D + 1.5P_A + 1.0T''$

2) $U = 1.0D \pm 0.05D + 1.25P_A + 1.0T' + 1.25DE$

3) $U = 1.0D \pm 0.05D + 1.0P_A + 1.0T + 1.0DDE$

4) $U = 1.0D \pm 0.05D + 1.0P_A + 1.0T + 1.0HE$

where:

U = required load capacity of section

P_A = load due to accident pressure

T = load due to maximum temperature associated with $1.0P_A$

T' = load due to maximum temperature associated with $1.25P_A$

T'' = load due to maximum temperature associated with $1.5P_A$

DDE = loads resulting from the double design earthquake

HE = loads resulting from the Hosgri event

(2) Internal Structure

For concrete structures, dead load, live load, earthquake load, compartment pressurization, pipe reactions associated with a postulated pipe rupture, jet forces, and missile loads are considered wherever occurring as follows:

$U = D + L + DDE + CP + R + J + M$

$U = D + L + HE + CP + R + J + M$

For annulus steel structures, the load combination are:

$U = D + DDE + THA + FV + RVOT$

$U = D + HE$

where:

CP = compartment pressurization associated with a pipe break

R = pipe reactions associated with a postulated pipe rupture

J = jet impingement load

M = missile impact load

THA = restrained thermal expansion loads of the supported piping.

FV = fast valve closure load

RVOT = relief valve opening thrust load

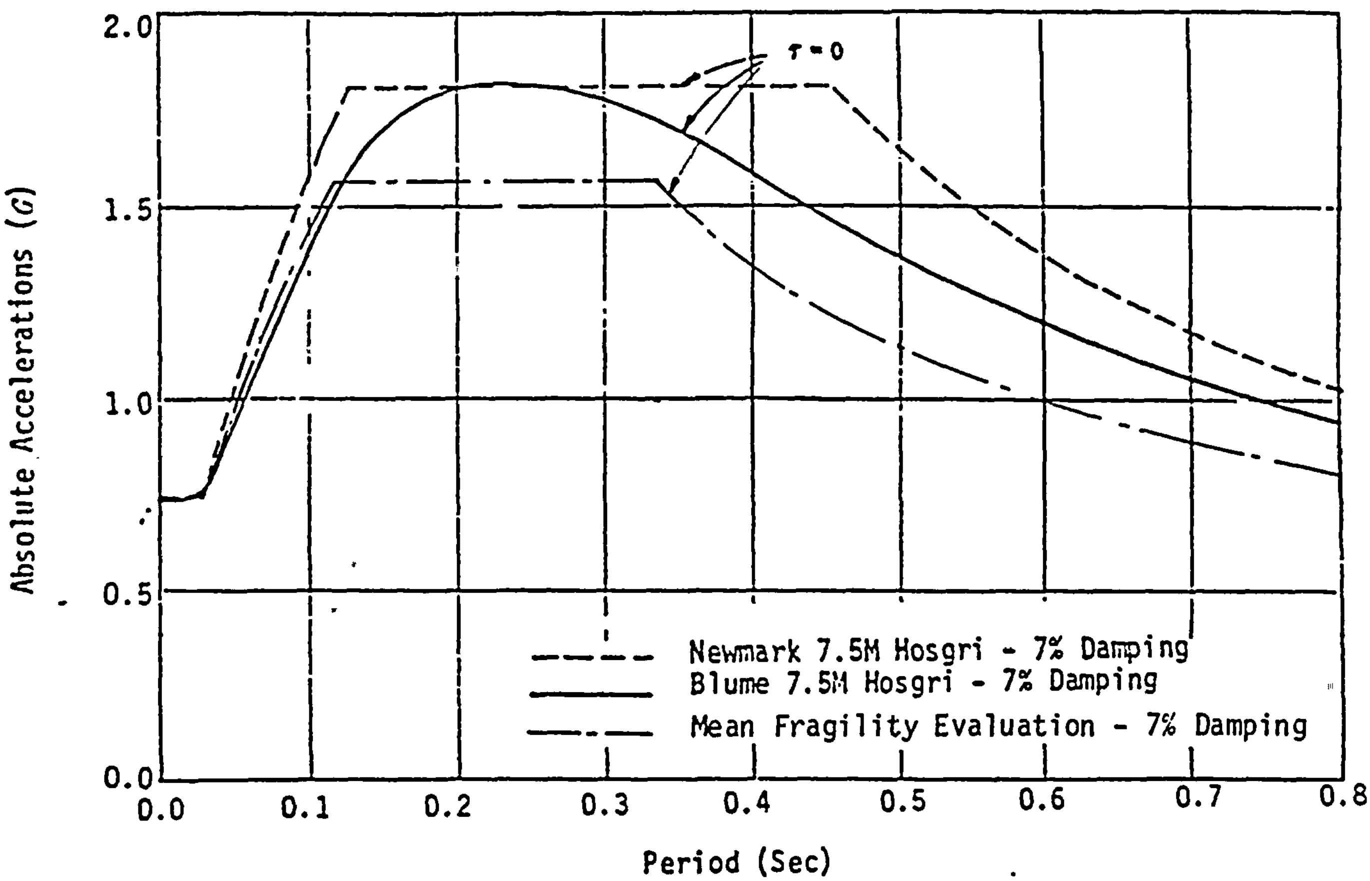

Figure 3-1. Comparison of Blume and Newmark (Unfiltered) Spectra with Mean 7% Damped Spectra used for the Fragility Evaluation

4. STRUCTURES

In this chapter, the approaches to assess the median factors of safety and logarithmic standard deviations for the important Diablo Canyon civil structures are developed. The auxiliary building is not included here. Based on these factors of safety, median capacities anchored to the 5% damped spectral acceleration in the 3 to 8.5 Hz range associated with seismic failure will be developed. For most of these structures, existing dynamic analysis results for the Hosgri event were used to determine the median factors of safety and logarithmic standard deviations for each of the variables associated with structure response. Nonlinear time history analyses were conducted for the east-west direction response of the turbine building. Thus, fragilities of the turbine building for response in the EW direction were developed based on the nonlinear analysis results. Seismic analyses of other structures were based on linear response model results of the Hosgri event.

4.1 Median Safety Factors and Logarithmic Standard Deviation

As discussed in Section 2.3, the seismic fragilities of structures and components are described in terms of the median ground spectral acceleration, A_{SA}, and random and uncertainty logarithmic standard deviations, β_R and β_U. In estimating these fragility parameters, it is computationally attractive to work in terms of an intermediate random variable called the factor of safety, F. The factor of safety is defined as the resistance capacity divided by the response associated with the Hosgri event. For equipment and structures qualified by analysis, it is easier to estimate the median factor of safety, F, and variability parameters, β_R and β_U, based upon the Hosgri stress analysis than it is to directly estimate the fragility parameters. Thus,

$$A_{SA} = F \cdot \left(A_{SA}\right)_{HOSGRI} \tag{4-1}$$

From existing analyses of the important civil structures together with a knowledge of the deterministic design criteria utilized, median factors of safety associated with the Hosgri level stresses can be estimated. These are most conveniently separated into those factors associated with the structures seismic capacity and those factors associated with the building response.

The factor of safety for the structure seismic capacity consists of the following parts:

1. The strength factor, F_S, based on the ratio of actual member strength to the Hosgri forces.

2. The inelastic energy absorption factor, F_μ, related to the ductility of the structure and to the earthquake magnitude range that is believed to contribute to most of the seismic risk.

Associated with the median strength factor, F_S, and the median inelastic energy absoprtion factor, F_μ, are the corresponding logarithmic standard deviations, β_S and β_μ. The structure strength factors of safety and logarithmic standard deviations vary from structure-to-structure and according to the different failure modes of a given structure.

The factor of safety, F_R, related to building response is assessed from a number of variables which include:

1. The response spectra used for design or Hosgri evaluation compared to the median-centered spectra for the site from multiple seismic events.

2. Damping used in the analysis compared with damping expected at failure.

3. Modal combination methods.

4. Combination of earthquake components.

5. Modeling accuracy.

6. Soil-structure interaction effects.

Based on the characteristics of the lognormal distribution, median factors of safety and logarithmic standard deviations for the various contributing effects can be combined to yield the overall estimates. For instance, the capacity factor of safety of a structure, F_{cap}, is obtained from the product of the strength and inelastic energy absorption factors of safety which, in turn, may include effects of more than one variable.

$$F_{cap} = F_S \times F_\mu \qquad (4\text{-}2)$$

The methods of assessing these safety factors are discussed in the following sections. The logarithmic standard deviation on capacity, β_{cap} is found by:

$$\beta_{cap} = \sqrt{\beta_S^2 + \beta_\mu^2} \qquad (4\text{-}3)$$

As discussed in Section 2.3, the logarithmic standard deviations are composed of both an inherent randomness and uncertainty in the median value.

Median factor of safety, F, and variability, β_R and β_U, estimates are made for each of the parameters affecting capacity and response. These median and variability estimates are then combined using the proper manner as Equation 4-2 and 4-3 to obtain the overall median factor of safety and variability estimates required to define the fragility curve for the structure.

For each variable affecting the factor of safety, the random variability, β_R, and the uncertainty, β_U, must be estimated separately. The random variability, β_R, represents those sources of dispersion in the factor of safety which cannot be reduced by more detailed evaluation or by gathering more data. Thus, β_R is due primarily to the variability of an earthquake time-history and, therefore, to a structure's response when the earthquake is only defined in terms of the peak spectral acceleration. The uncertainty, β_U, represents those sources of dispersion which could be reduced through better understanding or more knowledge. β_U is associated with such items as our lack of ability to predict the exact strength of materials (concrete and steel) and of structural elements (shear walls and diaphragms); errors in calculated response due to inaccuracies in mass and stiffness representations as well as load distributions; and use of engineering judgment in the absence of plant-specific data on fragility levels.

Each of the factors presented in Chapter 3 will be discussed in more detail in the following sections.

4.1.1. Structure Capacity

The primary lateral load-carrying systems of the Diablo Canyon structures that were analyzed are of reinforced concrete construction. The field erected tanks are essentially steel lined concrete tanks. For lateral load-carrying systems which are composed of concrete, the structure strength is a function of material strengths associated with the concrete and the reinforcing steel. The determinations of these material strengths are presented in the following two sections.

4.1.1.1 Concrete Compressive Strength

The evaluation of the strength of most concrete elements, whether loaded in compression or shear, is based on the concrete compressive strength, f'_c. Concrete compressive strength used for design is normally specified as some value at a specific time from mixing (for example, 28 or 90 days). This value is verified by laboratory testing of mix samples. The strength must meet specified values allowing a finite number of failures per number of trials. As previously stated, there are two major factors which justify the selection of a median value of concrete strength above the design strength.

1. To meet the design specifications, the contractor attempts to create a mix that has an "average" strength above the design strength.

2. As concrete ages, it increases in strength.

A variety of concrete mixes was used in the construction of the Diablo Canyon structures. Three basic mixes constitute the concrete, i.e. Type

[illegible]

A, Type B and Type C. Minimum specified and average test strengths and related statistical data of these mixes are given in Table 4-1. The concrete mixes used for the individual structural components of the various important structures are summarized in Reference 2 and are presented in Table 4-2. Note that slight variation in the average test strengths for same types of mix was observed from building to building. However, only one variability value, those shown in Table 4-1, was used for one type of mix, regardless of the difference in test strengths.

As concrete ages, its strengths increases. This must also be accounted for in determining the median strength compared to the design strength. Figure 4-1 from Reference 16 shows the increase in the concrete compressive strength with time assuming the concrete poured-in-the-field is adequately represented by the curve designated as "air-cured, dry-at-test." At 28 days, the concrete has a relative strength of 50 percent which approaches 60 percent asymptotically. The median factor relating the strength of aged concrete to the 28-day strength is, therefore, 1.2. No information is available on the standard deviation expected for aging. A logarithmic standard deviation associated with the 28-day aging factors was estimated to be 0.10. Median concrete compressive strengths and variabilities used in the fragility evaluations of the Diablo Canyon structures are listed in Table 4-2.

Other effects which could conceivably be included in the concrete strength evaluation include some decrease in strength in the in-place condition as opposed to the test cylinder strength, and some increase in strength resulting from rate of loading at the seismic response frequencies of the structure. The variation in the strength of in-place concrete compared with the test cylinder strength is accounted for to a large degree in the use of empirical representations of shear wall

[illegible]

[illegible]

[illegible]

capacities. These empirical capacities are typically developed by comparing actual wall strengths to the cylinder test strengths of the wall's concrete. Although experimental data on the in-place and rate effects are limited, that which is available would tend to indicate these effects are relatively small and of the same order magnitude. Since the two effects are opposite, they were neglected.

4.1.1.2 Reinforcing Steel Yield Strength

Both Grade 40 and 60 reinforcing steel were used in the construction of the Diablo Canyon structures. The results of tensile testing conducted on the reinforcement were reported in References 17 and 18 in terms of average yield strength. No variability in the yield strength was reported by these references. A review of the variability of the yield strength for reinforcing steel used in other nuclear power plants was conducted. Based on this survey and the average yield strength in References 17 and 18, the median yield strength, f_y, and the logarithmic standard deviations used in the structure fragilities calculations are listed in Table 4-3.

Two other effects must be considered when evaluating the yield strength of reinforcing steel. These are the variations in the cross-sectional areas of the bars and the effects of the rate of loading. A survey of information (Reference 19) determined that the ratio of actual to nominal bar area has a mean value of 0.99 and a coefficient of variation of 0.024. The same reference notes that the standard test rate of loading is 34 psi/sec. Accounting for the rate of loading anticipated in seismic response of structures results in a slight decrease in yield strength of reinforcing steel in tension. This effect is neglected in concrete compression.

4.1.1.3 Shear Strength of Concrete Walls

Recent studies have shown that the shear strength of low-rise concrete shear walls with boundary elements are conservatively predicted by the ACI 318-71 code provisions (Reference 15). This is particularly true for walls with height to length ratios in the order of 1 or less. Barda (Reference 20) determined that the ultimate shear strengths of low-rise walls tested could be represented by the following relationship:

$$v_u = v_c + v_s$$

$$= 8.3\sqrt{f'_c} - 3.4\sqrt{f'_c}\left(\frac{h_w}{\ell_w} - 0.5\right) + \rho_n f_y \qquad (4\text{-}4)$$

where:

v_u = Ultimate shear strength, psi

v_c = Contribution from concrete, psi

v_s = Contribution from steel reinforcement, psi

f'_c = Concrete compressive strength, psi

h_w = Wall height, in

ℓ_w = Wall length, in

ρ_n = Vertical steel reinforcement ratio

f_y = Steel yield strength, psi

The contribution of the concrete to the ultimate shear strength of the wall as a function of h_w/ℓ_w is shown in Figure 4-2. Also shown in Figure 4-2 are the available test values (References 20 through 23) and the corresponding ACI 318-71 formulation. The tests included load reversals and varying reinforcement ratios and h_w/ℓ_w ratios. Web crushing generally controlled the failure of the test specimens. Testing was performed with no axial loads, but an increase in shear capacity of $N/4\ell_w h$ was recommended, where N is the axial load in pounds, and h is the wall thickness in inches.

The contribution of the steel to the ultimate shear strength according to ACI 318-71 is:

$$v_s = \rho_h f_y \qquad (4\text{-}5)$$

where ρ_h = horizontal steel reinforcement ratio.

In order to estimate the effects that the horizontal and vertical steel have, the steel contribution to wall shear strength was determined from test values for the range of $0.5 < h_w/\ell_w < 2$. Test data from the above references were used. The effective steel shear strength was assumed to be in the form:

$$v_{se} = Av_{sn} + Bv_{sh} \qquad (4\text{-}6)$$

where A, B are constants and

$v_{sn} = \rho_n f_y =$ vertical steel contribution to shear strength

$v_{sh} = \rho_h f_y =$ horizontal steel contribution to shear strength

The constants A and B were then calculated assuming the concrete contribution to the ultimate strength is given as shown in Equation 4-4. Based on the results of this evaluation, the constants A and B can be shown to be:

$A = 1$	$B = 0$	$h_w/\ell_w \le 0.5$
$= -2.0\,(h_w/\ell_w) + 2.0$	$= 2.0\,(h_w/\ell_w) - 1.0$	$0.5 \le h_w/\ell_w \le 1.0$
$= 0$	$= 1$	$1.0 \le h_w/\ell_w$

and the median ultimate shear strength is given by:

$$v_u = v_c + v_{se}$$

$$= 8.3\sqrt{f'_c} - 3.4\sqrt{f'_c}\left(\frac{h_w}{\ell_w} - 0.5\right) + \frac{N}{4\ell_w h} + \rho_{se} f_y \qquad (4\text{-}7)$$

where $\rho_{se} = A\rho_n + B\rho_h$ with A and B determined as shown above. The logarithmic standard deviation was estimated to be 0.20 (Ref. 14).

The data used to substantiate the median shear strength equations presented above were derived from tests conducted on cantilever walls. The height h_w for these walls is known. However, the walls evaluated in this study typically span more than one story. For these walls, the equivalent cantilever wall height, h_{we} was taken as the ratio of the in-plane moment to the in-plane shear at the section under consideration. The equivalent height h_{we} was used to determine the median wall shear strength and provides a more accurate representation of the moment-shear interaction.

4.1.1.4 Strength of Shear Walls in Flexure Under In-Plane Forces

Equations to predict the overturning (in-plane) moment capacity of

rectangular shear walls containing uniformly distributed vertical reinforcement are found in Reference 22. These equations were derived from the basic ultimate strength design provisions for reinforced concrete members subjected to flexure and axial loads contained in Section 10.2 of ACI 318-71. These provisions are based upon the satisfaction of force equilibrium and strain compatibility.

Equation 1 of Reference 22 can be used to predict the flexural strength of rectangular walls having uniformly distributed reinforcement. The accuracy of this equation has been verified by testing. Equation 2 of Reference 22 shown as Equation 4-8 below, was presented as an adequate approximation to Equation 1.

$$M_u = 0.5\ A_s f_y \ell_w \left(1 + \frac{N_u}{A_s f_y}\right)\left(1 - \frac{c}{\ell_w}\right) \text{in - lb} \qquad (4\text{-}8)$$

where

A_s = Total area of vertical reinforcement at section, sq. in.

f_y = Yield strength of vertical reinforcement, psi

ℓ_w = Horizontal length of wall, in.

c = Distance from extreme compressive fiber to neutral axis, n

N_u = Axial load, positive in compression, lb.

f'_c = Compressive strength of concrete, psi

Inspection of Equation 4-8 reveals that the overturning moment capacity of a rectangular wall can be adequately represented by lumping the total

area of the uniformly distributed vertical reinforcement at midlength of the wall and applying the basic design provisions in Section 10.2 of ACI 318-71.

$$M_u = (A_s f_y + N_u)\left(\frac{\ell_w}{2} - \frac{\beta_1 c}{2}\right) \tag{4-9}$$

where β_1 is the ratio of the depth of the equivalent rectangular concrete stress block to the distance to the neutral axis (c).

This approach was typically used to predict the median flexural strength for walls without concentrated reinforcement. Concentrated reinforcement can be embedded steel columns well tied to the concrete wall or the vertical wall reinforcement bars within the effective flanges of the cross walls cast integrally with the wall evaluated. The compression flange steel is typically neglected since it is near the neutral axis, and its effect on the moment capacity is small. The total moment capacity of reinforced concrete shear walls including concentrated reinforcement is then:

$$M_u = (A_s f_y + N_u)\left(\frac{\ell_w}{2} - \frac{\beta_1 c}{2}\right) + A_f f_{fy}\left(d - \frac{\beta_1 c}{2}\right) \tag{4-10}$$

where

A_f = Area of concentrated reinforcement steel

d = Distance from the extreme compressive fiber to the centroid of concentrated reinforcement steel

4.1.2 Structure Inelastic Energy Absorption

A much more accurate assessment of the seismic capacity of a structure can be obtained if the inelastic energy absorption of the structure is considered in addition to the strength capacity. One tractable method involves the use of ductility modified response spectra to determine the deamplification effect resulting from the inelastic energy dissipation. Early studies indicated the deamplification factor was primarily a function of the ductility ratio, μ, defined as the ratio of maximum displacement to displacement at yield. More recent analytic studies (Reference 9) have shown that for single-degree-of-freedom systems with resistance functions characterized by elastic-perfectly plastic, bilinear, or stiffness-degrading models, the shape of the resistance function is, on the average, not particularly important. However, as opposed to the earlier studies, more recent analyses have shown the deamplification factor is also a function of the system damping.

The Riddell-Newmark ductility modified response spectra approach can be used to predict the inelastic energy absorption factor, F_μ, corresponding to some ductility ratio, μ, in the following manner:

$$F_\mu = [p\mu - q]^r \tag{4-11}$$

where $p = q + 1$

$q = 3.0\gamma^{-0.30}$ in the amplified acceleration region.

$\quad = 2.7\gamma^{-0.40}$ in the amplified velocity region.

$$r = 0.48\gamma^{-0.08} \quad \text{in the amplified acceleration region.}$$

$$= 0.66\gamma^{-0.04} \quad \text{in the amplified velocity region.}$$

γ = percent of critical damping.

For systems in the amplified acceleration region of the spectrum, Figure 4-3 from Reference 9, shows the deamplification function for several damping values as a function of the ductility ratio.

The ductility modified response spectra method was developed using single-degree-of-freedom models. For multi-degree-of-freedom systems such as the major Diablo Canyon civil structures, a system ductility must be developed. The approach used to determine the system ductility, μ_{syst}, for the various structures was discussed in Section 3.2.

One drawback of the ductility modified response spectra approach is that it does not reflect the relationship between earthquake magnitude and ductility. It is well known that lower magnitude earthquakes are not as damaging to structures and equipment as higher magnitude earthquakes with the same peak ground accelerations. The reason for this is that the lower magnitude earthquakes have lower energy content and shorter durations which develop fewer strong response cycles. Structures and equipment are able to withstand larger deformations (i.e., higher ductility) for a few cycles compared to the larger number of cycles resulting from longer duration events.

The method used in the Diablo Canyon fragilities evaluation to account for this effect was based on the use of an effective ductility, μ_{eff}, in conjunction with the Riddell-Newmark ductility modified spectra approach. The following formulation was developed in Section 3.2 to

calculate the effective ductility.

$$\mu_{eff} = 1.0 + C_D (\mu_{syst} - 1.0) \qquad (4\text{-}12)$$

where C_D = duration correction factor, is a function of the earthquake magnitude

μ_{syst} = overall system ductility developed in Section 3.2

A limited amount of the research is available for use in developing C_D factors. In Reference 24, structures with elastic frequencies of approximately 2, 3, 5 and 8 Hz were subjected to 12 earthquake records scaled to sufficient intensity to produce ductility ratios of approximately 1.9 and 4.3. Included was one artificial record which developed response spectra which envelope the US NRC Reg. Guide 1.60 spectra. The C_D factors used in the Diablo Canyon fragilities evaluation were based on the results from Reference 24. C_D is considered to be frequency-independent based on these limited data.

The factor of safety resulting from ductility effects, F_μ, is dependent on both duration and spectral shape. Figure 4-4 is reproduced from Reference 24 and clearly shows the effect of strong motion duration for a ductility ratio of approximately 4.3. However, F_μ, is most strongly influenced by the spectral shape and the frequency of the structure. Tables 4-4 and 4-5 also reproduced from Reference 24, show the F_μ factors for the various earthquake records and structure frequencies for the 1.9 and 4.3 ductility ratios, respectively. It is inappropriate to include results from Reference 24 for frequencies which lie in a steeply rising or falling portion of a sharply peaked region of the response spectra. As a structure reaches significant levels of inelastic response, there is a decrease in the resonant frequency of the

[illegible]

structure. If the elastic frequency of the structure is in a portion of the response spectrum where the frequency shift results in lower response, a relatively higher F_μ will be developed. Conversely, if the elastic frequency of the structure lies in a region of the response spectrum where the frequency shift results in increased response, a relatively lower F_μ will be predicted. A review of the data from Reference 24 indicates that many of the F_μ factors shown in Tables 4-4 and 4-5 do, in fact, lie in steeply rising or falling regions of the response spectra.

The Diablo Canyon median ground response spectra, however, are relatively broadband and contain significant energy throughout the frequency range from approximately 3 Hz to 10 Hz. Thus, even though a number of structures at Diablo Canyon have relatively high fundamental elastic frequencies, it is incorrect to use all the F_μ factors directly from the results from Reference 24 together with the Riddell-Newmark method and the Diablo Canyon median spectra. For earthquakes in the magnitude 6.5 to 7.5 range from Reference 24, an average value of F_μ of approximately 2.2 is indicated. Using the Riddell-Newmark formulation for F_μ given above together with the 4.27 ductility ratio and 7 percent of critical damping used in Reference 24, a value of 2.55 was calculated. Thus, for earthquakes in the magnitude 6.5 to 7.5 range, an effective ductility of about 3.2 with duration coefficient of 0.7 is indicated by using the Reference 24 results. The majority of seismic risk for the Diablo Canyon plant is expected to result from earthquakes centered around magnitude 7 range. Therefore, the effective duration coefficient of 0.7 is considered appropriate for the Diablo Canyon plant.

The following definition of the inelastic absorption factor was used for the Diablo Canyon structures whose fundamental frequencies are within

the amplified acceleration region:

$$F_\mu = \frac{S_{a_e}}{S_{a_\mu}} \qquad (4\text{-}13)$$

S_{a_e} = Spectral acceleration from the elastic response spectrum for the fundamental structure mode having a frequency in the amplified acceleration region.

S_{a_μ} = Deamplified spectral acceleration accounting for nonlinear structure response.

= Greater of $S_{a_{\mu,A}}$ or $S_{a_{\mu,RIG}}$, where

$$S_{a_{\mu,A}} = (p\mu_{eff} - q)^{-r} \, (S_{a_e}) \qquad (4\text{-}14)$$

$$S_{a_{\mu,RIG}} = (\mu_{eff})^{-0.13} \, (PGA) \quad \text{(for 10\% damping)} \qquad (4\text{-}15)$$

p,q,r - Equation 4-11

PGA = Peak ground acceleration

Equation 4-15 is also presented in Reference 9.

4.1.3 Spectral Shape, Damping and Modeling Factors

As previously discussed, important Diablo Canyon civil structures are

founded on competent bedrock. For the Hosgri evaluation, both Blume and Newmark type ground response spectra were used for the horizontal response analyses. Newmark's foundation filtering (Tau) effect was used in the Hosgri evaluation for horizontal response. Due to this filtering effect, reduction in base slab input were developed for the various Diablo Canyon structures as shown in Figures 3-2 through 3-5. The mean spectrum anchored to 0.75 g peak ground acceleration for the Phase IIIA fragilities evaluation was developed based on the discussion in Section 3.3.1. The spectral shape factor for each structure was based on the mode or modes contributing to most of the seismic response. The frequencies predicted by the Hosgri evaluation dynamic models were used. The spectral shape factor at the frequency under consideration is given by:

$$F_{ss} = \frac{S_{D_{\zeta} = S_D}}{S_{M_{\zeta} = S_M}} \tag{4-16}$$

where $S_{D_{\zeta=S_D}}$ represents the Hosgri spectral acceleration at the Hosgri damping value used for the structure evaluated and $S_{M_{\zeta} = S_M}$ represents the estimated site-specific response spectrum for median damping.

In computing the spectral shape factor of safety, it is convenient to combine the damping and ground response spectrum effects. In the development of logarithmic standard deviations on spectral shape, however, it is informative to consider the damping effects separately. This implies a factor of safety of unity on damping alone since it has already been included in the factor of safety on spectral shape.

For Diablo Canyon fragilities, a logarithmic standard deviation of 0.20 on the randomness of spectral shape was estimated to account for the peaks and valleys inherent in the response spectra of any real earthquakes compared to the smoothed mean spectra. No uncertainty on the spectral shape was included in the Diablo Canyon fragilities, i.e., $\beta_U = 0$.

The logarithmic standard deviation associated with damping, β_ζ, can be estimated from:

$$\beta_\zeta \simeq \ln \frac{S_{M_{\zeta = \zeta - 1\sigma}}}{S_{M_{\zeta = \zeta_M}}} \qquad (4\text{-}17)$$

where $S_{M_{\zeta = \zeta-1\sigma}}$ is the spectral acceleration from the median site-specific spectrum at mean minus one standard deviation damping, and $S_{M_{\zeta = \zeta M}}$ is the spectral acceleration from the median site-specific spectrum at median damping. Median minus one standard deviation material damping values are listed in Table 3-2. The randomness and uncertainty components of β_ζ were estimated to be approximately equal.

$$(\beta_R) = (\beta_U) = \frac{\beta_\zeta}{\sqrt{2}} \qquad (4\text{-}18)$$

The dynamic models used in the Hosgri evaluation were typically determined to be adequate to predict the seismic response. Modeling factors of unity typically were used. Variability in modeling predominantly influences the calculated mode shapes and modal frequencies. Since the concrete strength and, consequently, the stiffness of the structures is above the design values, calculated frequencies would be expected to be somewhat less than actual values, at

least for low-to-moderate levels of response. At response levels approaching failure, softening of the structures due to concrete cracking occurs, and for structures analyzed using uncracked section properties, some decrease in the actual frequencies compared to the calculated values is expected. The Hosgri calculated frequencies and mode shapes were generally assumed to be approximately median-centered.

Modeling uncertainties from both the mode shapes and modal frequencies enter into the uncertainty on calculated modal response as defined by β_M. Thus,

$$\beta_M = \sqrt{\beta_{MS}^2 + \beta_{MF}^2} \tag{4-19}$$

where β_{MS} and β_{MF} are estimated logarithmic standard deviations on structural response of a given point in the structure due to uncertainties in mode shape and due to uncertainties in modal frequencies, respectively. Based upon experience in performing similar analyses, β_{MS} was estimated to be typically about 0.15. The modal frequency variability shifts the frequency at which spectral accelerations are to be determined, so that:

$$\beta_{MF} \simeq \ln \left(\frac{S_{M_{f=f_\beta}}}{S_{M_{f=f_M}}} \right) \tag{4-20}$$

where f_M is the median frequency estimate, and f_β is the 84 percent exceedance probability frequency estimate. The logarithmic standard deviation on frequency was typically estimated to be approximately 0.30 for the structures evaluated.

4.1.4 Modal Combination

The Hosgri evaluation of Diablo Canyon structures was performed mostly by response analysis; therefore, phasing of the individual modal responses was unknown. Most current design analyses are normally conducted using response spectra techniques. For the Diablo Canyon structures as well as for the equipment, the SRSS method was used as discussed in Section 3.3.5. Many studies have been conducted to determine the degree of conservatism or unconservatism obtained by use of SRSS combination of modes. Except for the very low damping ratios, these studies have shown that SRSS combination of modal responses tends to be median-centered. The coefficient of variation (approximate logarithmic standard deviation) tends to increase with increasing damping ratios. Figure 4-5 (taken from Reference 25) shows the actual time-history calculated peak response versus SRSS combined modal responses for structural models with four predominant modes. Based upon these and other similar results, it is estimated that for ten percent or greater structural damping, the SRSS response is median-centered. The median modal combination factor of safety was therefore taken to be 1.0 for the Diablo Canyon structures and equipment fragilities based on the Hosgri evaluation information. Where individual modal responses were known, the absolute sum of these responses was used to estimate the coefficient of variation. The absolute sum is an upper bound estimated to be three standard deviations above the median SRSS response.

4.1.5 Combination of Earthquake Components

The Hosgri evaluation of the important Diablo Canyon structures was based on loads developed from the square-root-of-the-sum-of-the-squares (SRSS) of all three directions of input. Alternatively, it is recommended (Reference 11) that directional effects be combined by

[illegible]

taking 100 percent of the effects due to motion in one direction and 40 percent of the effects from the two remaining principal directions of motion. This was considered the median condition for the current evaluation.

Depending on the geometry of the particular structure under consideration together with the relative magnitude of the individual load or stress components, the expected stresses due to the 100%, 40%, 40% method of load combinations are increased when compared with those calculated using the SRSS method. For shear wall structures where the shear walls in the two principal directions act essentially independently and are the controlling elements, the two horizontal loads do not combine to a significant degree except for the torsional coupling. Thus, only the vertical component affects the individual shear wall stress. A moderate amount of vertical load slightly increases the ultimate shear load carrying capacity of reinforced concrete walls, while the overturning moment capacity may be more significantly affected. Typically, the effect of the vertical dead load on the wall capacities was conservatively neglected. In these cases, the effect of the vertical seismic component on the capacities and the earthquake component combination variabilities was not included since these capacities already contain conservatism due to not including the dead load. In other cases, where the increase in capacity due to the dead load was included, the effect of the vertical seismic response on the capacity and the earthquake component combination variability was also included.

The median strength factors for the structural failure modes were typically defined using the Hosgri loads combined by the median-centered method of directional component combination. Consequently, the median factor of safety on earthquake component combination is unity. The

coefficient of variation is calculated in the same manner as it was for the modal combination factor. The absolute sum of the three components is an upper bound, estimated to be three standard deviations above the median.

4.1.6 Soil-Structure Interaction

As discussed in Section 3.3.3, the Diablo Canyon structures are founded on competent bedrock. In the previous Hosgri evaluation, structural responses were obtained from dynamic analyses using fixed base models of the structures. For the fragilities evaluation reported here, no soil-structure interaction effect other than the statistical incoherence from the ground motion wave was considered. The factors of safety associated with this soil-structure interaction effect were developed as shown in Section 3.3.3. Currently, soil-structure interaction analyses accounting for embedment and other effects are underway, and these results will be incorporated in the final seismic PRA results.

4.2 Structure Fragilities

The significant failure modes for each of the important Diablo Canyon structures included in this study were evaluated. The resulting fragilities for each of these structures are discussed in the following sections. Most of the structures are founded on competent bedrock and are embedded into the ground. Thus, sliding-induced failure was considered not to be a credible failure mode for the Diablo Canyon structures.

4.2.1 Containment Building and Internal Structure

The containment building is a reinforced concrete structure consisting

[illegible]

of a circular cylindrical wall capped by a hemispherical dome. The containment wall is supported by a basemat bearing on the bedrock. Principal dimensions of the containment building are:

Mat	Radius	76' - 6"
	Thickness	14' - 6"
	Liner plate thickness	1/4"
Cylinder	Inside radius	70' - 0"
	Wall thickness	3' - 8"
	Liner plate thickness	3/8"
	Height to Springline	142' - 0"
Dome	Inside radius	70' - 0"
	Thickness	2' - 6"
	Liner plate thickness	3/8"

Concrete with a design compressive strength of 3000 psi at 28 days was used to construct the wall. The reinforcing in the cylinder wall consists of horizontal hoop bars, and inclined bars, oriented 60° from the horizontal. The inclined bars were extended past the springline and over the dome to form the dome reinforcing. After crossing the dome, the same bar once again becomes an inclined bar in the cylinder. Two layers of inclined cylinder wall reinforcing bars extend from the basemat to elevation 172 feet to provide additional capacity to resist seismic forces.

The controlling mode of failure for the containment building was found to be shear failure of the cylindrical wall near the base. The seismic shear forces were estimated based on the tangential membrane shear stresses due to the Hosgri-Newmark earthquake.

[illegible]

The results of scale model testing conducted to determine the strength of reinforced and prestressed concrete containment structures subject to seismic loads with and without internal pressure are summarized in Reference 26. The median shear strength of the containment wall was determined using empirical relationships derived from these test results. Resistance to horizontal seismic shear is provided by the concrete, the hoop reinforcing steel and the diagonal reinforcing steel. The components of the area of the diagonal bars in the hoop and meridional directions were added to the hoop and meridional stress capacities. Only the diagonal bars in one direction were included. The diagonal steel in the other direction is ineffective since it is parallel to the concrete struts formed by the horizontal shear.

The internal structure consists of the reactor shield wall, the fuel transfer canal, and the crane wall which provide support and restraint for all major equipment, components, and systems located within the containment building. These structures enclose the primary coolant system and also provide the biological shielding and missile protection. The internal structures are founded at EL 89 on the foundation mat common with the containment building. Anchorage to the foundation mat is achieved by cadwelding No. 18 wall reinforcing to either side of the steel base liner plate at the same locations. The reactor shield wall is an eight foot six inch thick reinforced concrete cylinder wall near the base. The upper reactor cavity wall is a four foot six inch thick reinforced concrete wall structurally connected to the fuel transfer canal. The crane wall is a three foot thick reinforced concrete cylinder with an inside diameter of 100 feet and an overall height of 51 feet.

Potential failure modes considered for the internal structure are shear

[illegible]

failure, flexural failure and shear transfer across the interface of the internal structure walls and basemat. The controlling failure modes for both the reactor shield wall and the crane wall were found to be shear failure. Seismic forces considered in the fragility analysis were obtained from the Hosgri evaluation using the Hosgri-Newmark earthquake input.

4.2.2 Intake Structure

The intake structure is a seismic design Class II structure housing the Class 1 auxiliary saltwater (ASW) pumps. The intake structure is a reinforced concrete box-type structure founded on a basemat bearing on competent bedrock. Keyways are provided into the bedrock at the basemat/bedrock interface to provide sliding resistance. Plan dimensions of the structure are approximately 240 feet by 100 feet with the long dimension running in the north-south direction. The major lateral force resisting system consists of concrete slabs and shear walls on the north, south and east sides of the intake structure.

The Hosgri evaluation seismic forces were used for the fragility analysis. These forces were obtained from the response spectrum analysis of the three-dimensional fixed base finite element model of the intake structure using the Newmark-Hosgri response spectrum. Load redistribution after yielding of the curtain wall and the gate guide wall was considered in the fragility evaluation, and the resulting additional torsional moment was included in the shear wall forces estimation.

4.2.3 Turbine Building

The turbine building of the Diablo Canyon plant is a Design Class II

[illegible]

structure that contains Design Class I equipment such as the component cooling heat exchangers, the emergency diesel generators, the 4.16 KV switchgear and other Class I systems. The building was originally dynamically analyzed to assure that it would not collapse and impair the Class I equipment during a design seismic event. During the Hosgri evaluation, the turbine building was reevaluated and upgraded to withstand the Hosgri seismic loads. Unit 1 and Unit 2 turbine buildings are very similar and share a common foundation basemat. The lateral force resisting system of the turbine building consists of structural steel frame superstructure above elevation 140 and reinforced concrete shear walls below elevation 140. There are four working floor levels at approximate elevations of 140, 119, 104, and 85 feet. all floors but the operating floor at elevation 140 and foundation base slab at elevation 85 consist of steel gratings, steel checkered plates and concrete slab. The operating floor is constructed of reinforced concrete slab. The turbine pedestal is located in the center of the building and is structurally isolated from the turbine building floors above a common foundation mat with a rattlespace.

In the Hosgri evaluation, a detailed linear elastic three-dimensional finite element model was constructed for the turbine building to perform response spectrum analyses. Modal responses were combined by SRSS and Double Algebraic Sum (DAS) methods. The horizontal seismic response was determined using 0.54g Blume and 0.50g Newmark-Hosgri response spectra. The accidental torsional response due to Newmark foundation filtering effect was accounted for by increasing the ground response spectra by 10%. Separate time history analyses were performed to generate in-structure response spectra for the equipment analysis in the Hosgri evaluation. For the fragility analysis of the turbine building, structural responses determined in the Hosgri evaluation were used

[illegible]

except the reinforced concrete shear walls in the east-west direction for which responses from the nonlinear time history analysis of the turbine building (Appendix C) were used.

Important structure components and their failure modes which were evaluated include:

1. Shear walls at column lines 19 and 31
2. Structural steel strut in the floor system at EL 119
3. Masonry block walls at EL 119 near the 4.16 KV switchgear

The following sections present the fragilities of each of the components evaluated.

4.2.3.1 Shear Walls at Line 19 and 31

In Phase II of the Long Term Seismic Program, the east-west oriented concrete shear walls were found not only to have relatively low capacity compared to other civil structures, but also to contain considerable uncertainty in the fragility. Consequently, in Phase IIIA a simplified two-dimensional inelastic model of the turbine building was developed to investigate the structure loads, load distributions and story drifts as well as develop in-structure response spectra for the structure at response levels close to failure. The model permitted inelastic response in the major E-W shear walls (Column Lines 19 to 31), the operating floor diaphragm, and the turbine pedestal, and allowed for impact between the operating floor and the turbine pedestal. The dispersion of structure response due to variabilities in structure properties and earthquake ground motion were included by using the Monte Carlo technique to vary the important structure properties such as damping, stiffness and strength of the elements and by employing the 25

time history records obtained from the LTSP Ground Motion Study Group for the nonlinear time history analysis. With this approach, a better estimate of uncertainty and randomness of the structure response was achieved.

Median capacity of the turbine building for response in the east-west direction was estimated by considering strengths of shear walls as well as shear story drift. Measurements in the laboratory and in the field have shown that structural damage to stiff low-rise walls can be related to story drift. For concrete walls with shear failure governing story drifts varying from 0.5% to 1.0% were observed. For turbine building fragility evaluation, a median shear story of 0.7% was judged to be appropriate.

4.2.3.2 Strut at EL 119'

The W 14 x 605 strut and corresponding strengthening of the floor diaphragm system at EL 119' of both units of the turbine building were installed in the 1983 modification in order to reduce the north-south direction Hosgri response of the concrete slab at EL 119' to reduce the seismic input to the 4.16 KV switchgear. The seismic loads in the strut were obtained from the response spectrum analysis of the turbine building for the Hosgri evaluation. Seismic loads developed by using the Double Algebraic Sum method for closely spaced modes were used.

4.2.3.3 Masonry Block Walls

The masonry block walls which are close to the safety related equipment in the turbine building are located at elevations of 119, 104 and 85 feet. These masonry walls have both horizontal and vertical reinforcing steel and the cells were fully grouted. In addition, the masonry walls are laterally braced by vertical wide flange steel columns. The walls

are attached to the columns by thru-bolts. Along the top and bottom edges, the walls are attached to the floor beams above and the concrete slab below by steel angle sections.

4.2.4 Refueling Water Storage Tanks and Condensate Storage Tanks

There are two refueling water storage tanks (RWST) and two condensate storage tanks (CST) at the Diablo Canyon site, one to serve each unit of the plant. The tanks were originally designed for the DDE simply as steel tanks. In a later modification, each tank was enveloped by a concrete shell. Studs were provided to tie the steel liner and the concrete shell together. The tanks are supported on concrete fill (with a minimum compressive strength of 3000 psi at 28 days) down to bedrock and are anchored to bedrock with rock anchors. Important dimensions are given below:

RWST

Inside diameter	40'-0"
Tank height	52'-6"
Steel liner thickness	Varies from 0.578" at the base to 0.25" at the dome
Concrete wall thickness	Varies form 36" at the base to 12" at the top
Concrete thickness at dome	8"

CST

Inside diameter	40'-0"
Tank height	47'-3"
Steel liner thickness	Varies form 0.60" at the

	base to 0.25" below the dome
Concrete wall thickness	Varies from 36" at the base to 12" at the top
Concrete thickness at dome	8"

Seismic forces were obtained from axisymmetric and non-axisymmetric dynamic analyses of the fixed base model with 7% damped Newmark-Hosgri ground response spectrum as input ground motion (Reference 27). No composite action of the steel liner and concrete shell was considered in the evaluation of the shear and flexural capacities of the tanks.

The structure configuration of the condensate tanks is very similar to that of the refueling water storage tanks. The height of the condensate tank and its design liquid depth are both 5.25 feet less than that of the RWST. Also, same amount of rock anchors were used for anchoring the condensate tank to the bedrock. Therefore, the median capacity of the condensate tank is expected to be somewhat greater than the refueling water storage tank.

4.2.5 Diesel Fuel Oil Storage Tank

The two diesel fuel oil storage tanks are located outside of the turbine building and are buried with the top of the crown at about 6 feet below grade. The tanks were constructed of steel plate with angle stiffeners spaced at 42 inches apart. The tank diameter is about 10½ feet and the length is 63 feet.

An extensive study of the tank was previously performed to analyze the behavior of these tanks under strong earthquake shaking (Reference 28) the computer program FLUSH was used in this study. For Newmark-Hosgri 7.5M ground motion, an artificial accelerogram with a peak ground

acceleration of 0.75g, was used as input.

4.2.6 Auxiliary Saltwater Piping

The auxiliary saltwater (ASW) pipelines are two 24-inch diameter pipes running from the intake structure to the turbine building. The ASW lines are buried at about 25 feet to 30 feet below the ground surface. The lines are restrained to the reinforced concrete circulating water intake conduit at 40 feet intervals. The concrete intake conduit was poured directly against the rock.

The fragility evaluation of the ASW lines is limited to the seismic induced dynamic strains in the pipelines. Failure due to gross movement of the ground was not considered in this study.

Table 4-1. Specified and Average Test Strengths of Concrete Used in Diablo Canyon Structures (Reference 2)

CONCRETE MIX	MINIMUM SPECIFIED f'_c (PSI) AT DAYS	AVERAGE TEST STRENGTH (PSI)	STANDARD DEVIATION (PSI)	COEFFICIENT OF VARIATION
A	5000 @ 60	6340	412	0.065
B	3000 @ 28	3870	369	0.095
C	5000 @ 28	5640	392	0.070

Table 4-2. Median Concrete Compressive Strength and Variabilities

STRUCTURE AND COMPONENT	CONCRETE MIX	AVERAGE TEST STRENGTH f'_c (PSI)	MEDIAN STRENGTH $\breve{f}'_c$ (PSI)	LOGARITHMIC STANDARD DEVIATION, β
CONTAINMENT STRUCTURE				
BASE SLAB TO ELEVATION 87'	A	6330	7100	0.12
SKIN POUR AT ELEVATION 89'	A	6330	7100	0.12
CONCRETE INTERNAL	A	6330	7100	0.12
EXTERIOR WALLS	B	3850	4600	0.14
DOME	B	3850	4600	0.14
TURBINE BUILDING				
SLAB AT ELEVATION 140'	A	6590	7400	0.12
SLABS EXCEPT AT ELEVATION 140' COLUMNS AND PEDESTAL	B	3870	4600	0.14
EXTERIOR WALLS ABOVE ELEVATION 85', EXCEPT SHEAR WALLS ALONG LINES 1 AND 35	B	3870	4600	0.14
SHEAR WALLS ALONG LINES 1, 35, 5, 17, 19 AND 31	C	5500	6600	0.12
REMAINDER	B	3870	4600	0.14
INTAKE STRUCTURE	B	3630	4300	0.14

Table 4-3. Median Reinforcement Yield Strength and Variabilities

STRUCTURE	GRADE	AVERAGE TEST YIELD STRENGTH (KSI)	MEDIAN YIELD STRENGTH (KSI)	LOGARITHMIC STANDARD DEVIATION
CONTAINMENT				
EXTERIOR #18's	60	67	67	0.10
INTERIOR #11's	60	68	68	0.10
TURBINE BUILDING	60	66	66	0.10
	40	51	51	0.09
INTAKE STRUCTURE	40	50	50	0.09

Table 4-4. Scale Factors Needed to Achieve μ = 1.85

a) Due to 6.5 - 7.5 Richter magnitude earthquakes

EARTHQUAKE RECORD (COMP.)	MODEL STRUCTURE FREQUENCY			
	8.54 Hz	5.34 Hz	3.20 Hz	2.14 Hz
Olympia, WA., 1949 (N86E)	1.36	1.11	1.49	1.70
Taft, Kern Co., 1952 (S69E)	1.20	1.25	1.50	1.78
El Centro Array No. 12 Imperial Valley, 1979 (140)	1.34	1.56	1.29	1.48
Pacoima Dam San Fernando, 1971 (S14W)	1.25	1.38	1.26	2.19
Hollywood Storage PE Lot, San Fernando, 1971 (N90E)	1.45	1.65	1.58	1.39
El Centro Array No. 5 Imperial Valley, 1979 (140)	1.58	1.60	1.34	1.51

Mean = 1.47 Median = 1.47 Range = 1.11 - 2.19

b) Due to 4.5 - 6.0 Richter magnitude earthquakes

EARTHQUAKE RECORD (COMP)	MODEL STRUCTURE FREQUENCY			
	8.54 Hz	5.34 Hz	3.20 Hz	2.14 Hz
UCSB Goleta Santa Barbara, 1978 (180)	1.35	1.65	1.41	1.49
Gilroy Array No. 2, Coyote Lake, 1979 (050)	1.36	1.93	2.00	1.86
Gavilan College Hollister, 1974 (S67W)	1.61	1.55	1.62	1.93
Melendy Ranch Barn, Bear Valley 1972 (N29W)	1.45	1.96	2.18	1.98

Mean = 1.71 Median = 1.64 Range = 1.35 - 2.18

Table 4-5. Scale Factors Needed to Achieve μ = 4.27

a) Due to 6.5 - 7.5 Richter magnitude earthquakes

EARTHQUAKE RECORD (COMP)	MODEL STRUCTURE FREQUENCY			
	8.54 Hz	5.34 Hz	3.20 Hz	2.14 Hz
Olympia, WA., 1949 (N86E)	1.56	1.54	2.61	3.75
Taft, Kern Co., 1952 (S69E)	1.25	1.65	2.05	3.38
El Centro Array No. 12 Imperial Valley, 1979 (140)	1.56	2.29	2.10	2.14
Pacoima Dam San Fernando, 1971 (S14W)	1.70	1.86	2.67	3.89
Hollywood Storage PE Lot, San Fernando, 1971 (N90E)	1.94	2.50	2.60	2.05
El Centro Array No. 5 Imperial Valley, 1979 (140	2.38	2.66	2.33	3.45

Mean = 2.33 Median = 2.22 Range = 1.25 - 3.89

b) Due to 4.5 - 6.0 Richter magnitude earthquakes

EARTHQUAKE RECORD (COMP)	MODEL STRUCTURE FREQUENCY			
	8.54 Hz	5.34 Hz	3.20 Hz	2.14 Hz
UCSB Goleta Santa Barbara, 1978 (180)	1.52	2.05	2.05	1.96
Gilroy Array No. 2, Coyote Lake 1979 (050)	1.56	3.85	4.36	3.03
Gavilan College Hollister, 1971 (S67W)	2.84	2.97	2.71	8.49
Melendy Ranch Barn, Bear Valley 1972 (N29W)	1.89	5.48	5.16	3.36

Mean = 3.33 Median = 2.91 Range = 1.52 - 8.49

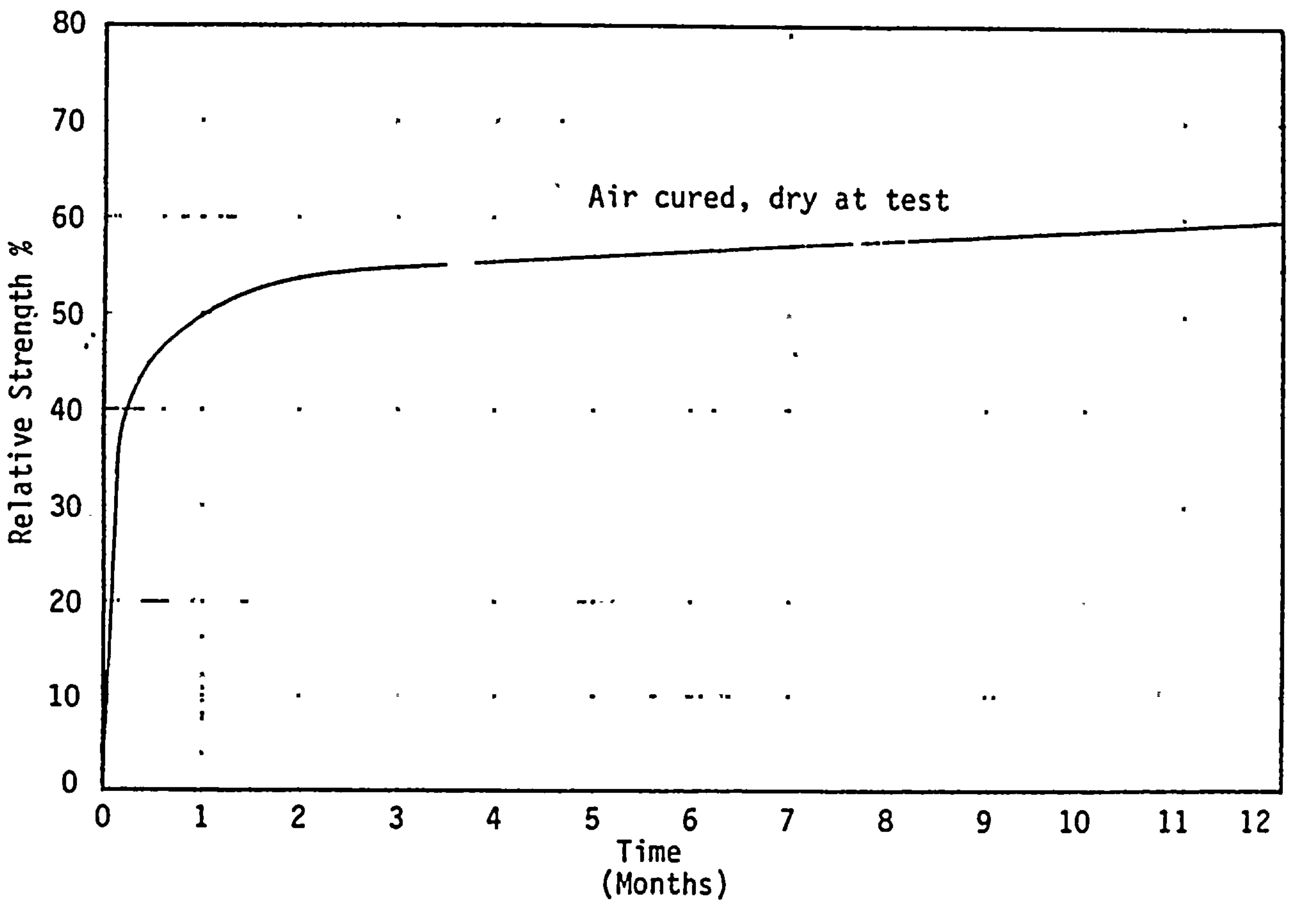

Figure 4-1. Effects of Time and Curing Conditions on Concrete Strength (From Reference 16)

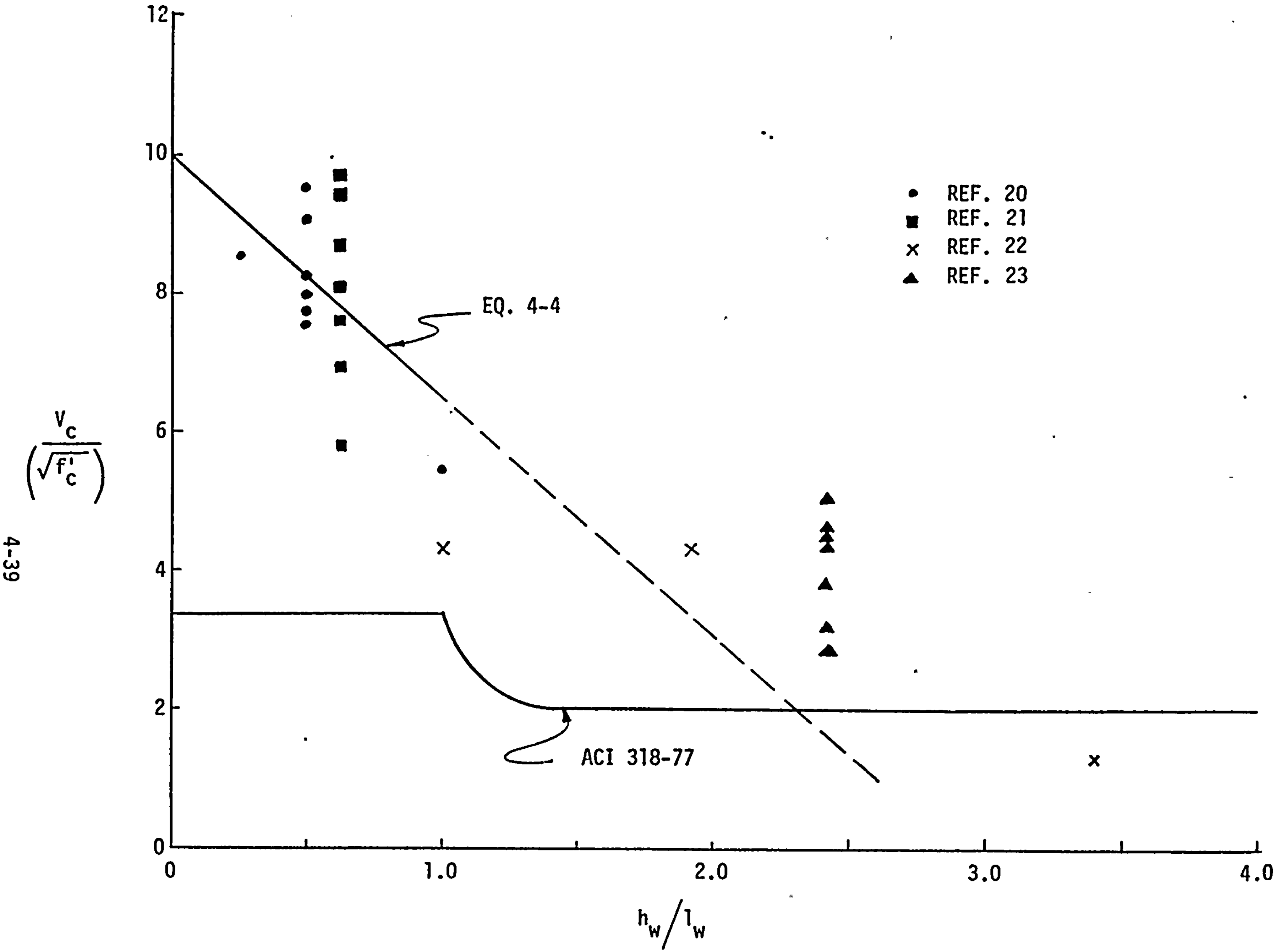

Figure 4-2. Strength of Concrete Shear Walls

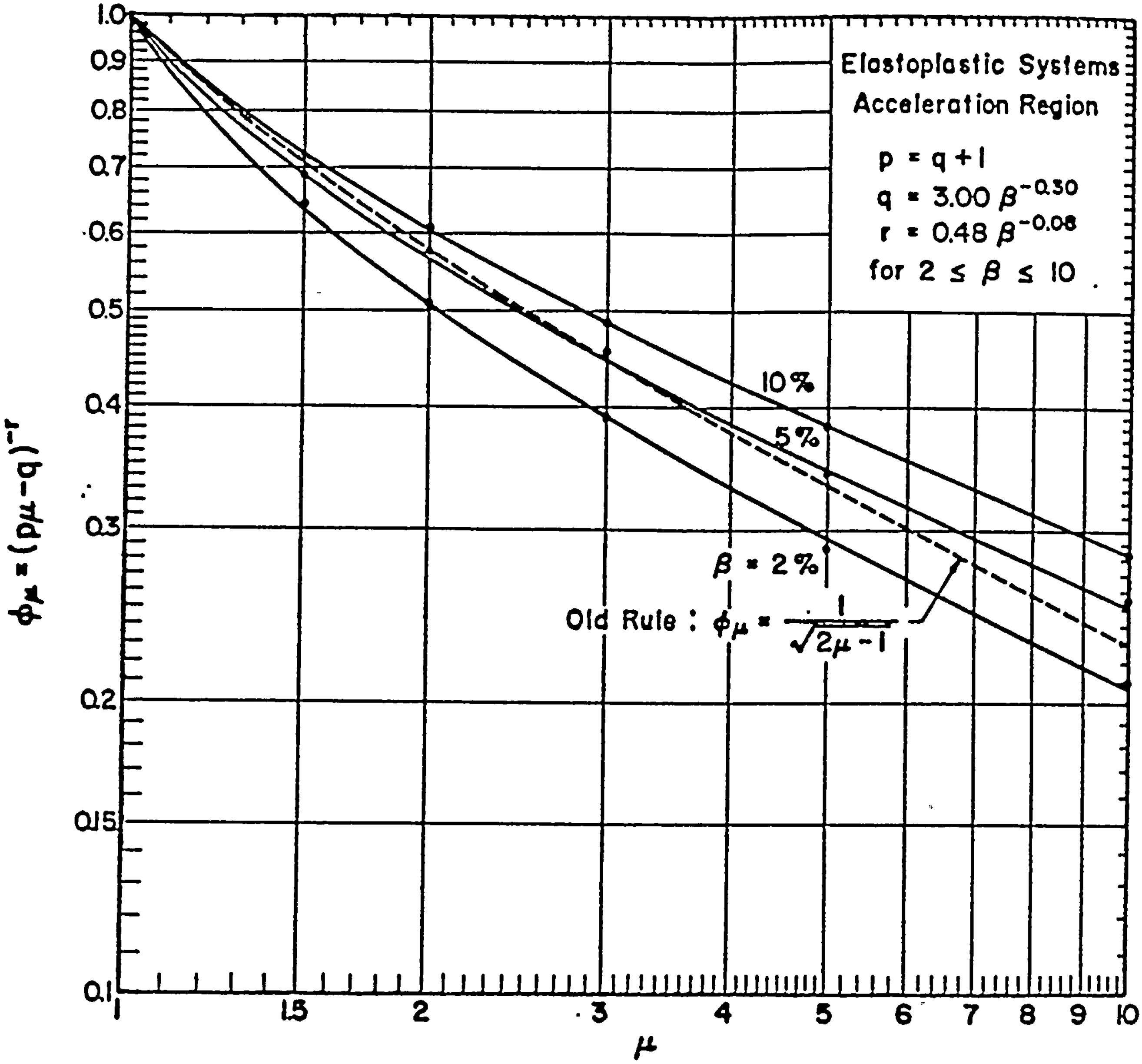

Figure 4-3. Deamplification Factors for Elastic-Perfectly Plastic Systems in the Acceleration Amplified Range (From Reference 9)

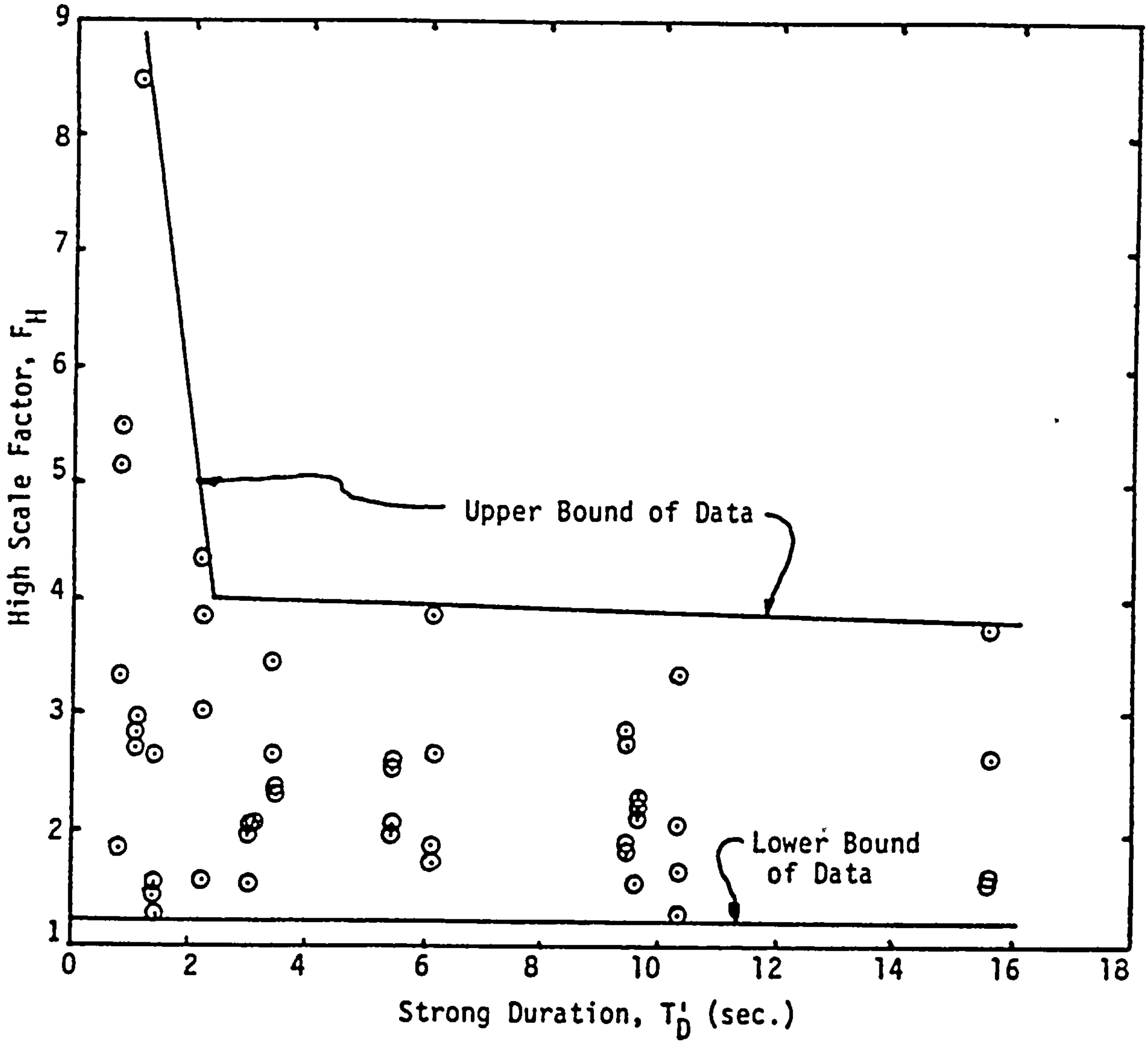

Figure 4-4. Scale Factor, F_H Versus Duration, T_D'
(From Reference 24)

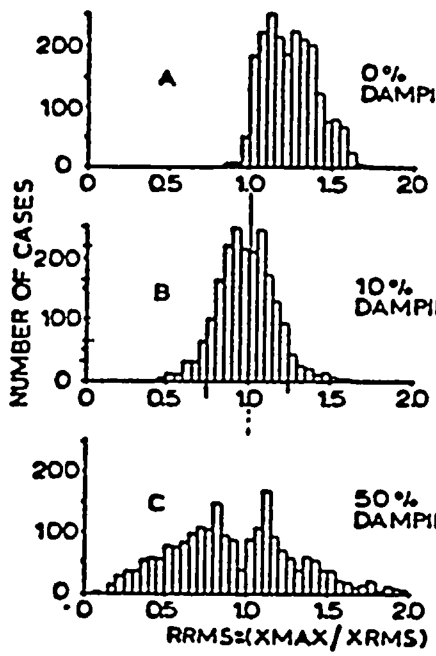

Figure 4-5. Histograms of Ratio of Peak Response to SRSS Computed Response for Four-Degree-of-Freedom Dynamic Models (From Reference 25)

5. EQUIPMENT FRAGILITY

This chapter describes the fragility development for seismically critical equipment within the Diablo Canyon Nuclear Power Plant. PG&E and Pickard, Lowe and Garrick have identified those equipment items which are essential to plant safety during and after a seismic event, and a fragility level and associated variabilities are determined for each of these components. Section 5.1 contains a general description of the equipment fragility methodology with a more in-depth treatment than was provided in Chapter 3.

5.1 Equipment Fragility Methodology

Fragility as used in probabilistic seismic safety studies is defined as a conditional probability of failure for a given hazard input. In this case, the fragility of a component or system is defined as the frequency of failure versus spectral ground acceleration. The development of these fragility descriptions combined with a discussion of the available information sources are the subject of this section.

5.1.1 Fragility Derivation

The procedure used in deriving fragility descriptions for equipment is similar to that used for structural fragility descriptions in that median factors of safety and their variability are first developed for equipment capacity and equipment response. These two factors, along with the median factor of safety on structural response, are then multiplied together to obtain an overall median factor of safety for the equipment item.

$$\check{F}_E = \check{F}_{EC} \cdot \check{F}_{ER} \cdot \check{F}_{SR} \tag{5-1}$$

[illegible]

[illegible]

$\check{F}_{EC}$ is the capacity factor of safety for the equipment relative to the floor acceleration used for design, $\check{F}_{ER}$ is the factor of safety inherent in the computation of equipment response, and $\check{F}_{SR}$ is the factor of safety in the structural response analysis that resulted in floor spectra for equipment design. Sections 5.1.1.1, 5.1.1.2, and 5.1.1.3 of this report contain a more thorough explanation of these three factors ($\check{F}_{EC}$, $\check{F}_{ER}$, and $\check{F}_{SR}$), respectively. The overall factor of safety, $\check{F}_E$, is then multiplied by the reference earthquake spectral ground acceleration to obtain fragility in terms of spectral ground acceleration.

$$\check{S}_A = \check{F}_E \cdot A_{Hos} \qquad (5\text{-}2)$$

where:

$\check{S}_A$ = Median spectral ground acceleration capacity

A_{Hos} = Spectral ground acceleration of the Hosgri earthquake for 5% damping in the 3 to 8-1/2 Hz range

Note that $\check{S}_A$ and F_E are random variables while A_{Hos} is a deterministic quantity. In most instances, Hosgri is used as the reference earthquake; however, the DE is used as a reference for those cases where the DE acceptance criteria governed the equipment design.

The logarithmic standard deviations, β_R and β_U, on the median acceleration capacity are obtained from the logarithmic standard deviations for each of the above factors based upon the lognormal model (Appendix A).

[illegible]

$$\beta_R = \left(\beta_{R_{EC}}{}^2 + \beta_{R_{ER}}{}^2 + \beta_{R_{SR}}{}^2\right)^{1/2}$$

$$\beta_U = \left(\beta_{U_{EC}}{}^2 + \beta_{U_{ER}}{}^2 + \beta_{U_{SR}}{}^2\right)^{1/2} \tag{5-3}$$

where βi_{EC}, βi_{ER}, and βi_{SR} are the randomness or uncertainty logarithmic standard deviations related to the parameters which make up the factors for equipment capacity, equipment response, and structural response, respectively.

5.1.1.1 Equipment Capacity Factor

The Equipment Capacity factor is defined as the failure threshold divided by the seismic design level. For the purposes of this study, the ultimate failure threshold is the acceleration level at which the component ceases to perform its intended function. This failure threshold could consist of a breaker tripping, excessive deflection of the control rod guide tubes or a support failure of a major vessel. Where several failure modes pertaining to the same component are found to have roughly the same capacity level, fragility descriptions for all significant failure modes are analyzed.

Like the structural seismic capacity factor, the median factor of safety related to equipment seismic capacity, $\check{F}_{EC}$, consists of two variables which are:

1. The Strength factor, F_S, computed as the ratio of the unused stress capacity to the stress level due to the designed for seismic event.

[illegible]

2. The Inelastic Energy Absorption factor, F_μ, related to the ductility of the system with which a given component is identified.

Therefore, in the identical form of Equation 4-2,

$$\check{F}_{EC} = \check{F}_S \cdot \check{F}_\mu \tag{5-4}$$

The logarithmic standard deviation on capacity can be derived by taking the SRSS of the logarithmic standard deviations on the Strength factor and the Ductility factor. The randomness and uncertainty portions of the variability can each be derived individually from Equation 5-5, by substituting the random or uncertainty β for the Strength factor and the Ductility factor (i.e., β_{S_R} for β_S and β_{μ_R} for β_μ, etc.).

$$\beta_{EC} = (\beta_S^2 + \beta_\mu^2)^{\frac{1}{2}} \tag{5-5}$$

5.1.1.1.1 Strength Factor

The Strength factor, F_S, is derived from the equation:

$$F_S = \frac{P_C - P_N}{P_{Hos}} \tag{5-6}$$

where P_C is the median limit state load or stress, P_N is the normal operating load or stress and P_{Hos} is the seismic load or stress. The normal and the seismic loads (P_N and P_{Hos}) are typically derived from the seismic qualification reports or other information sources described in Section 5.1.3. The calculation of the collapse or limit load, P_C, is a function of the failure mode for the specific equipment item. Equipment failures can be classified into three categories:

[illegible]

1. Elastic functional failures.
2. Brittle failures.
3. Ductile Failures.

Elastic functional failures involve the loss of intended function while the component is stressed below its yield point. Examples of this type of failure include:

1. Elastic buckling in tank walls and component supports.
2 Chatter and trip in electrical components.
3. Excessive blade deflection in fans.
4. Shaft seizure in pumps.

The limit state load for this type of a failure is defined as the load or stress level where functional failure occurs.

Brittle failures are defined in this study as those failure modes which have little or no system inelastic energy absorption capability. Examples of brittle type failures include:

1. Anchor bolt failures.
2. Component support weld failures.
3. Shear pin failures.

Each of these failure modes have the ability to absorb some inelastic energy on the component level, but the plastic zone is very localized and the system ductility for an anchor bolt or a support weld is very small. Thus, the collapse load for a brittle failure mode is defined as the median ultimate strength of the material. For example, consider a transformer structure where failure of the anchor bolts has been deter-

[illegible]

mined to be the critical failure mode. Under seismic loading, the massive transformer will typically be stressed well below its yield level while the bolts are being stressed well above the bolt yield level. The amount of system inelastic energy absorption provided by the bolts' plasticity is negligible when compared to the seismically-induced kinetic energy of the transformer structure, and thus, these bolts will fail in a brittle mode once the ultimate bolt strength is reached.

Ductile failures coincide much more closely with the structure failures which were described in Chapter 4. Ductile failure modes are those in which the structural system can absorb a significant amount of energy through inelastic deformation. Examples of ductile failure modes include:

1. Pressure boundary failure of piping
2. Structural failure of cable trays
3. Structural failure of ducting

The collapse load for ductile failure modes is defined as the <u>median</u> yield of strength of the material for tensile-type loading conditions. Therefore, a factor is applied to the code specified minimum yield strength value. Reference 28 gives the following to be appropriate median increase factors for typical materials used in power plant construction. More specific values can be used if supporting data are available.

[illegible]

MATERIAL	F
Carbon & Stainless Steel (Plate and Pipe)	1.25
Soft Bolts ($\sigma_U \approx 60$ ksi)	1.20
High Strength Bolts ($\sigma_U \geq 100$ ksi)	1.10

The code minimum value is typically taken to be a 95% confidence ($-1.65\beta_U$) lower bound value.

For bending-type failure modes, the collapse load is defined as the limit load or stress to develop a plastic hinge. Since failure does not occur when the outer fibre begins to yield, a section factor is applied to the capacity stress to represent the actual moment a member in bending can carry beyond the point of outer fibre yield. The median factor for rectangular and heavy wall pipe sections is taken to be 1.5 based upon the rules of the ASME Code. A section factor of 1.25 is estimated to represent a $-1.65\beta_U$ variation. Other cross sectional shapes have section factors defined in Appendix A of the ASME Code. For both tension and bending failures, the ductility factor quantifies the inherent safety factor above the collapse load to the failure threshold.

Each variable in Equations 5-6 has an associated lognormal probability distribution to express its combined randomness and uncertainty. To find the overall variance on the Strength factor, a technique commonly referred to as the "Second Moment Method" is utilized. The mean and variance of a function comprised of lognormally distributed variables

can be derived utilizing the moments (i.e., the mean and variances) of the logarithms of the distribution of each variable (Reference 29). The resulting equation for the logarithmic standard deviation on the Strength factor derived from Equation 5-6 is given below:

$$\beta_S = \left[P_C^2 \cdot \beta_C^2 + (P_N - P_C)^2 \cdot \beta_{Hos}^2 + P_N^2 \cdot \beta_N^2\right]^{1/2} \Big/ (P_C - P_N) \qquad (5\text{-}7)$$

where:

β_C = Logarithmic standard deviation on the collapse or limit load (stress).

β_{Hos} = Logarithmic standard deviation on the seismic load (stress).

β_N = Logarithmic standard deviation on the normal load (stress).

For components qualified by test, the test response spectrum generally envelopes the appropriate design floor spectrum by 10 percent or more depending upon the frequency. The qualification shake-table tests are intended to qualify the component both functionally and structurally for the specified seismic environment. Thus, significant functional or structural failures are not generally found during testing of the version of the item to be placed in the plant. As a result, the qualification tests do not constitute fragility tests and the component will generally function satisfactorily up to some acceleration above the qualification test level. For functional failures (i.e., relay chatter), the acceleration level corresponding to failure cannot be assumed to be significantly higher than the qualification acceleration and is usually set at 1.2 times the test level when no significant chatter is

[illegible]

noted during the test. For such failures, the test level is taken to be a 95% confidence (-1.65β) lower bound.

It should be noted that since fragility descriptions for tested equipment are conservatively based upon the qualification tests rather than an actual fragility test, tested equipment frequently show up in the risk analysis as important contributors to risk. More accurate fragility descriptions for tested equipment require the testing of such components to their malfunction level or specific structural analyses to determine structural capacity. During Phase IIIA, several electrical components shown to be significant contributors to risk in Phase II were reevaluated.

5.1.1.1.2 Inelastic Energy Absorption Factor

The inelastic energy absorption capability of an equipment component is quantified by the Inelastic Energy Absorption or Ductility factor, F_μ. Brittle failure modes and functional failure modes are considered to have a Ductility factor of 1.0, while ductile-type failure modes have values of F_μ which are a function of the deamplification in response due to inelastic behavior. Section 4.1.2 of this report describes the methodology utilized in deriving an appropriate Ductility factor for Diablo Canyon. The Ductility factor is based on the Riddell-Newmark methodology presented in Reference 8, updated to reflect the correlation between earthquake magnitude and system ductility. The median equipment Ductility factors and their variabilities are computed as a function of the component's natural frequency, and are summarized below:

a. For the amplified acceleration range of the appropriate floor spectra,

$$F_{\mu} = [(q+1)\cdot\mu^{*}-q]^{r} \qquad (5\text{-}8)$$

where

q = 3.0xj

r = 0.48xj

j = Percent of critical damping at failure.

μ^* = Effective ductility ratio

= $1.0 + C_D\,(\mu - 1.0)$

C_D = Factor accounting for the earthquake duration; For Diablo Canyon equipment, this factor equals 1.0, corresponding to moment resisting frames.

b. For the rigid (unamplified) range of the floor spectra,

$$F_{\mu} = \mu^{*0.13} \qquad (5\text{-}9)$$

where μ^* is as previously defined.

c. For the amplified acceleration range < f < rigid range of the floor spectra,

A log-log interpolation is applicable for ductile equipment with natural frequencies in this range. A point at the highest frequency of the smoothed and broadened amplified acceleration region should be plotted using F_{μ} from Equation

[illegible]

5-8 and another point should be plotted at the lowest unamplified (rigid) frequency for the floor spectrum using Equation 5-9. A line drawn between these two points on log-log graph paper will uniquely determine the Ductility factors in this frequency range.

The ductility ratio, μ, itself is based upon the recommendations given in Reference 8. This reference gives a range of ductility values to be used for design. The upper end of this range is considered to be a median value. Engineering judgment is utilized to match the applicable category from Reference 8 to a particular failure mode for the equipment component. Although the element ductility of a component, particularly those constructed of carbon or stainless steel, may be high (i.e., 10 to 20), the overall system ductility, μ, used in determining F_μ is generally substantially less.

The variabilities for the median Ductility factor derivations are evaluated by estimating a 1% probability (-2.33β) that the actual Ductility factor is less than 1.0. Thus, the following equations determine the composite variability, randomness and uncertainty, respectively.

$$\left.\begin{aligned} \beta_{\mu_C} &= \frac{1}{2.33} \ln (F_\mu) \\ \beta_{\mu_R} &= 0.8\, \beta_{\mu_C} \\ \beta_{\mu_U} &= 0.6\, \beta_{\mu_C} \end{aligned}\right\} \qquad (5\text{-}10)$$

5.1.1.2 Equipment Response Factor

Similar to that for equipment capacity, the median factor of safety related to equipment response, $\check{F}_{ER}$, is determined from an evaluation of a number of variables. However, the evaluation of each variable is dependent upon whether the equipment item was qualified for the seismic event by static or dynamic analysis or by dynamic testing. The various factors which make up the equipment response factor include:

1. The Qualification Method factor, F_{QM}, comparing the accelerations used in the design analysis or qualification test to the actual design floor response spectrum for the reference event.

2. The Spectral Shape factor, F_{SS}, evaluating the conservatism in the smoothing and broadening of the raw floor spectra and the conservatism or unconservatism in the time-history generation of the floor spectra.

3. The Damping factor, F_D, comparing the design equipment damping with the level of damping expected at or near failure of the equipment component.

4. The Modeling factor, F_M, assessing the uncertainty relative to the ability of the mathematical model to accurately determine the actual fundamental frequencies of the equipment modeled or the uncertainty related to the dynamic test boundary conditions.

5. The Mode Combination factor, F_{MC}, assessing the conservatism or unconservatism in the mode combination methodology used in

[illegible]

the design process or the ability of the test methodology to simultaneously excite all modes of a component qualified by test.

6. The Earthquake Component Combination factor, F_{ECC}, evaluating the conservatism or unconservatism in the method used to combine the responses from the various earthquake component directions during the design analysis or the unconservatism in the use of uniaxial or biaxial tests to duplicate actual earthquake response.

The median equipment response factor, $\check{F}_{ER}$, then becomes:

$$\check{F}_{ER} = \check{F}_{QM} \cdot \check{F}_{SS} \cdot \check{F}_{D} \cdot \check{F}_{M} \cdot \check{F}_{MC} \cdot \check{F}_{ECC} \qquad (5\text{-}11)$$

5.1.1.2.1 Equipment Qualification Method Factor

The Qualification Method factor is a measure of the conservatism or unconservatism involved in the seismic qualification method used to seismically qualify a component. There are three seismic qualification methods which are typically used for nuclear plant equipment:

1. Static Analysis
2. Dynamic Analysis
3. Testing

5.1.1.2.1.1 Static Analysis

The static coefficient method is intended to be a conservative upper bound method by which simple components may be qualified. Typically, the peak spectral acceleration is multiplied by a coefficient (i.e., 1.0

to 1.5) to account for multiple modes and this product is multiplied by the weight of the component to determine an equivalent static load to be applied at the subsystem center of gravity. If the component is comprised of more than one lumped mass, the same procedure may be applied at each lumped mass point in the static model or may be applied as a uniformly distributed load on the static model.

If the component is rigid (i.e., its fundamental frequency is above the frequency where the response spectrum returns to the zero period acceleration), the degree of conservatism in the response level used for design is the ratio of the specified static coefficient divided by the zero period acceleration of the floor level where the equipment is mounted. For such items, the variabilities due to spectral shape, combination of modal responses, damping, and for the most part, modeling errors are eliminated.

If the equipment is flexible and responds predominantly in one mode, the degree of conservatism is the ratio of the static coefficient to the spectral acceleration at the equipment fundamental frequency. In contrast, if the flexible component is judged to exhibit several dynamic modes, the response may be estimated on a mode-by-mode basis by estimating the frequencies and participation factors for each mode. The Qualification Method factor is then the ratio of the static coefficient response to the estimated dynamic response. The dynamic characteristic factors which could be eliminated for rigid components must be considered for flexible equipment.

5.1.1.2.1.2 Dynamic Analysis

Response spectrum, mode superposition time-history, and direct integration time-history dynamic analysis methods may be applied in subsystem

response analyses. Results from the response spectrum dynamic analysis method are judged to be median-centered. Similarly, the mode superposition time-history method or the direct integration time-history method are expected to give results which are median-centered assuming that the response spectrum and time-history inputs are compatible.

The response spectrum method was extensively used for dynamic analysis of components and systems within the Diablo Canyon Plant. If the applicable Diablo Canyon floor response spectra were utilized in the design analysis, the qualification method factor, F_{QM}, is equal to unity and the uncertainty variability is zero. If conservative generic spectra or envelope spectra were used to seismically qualify a component, F_{QM} is the ratio of the spectral acceleration from the generic spectrum divided by the spectral acceleration from the Diablo Canyon Hosgri event design floor spectrum evaluated at the components' fundamental frequency or frequencies on a mode-by-mode basis.

For components qualified by analysis, the Qualification Method factor is computed, as described above, for each of the earthquake components (both orthogonal horizontal directions and the vertical direction) with the final value of F_{QM} being an appropriately weighted average based upon the importance of each earthquake direction in contributing to the overall response of the component.

5.1.1.2.1.3 Testing

In vibration testing, the test response spectrum generally envelopes the required response spectrum by approximately ten percent or more depending on the frequency range. If the test response spectra are available within the test report, the overtest safety factor is accounted for in the Strength factor. The Qualification Method factor, F_{QM}, and varia-

[illegible]

bility, β_{QM}, will therefore be unity and zero, respectively. If the component is qualified by testing and the actual test response spectra are not available, F_{QM} and β_{QM} must be estimated, assuming a modest amount of overtest and quantifying the variability in the assumption.

5.1.1.2.2 Equipment Spectral Shape Factor

Floor response spectra for Diablo Canyon were computed by means of a simplified time-history seismic analysis of the structure. The overall dynamic response of each of the critical buildings was modeled by lumping the mass of the structure and the rigidly attached components at each floor level. The conservatism or unconservatism involved in developing the design floor response spectra from the ground response spectra is quantified by means of the equipment Spectral Shape factor. The conservatism or unconservatism involved in using the specified Diablo Canyon design ground response spectrum in lieu of a median site-specific spectrum is quantified in development of the Spectral Shape factor associated with structural response.

The response spectrum method for equipment dynamic analysis is often referred to as being conservative; however, the conservatism compared to a time-history analysis is primarily due to the method used in developing the design floor spectrum. Spectra used for design purposes are usually smoothed and the peaks are broadened such that the resulting design spectrum is conservative. In addition, conservatism is generally introduced in the development of the artificial time-history used to create the floor response spectra. The combined effect of these two conservatisms make up the equipment Spectral Shape factor.

[illegible]

5.1.1.2.2.1 Peak Broadening and Smoothing

The effect of smoothing and peak broadening varies with structure, elevation, frequency and damping. For any particular frequency, this peak broadening and smoothing safety factor can be computed as:

$$F_{SS_1} = \frac{S_a \text{ (broadened and smoothed)}}{S_a \text{(unbroadened and unsmoothed)}} \tag{5-12}$$

where

F_{SS_1} = Spectral Shape factor due to peak broadening and smoothing evaluated at the equipment frequency and design damping

S_a = Spectral acceleration value

The variability in this factor is a function of how well the equipment frequency can be defined. If the frequency can only be defined within a certain range, then the variability is established by calculating the range of F_{SS1} values for the frequency range. Since the variability, β_{SS}, is due to the uncertainty in the frequency, it is considered to be all uncertainty.

For the Diablo Canyon plant, both smoothed and broadened design floor spectra and raw (unsmoothed and unbroadened) spectra were available having been generated from the time history analysis of the various structures. Therefore the effects of smoothing and broadening could be accurately determined for each equipment component evaluated based upon its fundamental mode frequency.

[illegible]

5.1.1.2.2.2 Artificial Time-History Generation

Studies have been conducted which show that conservatism is involved in the current practice of generating floor spectra in structures using artificial time-histories. These artificial time-histories result in response spectra that conservatively envelope the applicable ground spectra. For instance, Reference 31 indicates that the average U.S. industry-generated artificial time-history tends to introduce about 10 percent conservatism except at high frequencies for which the conservatism is about 20 percent at 33 Hz.

Comparisons made between the 5% and 7% damped Diablo Canyon design ground response spectra and the response spectra generated from the synthetic Hosgri earthquake time-history used to compute in-structure floor spectra indicate that the factor of conservatism due to the artificial earthquake time-history generation factor, F_{SS_2} obtained directly from such a comparison at the building fundamental frequencies is approximately unity.

The overall spectral shape factor, applicable to equipment qualified by either analysis or tests, is generated by taking the product of the peak broadening and smoothing factor times the artificial time-history factor.

$$F_{SS} = F_{SS_1} \cdot F_{SS_2} = F_{SS_1} \qquad (5\text{-}13)$$

5.1.1.2.3 Damping Factor

The basis for the damping factor has been addressed in Section 3.3.2 of this report in the discussion on system damping. Table 5-1 shows the

[illegible]

[illegible]

[illegible]

damping values used for the Hosgri evaluation analysis of various types of equipment associated with the Diablo Canyon Non-NSSS and NSSS Systems. Median damping values and their variabilities are a function of the material, construction details, size and stress level. Reference 31 suggests that median damping for equipment at the SSE level for U.S. plants is about five percent. Thus, for single-degree-of-freedom systems, the damping factor for equipment is:

$$F_D = Sa_{DD}/Sa_{DM} \qquad (5\text{-}14)$$

where

Sa_{DD} = Spectral acceleration from the design floor spectra evaluated at the equipment fundamental frequency using design analysis damping.

Sa_{DM} = Spectral acceleration from the design floor spectra evaluated at the equipment fundamental frequency using the expected median damping.

For multi-degree-of-freedom systems, Equation 5-14 can be altered to reflect the summation of the spectral accelerations at each frequency multiplied by their associated mass participation factors.

There is uncertainty variability in the median damping value and the associated response that must be considered. It is indicated within Reference 31 that for a median damping value of 5 percent, the minus one logarithmic standard deviation value is about 3.5 percent. The uncertainty in damping results in a logarithmic standard deviation on response equal to:

[illegible]
[illegible]
[illegible]

[illegible]
[illegible]
[illegible]
[illegible]
[illegible]
[illegible]

[illegible]
[illegible]
[illegible]
[illegible]
[illegible]
[illegible]
[illegible]

$$\beta_{D_U} = \ell n\left(\frac{S_{a_{\zeta = 3.5\%}}}{S_{a_{\zeta = 5.0\%}}}\right) \tag{5-15}$$

where $Sa_{\zeta=5.0\%}$ is the 5 percent damped spectral acceleration and $Sa_{\zeta=3.5\%}$ is the 3.5 percent damped spectral acceleration taken at the equipment fundamental frequency using the applicable floor response spectra. The resulting logarithmic standard deviation on the damping response factor, from Equation 5-15 above, is considered to be all uncertainty.

For components qualified by test, the damping level achieved during the test is by definition, the median value. Even though the actual test damping level is unknown, the Qualification Method factor for tested equipment is based upon a comparison of the Test Response Spectra (TRS) and the design floor spectra at like values of damping. Therefore, F_D for tested components is unity and the randomness and uncertainty variabilities are zero.

5.1.1.2.4 Modeling Factor (Analysis) and Boundary Conditions Factor (Testing)

In any dynamic analysis, there is uncertainty in the computed response due to assumptions made in modeling the component, modeling boundary conditions, and representing material behavior. Modeling of complex systems is usually conducted using nominal dimensions, weights, and material properties and is done in such a manner that further refinement of mesh size in a finite element representation will not significantly alter the calculated response. Representation of boundary conditions in a model may have a significant influence on the response. The misrepresentation of boundary conditions in the dynamic model by assuming great-

[illegible]

er or lesser stiffness or treating nonlinear gap effects linearly cannot be quantified generically and each model must be treated specifically to determine a response factor for modeling. If it is judged that the analyst has done his best job of modeling, modeling accuracy is considered to be median-centered (i.e., $F_M = 1.0$) with the variability in each of the modeling parameters amounting to variability in calculated mode shapes and frequencies. The error in calculation of mode shapes and frequencies then has an effect on the computed response.

For Diablo Canyon, the actual modeling variability is based upon an assumed variation on the fundamental frequency computed in the design analysis or dynamic test. The frequency variation is represented by a β ranging from 0.085 to 0.020 depending upon the qualification boundary conditions. Similarly, there is uncertainty with regard to the actual structural frequency determined during the finite element analysis of the various structures. The variation on structure frequency is represented by a β ranging from 0.05 to 0.25 depending upon the failure mode of interest (i.e., diaphragm mode, concrete shear wall mode, etc.). In assessing the overall variability on response due to uncertainty in the equipment and structural frequency, the corresponding values of β_u on frequency are combined by SRSS to determine the frequency range of interest. The variation in response which could occur in that frequency range is taken to represent $\pm 1\beta$ variation. The variability on response in the range of frequency variation is taken to be all uncertainty.

The boundary conditions utilized in equipment seismic testing can be a significant source of variability that depends almost solely upon the diligence of the test laboratory and the qualification review organization. In general, a component that is bolted to the floor in a nuclear power plant and which is similarly bolted to a shake table for qualification testing, will exhibit little variability in the response factor

accounting for boundary conditions. Carelessness on the part of the various organizations involved in design, fabrication, testing and installation can result in a significant variability. For instance, the lack of a specified bolt torque at the mounting interface can result in a difference between the testing and installation condition which could have a pronounced impact on the response factor. Where the component is bolted to the test fixture during test and welded to embeddments on installation, the uncertainty on frequency is judged to be low.

The variability of the subsystem response due to test boundary conditions comes primarily from differences in mode shape and frequency shift. The variability of mode shape, frequency, and resulting response due to boundary conditions varies considerably for different generic types of equipment. For a large majority of tests conducted by reputable testing laboratories, the boundary condition factor is judged to be 1.0. Engineering judgment must be utilized in calculating boundary condition factors for those cases where the component to test table attachment mechanism is not representative of the actual in-plant condition. The variability is all uncertainty and can be derived from the variability in spectral accelerations obtained from estimating confidence bounds on the equipment frequency. The boundary condition uncertainty is generally estimated to be about 0.11 based on values derived in the SSMRP study (Reference 31).

5.1.1.2.5 Mode Combination Factor (Analysis) and Spectral Test Method Factor (Testing)

The modal combination technique utilized for most current seismic design analyses is the square-root-of-the-sum-of-the-squares (SRSS) methodology. For some equipment such as piping, the 10% grouping method is used to account for closely-spaced modes. The SRSS method is considered

median-centered. The response factor for the combination of modes is taken to be 1.0 for such analyses. The variability associated with mode combination depends upon the complexity of the model. For multi-degree-of-freedom systems, Reference 31 recommends that the coefficient of variation (COV) due to mode combination be taken to be approximately 0.15. For single-degree-of-freedom systems, the COV is by definition, zero. The variability due to mode combination is considered to be all randomness due to the random phasing of modes.

Synthesized time-histories are generally developed directly from the Required Response Spectrum at most testing laboratories. A much better approach, as recommended in Reference 32, is to synthesize a time-history that corresponds to a power spectral density which closely envelopes the RRS rather than make the direct step from the RRS to the synthesized time-history. This approach tends to smooth out the input time-history, resulting in less chance for an equipment mode to coincide with a significant peak or valley. Reference 31 recommends a Spectral Test Method factor of unity with a total variability of 0.20. The variability is all uncertainty since the use of more accurate techniques could eliminate most of the uncertainty.

For tested equipment which exhibit only one dynamic fundamental frequency, a series of single frequency sine beat tests is generally considered adequate to excite the dynamic modes of the component to the level of the Required Response Spectrum (RRS). However, such tests may be unconservative for flexible equipment with multiple dynamic modes since the modes are not simultaneously excited to the required levels. The value of F_{MC} is evaluated on a case-by-case basis considering an estimate of the participation factor for each mode.

[illegible]

5.1.1.2.6 Earthquake Component Combination Factor (Analysis) and Multi-Directional Effects Factor (Testing)

Two methods of combining earthquake components have been determined to provide approximate median-centered results. The first method is the square-root-of-the-sum-of-the-squares (SRSS) and the second method is the 100%, 40%, 40% method contained in Reference 13. Reference 13 recommends that the response be represented by combining the worst case horizontal response with 40 percent of the orthogonal horizontal response and 40 percent of the vertical response. The SRSS method must be applied to the end item of interest, while the 100%, 40%, 40% method can be applied at the input seismic load stage or at the response stage with equivalent results. For this reason, the 100%, 40%, 40% methodology is convenient when the responses from the three earthquake component directions are not separately available. In the Diablo Canyon equipment design analyses, earthquake components were generally combined by the absolute sum of the worst horizontal plus the vertical method. For this combination method, the magnitude of the Earthquake Component Combination factor, F_{ECC}, depends on the orientation, failure mode, and response characteristics of the equipment component under consideration.

A generic study was conducted to develop earthquake component combination response factors and their variabilities for common two- and three-dimensional equipment idealizations. The amount of conservatism or unconservatism and the associated variability on this factor are generally a function of the following:

1. The number and direction of earthquake components which affect the failure mode under consideration (e.g., piping failures can be influenced by all three directional responses, but a particular relay might fail due to a partic-

[illegible]

ular horizontal seismic excitation while remaining unaffected by the vertical and the other horizontal directions).

2. The amount of coupling that exists between directional response (i.e, does an x direction excitation cause a response in the y and z directions).

3. The relative magnitude of the response quantity attributed to each of the earthquake component directions.

The variability involved in the phasing of the three earthquake directional components is considered to be all randomness, while the variability due to the degree of coupling involved between directions is considered to be all uncertainty. Table 5-2 presents the earthquake component combination response factors for the worst horizontal plus vertical method which is most commonly applicable for Diablo Canyon equipment.

The Multi-Directional Effects factor is a measure of the conservatism or unconservatism and corresponding variability involved in testing the three different earthquake directional components. Triaxial, biaxial and uniaxial tests are the types of dynamic tests which are usually conducted. A triaxial test is by definition, median-centered for all failure modes.

Biaxial qualification tests are conducted by exciting the equipment in one horizontal direction at a time along with the vertical direction, using randomly phased input time-histories. Biaxial testing is conducted for most equipment qualified for nuclear service. A biaxial test is judged to be median-centered for certain functional failures such as relay chatter in an electrical cabinet but can be somewhat unconserva-

[illegible]

tive for structural failures where either the two horizontal directions or all three direction components contribute significantly to the failure response. The degree of unconservatism associated with biaxial testing can be defined as the median response vector for biaxial testing divided by the median three-axis response. The Multi-Directional Effects factor and its associated variabilities for random vibration biaxial testing are:

Functional Failure	Structural Failure
$F_{MDE} = 1.00$	$F_{MDE} = 0.814$
$\beta_R = 0.00$	$\beta_R = 0.00$
$\beta_U = 0.00$	$\beta_U = 0.07$

Uniaxial qualification tests, on the other hand, are conducted by testing each of the three directions independently. A uniaxial test is, in general, unconservative for all failure modes in that coupling and phasing between the three-directional earthquake components is not accounted for. The degree of unconservatism associated with uniaxial testing can be defined as the median response vector for uniaxial testing divided by the median three-axis response. Thus the Multi-Directional Effects factor and its associated variabilities for uniaxial testing are:

Functional Failure	Structural Failure
$F_{MDE} = 0.819$	$F_{MDE} = 0.686$
$\beta_R = 0.00$	$\beta_R = 0.00$
$\beta_U = 0.09$	$\beta_U = 0.11$

[illegible]

[illegible]

[illegible]

As with F_{ECC} for components qualified by analysis, the variability due to phasing is a function of the earthquake and thus, is all randomness while the variability due to coupling and relative response magnitude is all uncertainty.

5.1.1.3 Structural Response Factors

The Structural Response factor, $\check{F}_{SR}$, for equipment evaluates the effect of the conservatism or unconservatism of the structural analysis on the actual equipment response. Structural response factors as they relate to structural capacity for the safety-related structures are described in Section 4.8 of this report. The variables pertinent to the structural response analyses used to generate floor spectra for equipment design are the only variables of interest relative to equipment fragility. The applicable variables for equipment from those analyses are:

1. Spectral shape
2. Damping
3. Modeling (mode shape)
4. Soil-Structure Interaction
5. Inelastic Response
6. Ratio of vertical to horizontal excitation

It should be noted that the combination of earthquake components is not included in structural response since that variable is addressed for specific equipment orientation in the treatment of equipment response. Several of these response factors have different median values and variabilities depending upon whether the structure is responding elastically or is approaching its yield capacity at the point defining equipment failure. Therefore, it is important to know the relationship between the failure capacity of a particular equipment item and the yield capacity of the structure in which it is located.

[illegible]

Reference 10 recommends the use of 5% damping to characterize the response of reinforced concrete structures at the one-half yield condition and 10% damping to characterize the response of such structures at or just below the yield condition. The higher level of damping is generally considered appropriate when the load level in the structure or structural element is greater than or equal to the three-quarter yield condition.

Although the vast majority of equipment used in nuclear power plants are acceleration sensitive, there are cases where equipment is displacement sensitive. An example is that of interconnecting piping systems which run between separate structures or enter a structure from an underground pipe channel. In such cases, the inelastic response of the structure may place greater loads on the piping system. Such systems for Diablo Canyon have been designed with sufficient flexibility between fixed anchors or between fixed anchors and rigid supports to accommodate differential building motion.

Although acceleration response in the amplified region near the peak of the floor response spectra tends to deamplify as the structure goes inelastic, this is not necessarily the case in the higher frequency ranges. Inelastic response above the peak frequency range is highly structure and earthquake ground motion frequency content dependent and may be either higher or lower than that predicted by the elastic model. To account for the possibility that the actual high frequency inelastic response is higher or lower than the elastic response, randomness and uncertainty variabilities of 0.17 and 0.10, respectively, are recommended based upon limited data.

During the design analysis, certain assumptions are made regarding the relative magnitudes of the horizontal and vertical components of earthquake. Reference 1 specifies that for Diablo Canyon, the vertical component is assumed to be equal to two-thirds of the horizontal component. In real earthquakes, the ratio of vertical to horizontal peak ground motion may vary. Therefore, an assessment is made of the conservatism or unconservatism in this design assumption and its randomness variability. The effect of this assumption on $F_{V/H}$ and β_R is weighted by the relative importance of the vertical earthquake on the overall response. Generally, the ratio of peak vertical ground motion acceleration to peak horizontal ground motion acceleration used for design is judged to be median-centered when based on sound geotechnical studies. For equipment qualified by analysis or tests

$$F_{V/H} = 1.00$$

$$\beta_{U_{V/H}} = 0.0 \text{ (Unless component frequencies are unknown)}$$

$$\beta_{R_{V/H}} = \left[\frac{1}{-2.0} \ln \; Rv_D/Rv_{MX}\right] C_I \quad (0.40_I \text{ for Diablo Canyon}) \qquad (5\text{-}16)$$

where

Rv_D = Ratio of vertical acceleration, A_V, to horizontal acceleration A_H, used for design (taken as 0.67 for Diablo Canyon).

Rv_{MX} = Maximum probable ratio of A_V/A_H (taken as 1.5 for Diablo Canyon).

[illegible]

[illegible]

C_I = Coefficient reflecting the importance of the vertical earthquake component to overall equipment response.

It should be noted that the structural response factors associated with the behavior of the building are not appropriate for equipment located at the basemat. In such cases, only the Spectral Shape, Soil-Structure Interaction, and vertical to horizontal seismicity factors should be included and the Spectral Shape factor must be recomputed at the equipment fundamental frequency. Since the Structural Response factor is frequently computed for structural elements located well up in the structure, it is considered reasonable to interpolate between this value and a value computed for the basemat for equipment located low in the structure but above the basemat.. It should also be noted that the Soil-Structure Interaction factor is only appropriate for failure modes driven by the horizontal earthquake components and should not be included for failure modes resulting from the vertical component of earthquake.

5.1.2 Information Sources

Several sources of information are utilized in a PRA from which plant-specific and generic fragilities for equipment are developed. These sources include:

1. Seismic Qualification Design Reports
2. Seismic Qualification Test Reports
3. Final Safety Analysis Report (FSAR)
4. Seismic Qualification Review Team (SQRT) Submittals
5. Past Earthquake Experience
6. United States Corps of Engineers Shock Test Reports
7. Specifications for the Seismic Design of Equipment

The first four of these information sources are termed "plant-specific" since they pertain to specific equipment within the plant. The remaining three information sources are termed "generic" since they constitute data generated for similar types of equipment or are definitions of design requirements, in lieu of actual design results. Plant-specific sources are preferred since they have been generated for the specific items in question and their uncertainty level is reduced from those of the generic sources.

Depending upon the uniqueness of the equipment, the failure mode, the inelastic energy absorption capability of the equipment, and its dynamic characteristics, either a plant-specific or a generic derivation of the fragility description may be appropriate. The factors of safety relative to the Hosgri Earthquake are widely variable. In general, flexible equipment such as piping, which possess the ability to undergo large inelastic deformation, will have a factor of safety against failure of many times the Hosgri Earthquake even if stressed to the maximum code allowable stress. Such equipment is a prime candidate for a generic derivation of fragility. The increased uncertainty inherent in a generic derivation does not have much influence on the outcome of the seismic risk analysis if large safety factors can be demonstrated. On the other hand, if rigid equipment with relatively brittle failure modes are stressed to code allowable for the Hosgri Earthquake, the factor of safety against failure may be considerably smaller and a generic treatment may result in unsatisfactory risk predictions. Fortunately, plant-specific analyses have shown that most rigid equipment have stresses well below the allowable and large safety factors are present.

Table 5-1. Comparison of Damping Values for Equipment

EQUIPMENT TYPE	DAMPING (% OF CRITICAL)		
	DDE (REF. 1,2)	HOSGRI (REF. 1,2)	FRAGILITY (REF. 8,11,12)
REACTOR COOLANT LOOP	1.0	4.0	5.0
MECHANICAL COMPONENTS	2.0	4.0	5.0
VITAL PIPING (≤ 12")	0.5	2.0	5.0
(> 12")	0.5	3.0	5.0
CABLE TRAYS	7.0	7.0 - 15.0	7.0 - 15.0

[illegible] [illegible]

[illegible]

[illegible]

[illegible]

[illegible]

[illegible]

[illegible] [illegible]

Table 5-2. Earthquake Component Combination Factors (H_{MAX} + V)

CASE	DESCRIPTION	F_{ECC}^{V}	β_R	β_U
1	3D Case - All 3 directional components contribute to failure	0.96	0.12	0.10
2	2D Case - Median Coupling - Both horizontal contribute to failure	0.87	0.10	0.10
3	2D Case - No Coupling - Both horizontals contribute to failure	0.71	0.06	0.00
4	2D Case - Median Coupling - 1 horizontal and the vertical contribute to failure	1.07	0.09	0.05
5	2D Case - No Coupling - 1 horizontal and vertical contribute to failure	1.00	0.03	0.00
6	1D Case - Any one of the directional components alone is responsible for the failure	1.00	0.0	0.00
7	Systems of components for which any of the above cases could apply (piping, cable trays, ducting, etc.)	0.96	0.12	0.09

[illegible]

REFERENCES

1. Pacific Gas and Electric Company, "Final Safety Analysis Report," PG and E, San Francisco, California (1974).

2. Pacific Gas and Electric Company, et al, "Seismic Evaluation for Postulated 7.5M Hosgri Earthquake," PG and E, San Francisco, California (November 1977 with amendments).

3. Freudenthal, A.M., J.M. Garrelts, and M. Shinozuka, "The Analysis of Structural Safety," Journal of the Structural Division, ASCE, ST 1, pp. 267-325, February 1966.

4. Kennedy, R.P., A Statistical Analysis of the Shear Strength of Reinforced Concrete Beams, Technical Report No. 78, Department of Civil Engineering, Stanford University, Stanford, California, April 1967.

5. Newmark, N.M., "A Study of Vertical and Horizontal Earthquake Spectra," WASH 1255, Nathan M. Newmark Consulting Engineering Services, prepared for USAEC, April 1973.

6. ACI Committee 318, "Building Code Requirements for Reinforced Concrete (ACI 318-63)," American Concrete Institute, Detroit, Michigan (1963).

7. "Manual of Steel Construction," 7th Edition, American Institute of Steel Construction, Chicago, Illinois (1970).

8. Newmark, N.M., "Inelastic Design of Nuclear Reactor Structures and Its Implications on Design of Critical Equipment," SMiRT Paper K 4/1, 1977 SMiRT Conference, San Francisco, California.

9. Riddell, R., and N.M. Newmark, "Statistical Analysis of the Response of Nonlinear Systems Subjected to Earthquakes," Department of Civil Engineering, Report UILU 79-2016, Urbana, Illinois, August 1979.

10. USNRC, "Damping Values for Seismic Design of Nuclear Power Plants," USNRC Regulatory Guide 1.61, October 1973.

11. Newmark, N.M., and W.J. Hall, "Development of Criteria for Seismic Review of Selected Nuclear Power Plants," NUREG/CR-0098, May 1978.

12. Kennedy, R.P., et al, "Probabilistic Seismic Safety Study of an Existing Nuclear Power Plant," Nuclear Engineering and Design, Vol. 59, No. 2, pp. 315-338.

13. Benjamin, J. and J. Reed, "Recommended Evaluation Criteria for Diablo Canyon Nuclear Power Plant Auxiliary Building Walls and Diaphragms", February 11, 1983.

14. Kennedy, R.P. etal, "Engineering Characterization of Ground Motion" NUREG/CR-3805, Vol. 2 and Vol. 5, March 1985.

15. ACI 318-71, "Building Code Requirements for Reinforced Concrete", American Concrete Institute, 1971.

16. Troxell, G.E., and H.E. Davids and J.W. Kelly, Composition and Properties of Concrete, McGraw-Hill, 1968.

17. Pacific Gas and Electric Company Design Criteria Memorandum No. C-65, dated April 15, 1983.

18. Material Test Data of Intake Structure, QA Document No. 34001.01 M-223A.

19. Mirza, S.A., Hatzinikolas, M., and J.G. MacGregor, "Variability of Mechanical Properties of Reinforcing Bars", Journal of Structural Division, ASCE, May, 1979.

20. Barda, F., Hanson, J.M., and W.G. Corley, "Shear Strength of Low-Rise Walls with Boundary Elements', ACI Symposium, "Reinforced Concrete Structures in Seismic Zones", ACI, Detroit, Michigan, 1976.

21. Shiga, T., Shibata, A., and J. Tabahashi, "Experimental Study on Dynamic Properties of Reinforced Concrete Shear Walls", 5th World Conference on Earthquake Engineer, Rome, Italy, 1973.

22. Cardenas, A.E., et al, "Design Provisions for Shear Walls", ACI Journal, Vol. 70, No. 3, March, 1973.

23. Oesterle, R.G., et al, "Earthquake Resistant Structural Walls - Tests of Isolated Walls - Phase II", Construction Technology Laboratories (Division of PCA), Skokie, Illinois, October, 1979.

24. Kennedy, R.P., et al, "Engineering Characterization of Ground Motion Effects of Characteristics of Free-Field Motion on Structural Response", SMA 12702.01, prepared for Woodward-Clyde Consultants, April, 1983.

[illegible]

25. Merchant, H.C., and T.C. Golden, "Investigations of Bounds for the Maximum Response of Earthquake Excited Systems", Bulletin of the Seismological Society of America, Vol. 64, No. 4, pp. 1239-1244, August, 1974.

26. Ogaki, Y., et al. "Shear Strengths Tests of Prestressed Concrete Containment Vessels", Paper J4/3, Sixth International Conference on Structural Mechanics in Reactor Technology, Paris, France 1981.

27. "Outdoor Water Storage Tanks Dynamic Seismic Analysis for the 7.5M Hosgri Criteria", prepared for Pacific Gas and Electric Company by URS/John A. Blume and Associates, Engineers, March 1979.

28. "Geotechnical Studies Diesel Fuel Oil Storage Tanks Diablo Canyon Nuclear Power Plants", prepared for Pacific Gas and Electric Company by Harding Lawson Associates, August 19, 1983.

29. Ang, A.H., and Wilson H. Tang, Probability Concepts in Engineering Planning and Design, John Wiley and Sons, Inc., 1975.

30. Smith, P.D., and O.R. Maslenikov, "LLNL/DOR Seismic Conservatism Program, Part III: Synthetic Time Histories Generated to Satisfy NRC Regulatory Guide 1.60," UCID-17964 (draft report), Lawrence Livermore Laboratory, Livermore, California, April 1979.

31. NUREG/CR-1706, UCRL-15216, Kennedy, R.P., et al., "Subsystem Response Review, Seismic Safety Margin Research Program," October, 1980.

32. "Seminar on Understanding Digital Control and Analysis in Vibration Test Systems," sponsored by Goddard Space Flight Center, Jet Propulsion Laboratory and the Shock and Vibration Information Center held at Goddard Space Flight Center on 17-18 June 1975 and at the JPL on 22-23 July 1975.

33. NUREG/CR-2405, UCRL-15407, Kennedy, R.P., R.D. Campbell, G.S. Hardy, and H. Banon, "Subsystem Fragility - Seismic Safety Margins Research Program (Phase I)," Structural Mechanics Associates, Inc., prepared for U.S. Nuclear Regulatory Commission, February 1982.

34. ASTM DS 552, "An Evaluation of the Yield, Tensile, Creep and Rupture Strengths of Wrought 304, 316, 321 and 347 Stainless Steels at Elevated Temperatures," American Society of Testing Materials.

35. Westinghouse Electric Co. letter Report, PGE-87-009, "Diablo Canyon Long Term Seismic Program Reactor Coolant Pump Seismic Qualification Information", dated January 14, 1987.

[illegible]

36. PG&E, "Diablo Canyon Power Plant Units 1 & 2, Seismic Qualification of Class 1E Electrical Equipment - File ES 24 Vital load centers, Bus F, Bus G, and Bus H (480V)", dated September 6, 1984.

37. Ravindra, M.K., and R.P. Kennedy, "Lessons Learned from Seismic PRA Studies," Paper M6/4, Proceedings, Seventh Conference on Structural Mechanics in Reactor Technology, Chicago, Illinois, August 1983.

38. Hardy, G.S., and R.D. Campbell, "Development of Fragility Descriptions of Equipment for Seismic Risk Assessment of Nuclear Power Plants," ASME Pressure Vessel and Piping Conference, Portland, Oregon, June 1983.

39. NUREG/CR-0261, Rodabaugh, E.C., and S.E. Moore, Evaluation of the Plastic Characteristics of Piping Products in Relation to ASME Code Criteria, Battelle Columbus Laboratories, ORNL/SUB-2913/8, July 1978.

40. EQE Inc. (1982), Program for the Development of an Alternative Approach to Seismic Equipment Qualification, Volume I: Pilot Program Report, Volume II: Pilot Program Report Appendices, September 1982, prepared for the Seismic Qualification Utility Group.

41. NUREG/CR-2137, "Realistic Seismic Design Margins of Pumps, Valves and Piping," by E.C. Rodabaugh and K.D. Desai, June 1981.

42. IE Bulletin No. 79-02, "Pipe Support Base Plate Designs Using Concrete Expansion Anchor Bolts," USNRC.

43. NUREG/CR-2015, Smith, P.E., et al., Seismic Safety Margins Research Program, Phase I Final Report, "Overview," UCRl-53021, Lawrence Livermore National Laboratory, Livermore, California, Vol. I, 1981.

APPENDIX A

CHARACTERISTICS OF THE LOGNORMAL DISTRIBUTION

[illegible]

CHARACTERISTICS OF THE LOGNORMAL DISTRIBUTION

Some of the characteristics of the lognormal distribution which are useful to keep in mind when generating estimates of $\check{A}$, β_R, and β_U are summarized in References A1 and A2. A random variable X is said to be lognormally distributed if its natural logarithm Y given by:

$$Y = \ell n\ (X) \tag{A-1}$$

is normally distributed with the mean of Y equal to $\ell n\ \check{X}$ where $\check{X}$ is the median of X, and with the standard deviation of Y equal to β, which will be defined herein as the logarithmic standard deviation of X. Then, the coefficient of variation, COV, is given by the relationship:

$$COV = \sqrt{\exp\ (\beta^2)-1} \tag{A-2}$$

For β values less than about 0.5, this equation becomes approximately:

$$COV \approx \beta \tag{A-3}$$

and COV and β are often used interchangeably.

For a lognormal distribution, the median value is used as the characteristic parameter of central tendency (50 percent of the values are above the median value and 50 percent are below the median value). The logarithmic standard deviation, β, or the coefficient of variation, COV, is used as a measure of the dispersion of the distribution.

The relationship between the median value, $\check{X}$, logarithmic standard deviation, β, and any value x of the random variable can be expressed as:

$$x = \check{X} \cdot \exp(\eta \cdot \beta) \tag{A-4}$$

where η is the standardized Gaussian random variable, (mean zero, standard deviation one). Therefore, the frequency that X is less than any value x' equals the frequency that η is less than η' where:

$$\eta' = \frac{\ln (x'/\check{X})}{\beta} \tag{A-5}$$

Because η is a standardized Gaussian random variable, one can simply enter standardized Gaussian tables to find the frequency that η is less than η' which equals the probability that X is less than x'. Using cumulative distribution tables for the standardized Gaussian random variable, it can be shown that $\check{X} \cdot \exp(+\beta)$ value of a lognormal distribution corresponds to the 84th percentile value (i.e., 84 percent of the data fall below the $+\beta$ value). The $\check{X} \cdot \exp(-\beta)$ value corresponds to the value for which 16 percent of the data fall below.

One implication of the usage of the lognormal distribution is that if A, B, and C are independent lognormally distributed random variables, and if

$$D = \frac{A^r \cdot B^s}{C^t} \; q \tag{A-6}$$

where q, r, s and t are given constants, then D is also a lognormally distributed random variable. Further, the median value of D, denoted by $\check{D}$, and the logarithmic variance β_D^2, which is the square of the logarithmic standard deviation, β_D, of D, are given by:

[illegible]

$$\check{D} = \frac{\check{A}^r \cdot \check{B}^s}{\check{C}^t} q \qquad \text{(A-7)}$$

and

$$\beta_D^2 = r^2\beta_A^2 + s^2\beta_B^2 + t^2\beta_C^2 \qquad \text{(A-8)}$$

where $\check{A}$, $\check{B}$, and $\check{C}$ are the median values, and β_A, β_B, and β_C are the logarithmic standard deviations of A, B, and C, respectively.

The formulation for fragility curves given by Equation 2-1 and shown in Figure 2-1 and the use of the lognormal distribution enables easy development and expression of these curves and their uncertainty. However, expression of uncertainty as shown in Figure 2-1 in which a range of peak accelerations are presented for a given failure fraction is not very usable in the systems analyses for frequency of radioactive release. For the systems analyses, it is preferable to express uncertainty in terms of a range of failure fractions (frequencies of failure) for a given ground acceleration. Conversion from the one description of uncertainty to the other is easily accomplished as illustrated in Figure A-1 and summarized below.

With perfect knowledge (i.e., only accounting for the random variability, β_A), the failure fraction, f(a), for a given acceleration a can be obtained from:

$$f(a) = \Phi\left(\frac{\ell n(a/\check{A})}{\beta_R}\right) \qquad \text{(A-9)}$$

in which $\Phi(\cdot)$ is the standard Gaussian cumulative distribution function, and β_R is the logarithmic standard deviation associated with the underlying randomness of the capacity.

For simplicity, denote $f = f(a)$. Similarly, f' is the failure fraction associated with acceleration a', etc. Then, with perfect knowledge (no uncertainty in the failure fractions), the ground acceleration a' corresponding to a given frequency of failure f' is given by:

$$a' = \check{A} \exp\left[\beta_R \, \Phi^{-1}(f')\right] \tag{A-10}$$

The uncertainty in ground acceleration capacity corresponding to a given frequency of failure as a result of uncertainty of the median capacity can then be expressed by the following probability statement:

$$P\left[A > a'' | f'\right] = 1 - \Phi\left[\frac{\ell n(a''/A)}{\beta_U}\right] \tag{A-11}$$

in which $P[A > a''|f']$ represents the probability that the ground acceleration A exceeds a'' for a given failure fraction f'. This probability is shown shaded in Figure A-1. However, it is desirable to transform this probability statement into a statement on the probability that the failure fraction f is less than f' for a given ground acceleration a'', or in symbols $P[f \leq f'|a'']$. This probability is also shown shaded in Figure A-1. It follows that:

$$P[f \leq f'|a''] = P[A > a''|f'] \tag{A-12}$$

Thus, from Equations A-10 and A-11:

$$P[f \leq f'|a''] = 1 - \Phi\left[\frac{\ell n\left(a''/A \exp\left[\beta_R \, \Phi^{-1}(f')\right]\right)}{\beta_U}\right] \tag{A-13}$$

from which:

[illegible]

[illegible]
[illegible]
[illegible]
[illegible]

[illegible]

[illegible]

[illegible]

[illegible]

[illegible]
[illegible]

$$P[f > f' | a''] = \Phi\left(\frac{\left(\ln a''/\check{A} \exp\left[\beta_R \Phi^{-1}(f')\right]\right)}{\beta_U}\right) \qquad \text{(A-14)}$$

which is the basic statement expressing the probability that the failure fraction exceeds f' for a ground acceleration a" given the median ground acceleration capacity $\check{A}$, and the logarithmic standard deviations β_R and β_U associated with randomness and uncertainty, respectively.

As an example, if:

$\check{A} = 0.77,\qquad \beta_R = 0.36,\qquad \beta_U = 0.39$

then from Equation A-14 for typical values of f and a".

$$P[f > 0.5 | a'' = 0.40g] = 0.05$$

which says that there is a 5 percent probability that the failure frequency exceeds 0.5 for a ground acceleration of 0.40g.

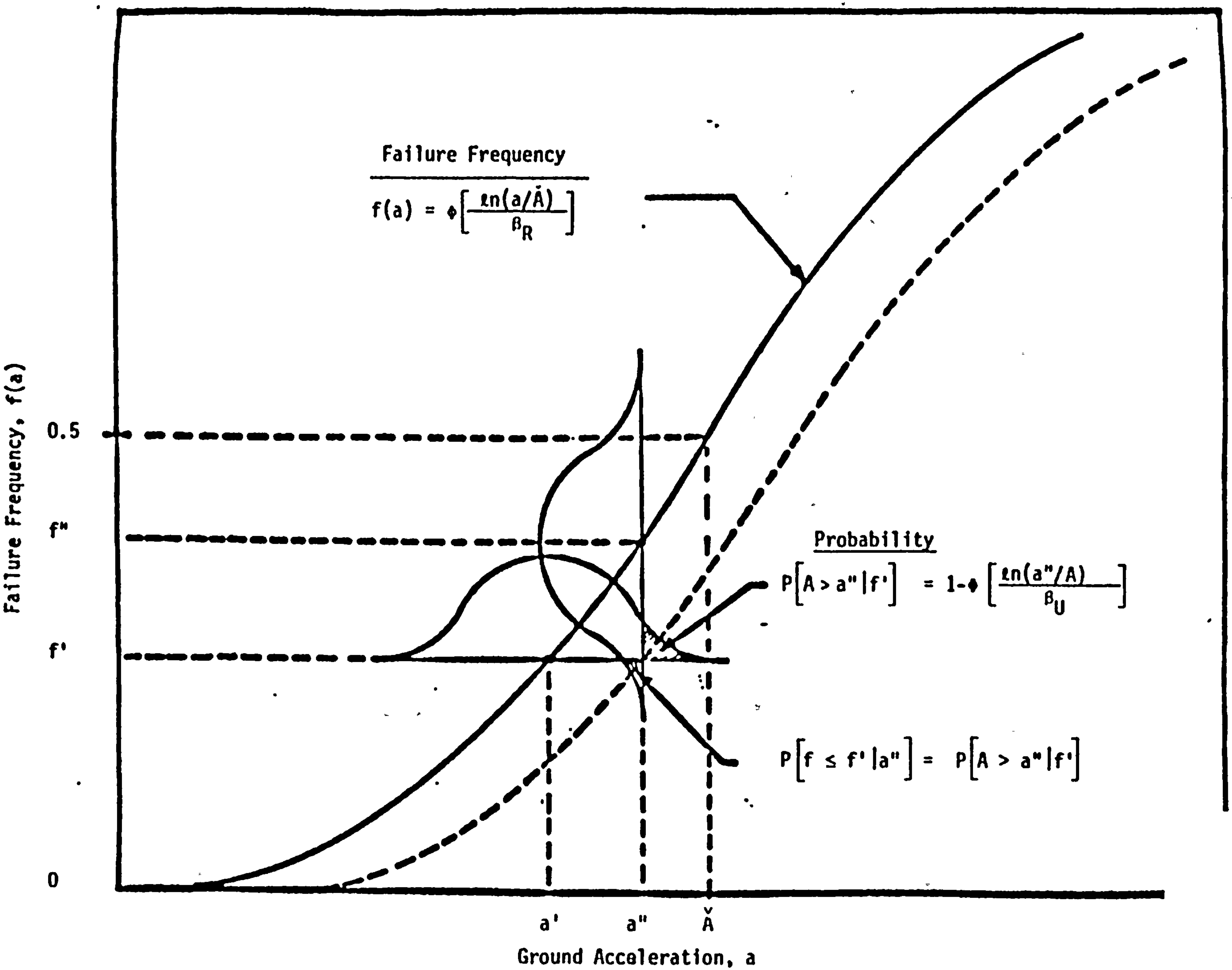

1611-A

Figure A-1. Relationship Between Uncertainty in Ground Acceleration for a Given Failure Fraction and Uncertainty in Failure Fraction for a Given Ground Acceleration

APPENDIX B

CHECK ON SEPARATION OF VARIABLES

[illegible]

INTRODUCTION

Since the late 1970's, a number of probabilistic risk assessment (PRA) studies have been conducted on nuclear power plants. One of the results observed from these PRA's is that seismic events play a significant role in contributing to overall plant risk. Now, since a large portion of plant risk has been associated with earthquake events, seismic risk analysis has itself become of paramount importance.

The primary objectives of a seismic risk analysis are to estimate the frequencies of occurrence of earthquake-induced accidents and to identify key risk contributors. Because of the generally large uncertainties associated with the fragilities of components, and because of an earthquakes ability to fail these components in redundant systems, one of the more important elements of a seismic risk analysis is the calculation of component fragilities. Other key elements of the analysis include:

1. the seismic hazard at the site

2. the response of plant systems and structures

3. plant systems and accident sequences, and

4. consequences.

In fragility analysis the main goal of the analyst is to estimate the peak ground acceleration for which the seismic response of a component exceeds the component capacity resulting in failure.

This value is defined as the item's "ground acceleration capacity", A. Because there is both inherent randomness and uncertainty due to imperfect modeling of any system, component fragilities have been cast in a probabilistic format consisting of a median ground acceleration capacity (A), and two random variables ε_R and ε_U. Thus, seismic fragility (mathematical description of an item's ground acceleration capacity) is given by:

$$A = A\ \varepsilon_R \varepsilon_U \qquad (1)$$

in which ε_R and ε_U are random variables with unit medians values. These variables represent the inherent randomness and uncertainty in the median value, respectively (Kennedy, 1984). It is furthermore assumed that ε_R and ε_U are lognormally distributed with lognormal standard deviations β_R and β_U. With this format it is evident that a component's fragility takes on meaning only when it is associated with a probability level. Therefore, the formal definition of an item's seismic fragility is given as the conditional frequency of failure for a given value of a seismic response parameter (e.g., stress, deflection, and spectral acceleration). This description enables the fragility curve to be represented as a set of shifted curves with attached uncertainty levels (Figure 1).

As part of an ongoing PRA for Diablo Canyon standard the method used for determining the seismic fragility parameters $\left((A, \beta_R, \beta_U)\right)$ for components and structures has been verified by an independent approach. The standard method, herein called the separation of variables approach, makes certain assumptions which have not previously been substantiated. Because of this, it was desired to perform an independent, rigorous analysis in order to check the validity of the method. In addition to checking the method, it was also desired to

[illegible]

[illegible]

[illegible]

ascertain whether or not subsystem component failures were highly correlated and whether or not the fragility curves could be cut off at low levels of probability.

This appendix discusses and illustrates the results of a check performed on the current state of the art technique used for estimating the seismic response of subsystems for use in fragility analysis. The separate issue of correlation between failure modes is addressed in Appendix D.

This appendix presents a description of the separation of variables technique. It then describes the method used for checking the technique (Monte Carlo Simulation) and orients the reader with the system selected for use in the simulation. The appendix then describes an importance sampling technique used in obtaining the Monte Carlo trials. It then describes in detail the procedures used in estimating the response parameters for the sample system. Finally, it gives the reader the results of both the simulation and the separation of variables analysis completed on the same system. Some limitations of the study are that; (1) only linear analyses are performed, (2) no strength model was checked, (3) only 200 Monte Carlo trial were used, and (4) only 25 earthquake time histories were used.

Separation of Variables Technique

Most often in estimating the fragility parameters (A, β_U, β_R) the analyst works in terms of a factor of safety, F, on ground acceleration capacity above the safe shutdown earthquake level specified for design, A_{SSE}. This factor is defined as follows:

$$A = F\,A_{SSE} \tag{2}$$

[illegible]

[illegible]

[illegible]

[illegible]

[illegible]

[illegible]

[illegible]

[illegible]

[illegible]

[illegible]

[illegible]

[illegible]

[illegible]

[illegible]

[illegible]

[illegible]

[illegible]

$$F = \frac{\text{ACTUAL CAPACITY}}{\text{DESIGN RESPONSE DUE TO SSE}} \quad (3)$$
$$\times \frac{\text{DESIGN RESPONSE DUE TO SSE}}{\text{ACTUAL RESPONSE DUE TO SSE}}$$

The best estimate (median) factor of safety, F, is related to the median ground acceleration capacity as:

$$\check{F} = A/A_{SSE} \quad (4)$$

The logarithmic standard deviations of $\check{F}$ are β_U and β_R. These are identical with those for the ground acceleration capacity $\check{A}$. In essence, then, the process of formulating a fragility description for any system is reduced to determining the median factor of safety above design levels with the associated uncertainty and inherent randomness.

The most common method used in practice today for estimating these fragility parameters is a first order second moment approach referred to as the method of separation of variables (SOV). In this method, the factor of safety, F, (Equation 3), is made up of three parts consisting of a capacity factor, F_C, a structure response factor, F_{RS}, and an equipment response (relative to the structure) factor F_{RE}. Thus,

$$F = F_C \, F_{RE} \, F_{RS} \quad (5)$$

The separation of variables terminology comes from the fact that by using this approach each of the three factors, may be calculated independently.

Each of the factors is considered to be lognormally distributed with

[illegible]

[illegible]

[illegible]

[illegible]

corresponding uncertainty measures β_R (inherent randomness) and β_U (uncertainty). Following a first order second moment approach the median value, F, and the total uncertainty, β_C, on the factor of safety is obtained as follows:

$$\check{F} = \check{F}_C \check{F}_{RE} \check{F}_{RS} \tag{6}$$

$$\beta_U = (\beta_{U_C}{}^2 + B_{U_{RE}}{}^2 + \beta_{U_{RS}}{}^2)^{1/2} \tag{7}$$

$$\beta_R = (\beta_{R_C}{}^2 + \beta_{R_{RE}}{}^2 + \beta_{R_{RS}}{}^2)^{1/2} \tag{8}$$

$$\beta_C = (\beta_U{}^2 + \beta_R{}^2)^{1/2} \tag{9}$$

The use of the composite variability, β_C, along with the median factor of safety, F is often used as a single "best estimate" fragility curve which does not explicitly separate out uncertainty from underlying randomness (Figure 1).

The capacity factor, F_C, for equipment is the ratio of the acceleration level at which the equipment fails to the seismic design level. The factor is composed as the product of a strength factor, F_S, and a ductility factor F_{μ}. The nature of the capacity factor lends itself to a rather simple derivation and the methods used in obtaining it are recognized as sound; therefore, this factor was not examined in this study.

The equipment response factor, F_{RE}, is the ratio of equipment response calculated in design to the realistic equipment response. Both responses are calculated using design floor spectra. When dynamic analysis is used in the design, the equipment response factor may be modeled as a product of factors influencing the response variability.

$$F_{RE} = F_{EC} \cdot F_{MC} \cdot F_{\delta} \cdot F_{SA} \cdot F_{M} \cdot F_{QM} \tag{9}$$

where: F_{QM} = factor accounting for variability introduced in response by the qualification method (analytical procedure).

F_{SA} = spectral shape factor representing the variability in ground motion and the associated ground response spectra

F_{δ} = damping factor representing the variability in response due to difference in actual damping and design damping.

F_{M} = modeling factor accounting for the uncertainty in response due to modeling assumptions.

F_{MC} = mode combination factor accounting for the variability in response due to the method used in combining dynamic modes of response.

F_{EC} = earthquake component combination factor accounting for the variability in response due to the method used in combining the earthquake components.

The median and logarithmic standard deviation of F_{RE} are expressed as:

$$\check{F}_{RE} = \check{F}_{EC}\, \check{F}_{MC}\, \check{F}_{\delta}\, \check{F}_{SA}\, \check{F}_{M}\, \check{F}_{QM} \tag{10}$$

and $$\beta_{RE} = (\beta_{EC}^{2} + \beta_{MC}^{2} + \ldots)^{1/2} \tag{11}$$

The logarithmic standard deviation, β_{RE}, is further broken down into a random component, β_{R}, and a uncertainty component, β_{U}.

[illegible]

The structure response factor, F_{RS}, is the ratio of structure response used in design to the realistic, or median centered, structure response. It is based on the structural properties which affect the structure response at the desired location (for example, floor response for equipment). The structure response factor is given as:

$$\check{F}_{RS} = \check{F}_{SA} \cdot \check{F}_{\delta} \cdot \check{F}_{M} \cdot \check{F}_{SSI} \tag{12}$$

where F_{SA} = spectral shape factor

$\check{F}_{\delta}$ = damping factor

$\check{F}_{M}$ = modeling factor

$\check{F}_{SSI}$ = soil structure interaction factor

F_{SA}, F_{δ}, and F_M are similar to those used in calculating the equipment response factor. The soil structure interaction factor, F_{SSI}, accounts for any conservatism (or unconservatism) introduced into the design by introducing improper boundary conditions at the soil level. The lognormal standard deviation on uncertainty (β_U) and on randomness (β_R) are calculated as the square root of the sum of the squares of each component's term:

$$\beta = (\beta_{SA}^2 + \beta_{\delta}^2 + \beta_M^2 + \beta_{SSI}^2)^{1/2} \quad \text{(for both U and R)}$$

<u>Method for Checking the SOV Technique</u>

The fragility analyst is typically given no more information about a piece of equipment than what is available to the designer. In addition to the design of the item, the analyst usually is given floor spectra at

[illegible]
[illegible]
[illegible]
[illegible]
[illegible]

[illegible]

[illegible]
[illegible]
[illegible]
[illegible]
[illegible]

[illegible]
[illegible]

different damping levels (3, 5, 7 percent are common). Sometimes, albeit infrequently, the analyst also has spectra which are not peak smoothed and broadened. Using this information and sound engineering judgement the analyst can make rather good estimates of a subsystems fragility description with the separation of variables techniques.

A Monte Carlo simulation is a good way to check the separation of variables approach usually taken by the analyst with his limited information. Variables for the simulation should cover the distributions on the inherent earthquake variability, the capacity factor, the equipment response factor, and the structural response factor. Primarily of interest, however, are the response factors. The capacity factor is more deterministic by nature, since the distributions on such strength characteristics as material properties are well defined.

The distribution on response may be taken into account through a simulation process by varying the following:

1. Earthquake Time Histories
2. Structure Frequency
3. Structure Damping
4. Equipment Frequency
5. Equipment Damping

Dynamic time history runs may then be run which yield distributions on response. From this distribution, a median response factor,

$$\check{F}_R = \check{F}_{RS} \cdot \check{F}_{RE}$$

and a composite uncertainty value, β_C, may be obtained. These values

[illegible]

could then be compared to values computed using a SOV approach.

For the SOV approach spectra generated from the time history runs may be used as input. The analyst must then use the equipment frequencies as median centered and approximate the safety (Equation 9 and 10) factors in the same manner in which most fragilities are calculated today. A direct comparison of the two resulting distributions (Monte Carlo, SOV) on response would then provide a check on the SOV approach.

System Selected

In order to provide a reasonable check on the SOV technique a generic structure subsystem assembly is required. The ideal system would model items of various natural frequencies at different locations on a site. For simplicity, however, a system was selected which includes one structure and four pieces of equipment located on two different floors.

Equipment

Components typically found in fragility analyses have fundamental frequencies ranging from 3 hz to rigid. These items are most often located on various floor levels and with different mounting schemes. In order to adequately model these subsystems in the frequency range of interest four items with central frequencies of 5, 8, 14 and 24 hz were selected. Experience has shown that frequency may be modeled with a lognormal distribution [5]. A lognormal standard deviation of 0.20 on equipment frequency is reasonable. Median equipment damping was taken as 5 percent of critical. Damping is also assumed to follow a lognormal distribution with a lognormal standard deviation of 0.35. The four items were located both high in the structure (elevation 140') and low in the structure (elevation 100'). This arrangement accounted for the

effect of location in the structure and later proved to be useful in the correlation analysis.

Table 1. Equipment Parameters

	Median Value	β	Cut-off	Range
Frequency	5	0.20	$\pm 2\beta$	3.4 - 7.5
	8	0.20	$\pm 2\beta$	5.4 - 11.9
	14	0.20	$\pm 2\beta$	9.4 - 20.9
	24	0.20	$\pm 2\beta$	16.1 - 35.8
Damping	.05	0.35	$\pm 2\beta$	0.025 - .10

Structure

A simplified model representative of an auxiliary building was used as the structural system. The model was a fixed base, five degree of freedom, two dimensional representation of the Diablo Canyon auxiliary building above basemat elevation. The fundamental frequency of the building model was assumed as 8.1 Hz which includes some frequency shift due to softening of the building at higher shaking levels. In addition, a lognormal distribution is assigned to stiffness with a lognormal standard deviation (β) of 0.5, which results in a β on frequency of 0.25.

Median structure damping at high response levels expected for equipment failure is estimated as 7% of critical with an expected lognormal standard deviation of 0.35.

Table 2. Structure Parameters

	Median	β	Cut-off	Range
Frequency	8.1 hz	0.25	±2β	4.9 - 13.4
Damping	0.07	0.35	±2β	0.035 - 0.14

In order to avoid unrealistic values on certain parameters (damping, stiffness), the range of values allowed for any given sample set was limited to a smaller range than a lognormal distribution would generate. Cut-offs on individual parameters of ±2β were used in this study in order to circumvent this use of unrealistic values. The resulting permissable ranges on the parameters are shown in the preceeding Tables 1 and 2.

Monte Carlo Simulation

The total number of trials comprising the Monte Carlo Sample Space was 200. Time histories used consisted of horizontal components of historical and numerically generated earthquake records. Orthogonal records of pairs of horizontal components were treated as independent records. In order to eliminate some variability due to differences in earthquake energy content, and to accurately model a large scale event each time history was scaled to an average 7% damped spectral acceleration of 2.0 g from 5 to 14 hz. This frequency range is centered on the fundamental frequency of the structure (8.1 hz). The time histories with scaling factors are shown in Table 3.

[illegible]

In order to assure that the resulting distribution on response would be densely populated in the region of interest (high response). Importance sampling was used in generating the structure parameters. A weighting function was selected which resulted in shifting the damping values toward low values, and shifting the frequency of the equipment toward resonance with the structure (8.1 hz). The importance sampling technique used is as follows:

Each parameter, y_i is assumed to be lognormally distributed.

$$y_{i,j} = \check{Y}_i \exp(\beta_i \mu_j) \qquad \text{(for } j = n \text{ trials)} \qquad (13)$$

where $\check{Y}_i$ = median value for parameter i

β_i = lognormal standard deviation for parameter i

μ_j = a specific trial from the standard normal function

The standard normal function is given as;

$$\text{PDF: } f(\mu) = \phi(\mu) = \frac{1}{\sqrt{2\pi}} \exp(-\mu^2/2)$$

$$\text{CDF: } F(\mu) = \Phi(\mu) = \frac{1}{\sqrt{2\pi}} \int_{\infty}^{\mu} \exp(-x^2/2)dx$$

multiply the PDF ($\phi(\mu)$) by a weighting function W (μ) to obtain a weighted PDF

$$\phi'(\mu) = \frac{W(\mu)}{\sqrt{2\pi}} \exp(-\mu^2/2) \qquad (14)$$

The weighting function selected in this case was:

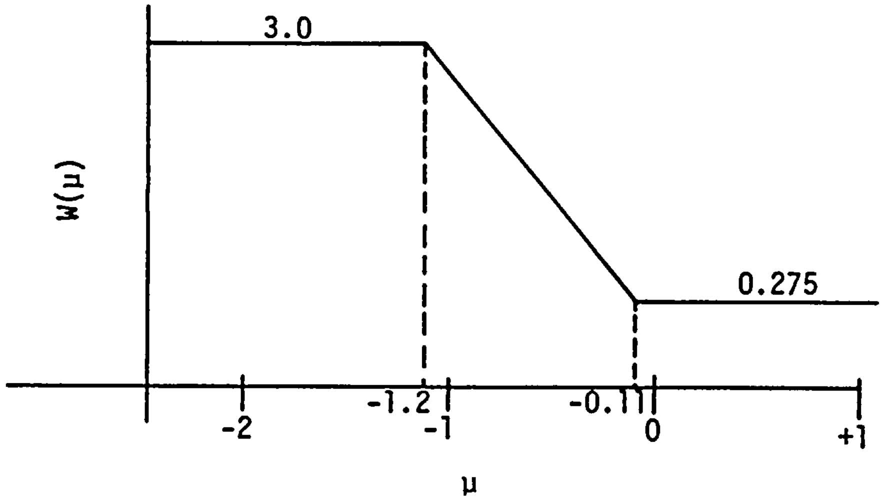

Figure 2. Weighting Function

$$
\begin{aligned}
W(\mu) &= 0.275 && \text{for } \mu \geq -0.11 \\
W(\mu) &= -2.5\mu && \text{for } -0.11 \geq \mu \geq -1.2 \\
W(\mu) &= 3.0 && \text{for } -1.2 \geq \mu
\end{aligned}
\tag{15}
$$

Substituting these into Equation 14 and integrating yields the weighted CDF:

$$\Phi'(\mu) = 3\Phi(\mu) \qquad \text{for } \mu \leq -1.2$$

$$\Phi'(\mu) = 0.8505 - \sqrt{\frac{2.5}{2\pi}} \left[0.9940 - \exp(-\mu^2/2)\right] \qquad \text{for } -1.2 \leq -.11$$

$$
\begin{aligned}
\Phi'(\mu) &= 1.0 - 0.275\ \Phi(-\mu) \qquad \text{for } -0.11 \leq \mu \\
&= 0.725 + .275\ \Phi(\mu)
\end{aligned}
$$

Rewriting these into μ for $\Phi'(\mu)$ gives:

$$\Phi(\mu) = 1/3\ \Phi'(\mu) \qquad \text{for } \Phi'(\mu) \leq .345$$

[illegible]

$$\mu = -\sqrt{-2\ln\,[1.0026\;\Phi'(\mu) + 0.1413]} \qquad \text{for } .345 \le \Phi'(\mu) \le .850 \qquad (16)$$

$$\Phi(\mu) = \frac{\Phi'(\mu) - 0.725}{0.275} \qquad \text{for } .850 \le \Phi'(\mu)$$

These equations may then be used for determining the variable μ to be used in Equation 13 for generating trials. Summarizing, then, the process for generating the random samples with importance sampling is as follows:

1. Randomly select N trials for the weighted CDF, $\Phi'(\mu)$, using random numbers from 0.0 to 1.0

2. Determine μ from Equation 16 and the corresponding weight (W_μ) from Equation 15

3. Determine parameter $y_{i,j}$ from Equation 13

The resulting distribution on the parameters is obtained by assigning the probability of non-exceedance "P" or $F_Z(z')$ a value of:

$$P = F_Z(z') = \frac{1}{n}\sum_{i=1}^{n} I(y_i) \cdot \frac{1}{W(y_i)} \qquad (17)$$

where $I(y_i) = 1.0$ if $y_i \le z'$ and 0.0 if $y_i > z'$

$W(y_i)$ = the weight corresponding to sample point y_i (From Equation 15)

n = number of trials

The final distribution on response of the subsystem, $F_Z(z')$, (a function of all four random variables) is dependent on the vector $\underline{y}$, and is

[illegible]

[illegible]

obtained by allowing the function I(y) to become I($\underline{y}$) and W(y) to become W($\underline{y}$) therefore, the estimator P, for a given value z', becomes:

$$P = F_Z\ (z') = \frac{1}{n} \sum_{i=1}^{n} I(\underline{y}_i) \frac{1}{W(\underline{y}_i)} \tag{18}$$

where $I(\underline{y}_i)$ = 1.0 if $z(\underline{y}_i) \le z'$ and
0.0 if $z(\underline{y}_i) > z'$

$W(\underline{y}_i)$ = $\Pi W(yi) = W(y_1) \cdot W(y_2) \cdot \cdot \cdot W(y_n)$ for independent y

P = is an estimate of $P(Z \le z')$ or $F_Z(z')$

n = number of trials

Each sample set for the individual Random Variables (damping, frequency) was generated using this method. An example set for equipment damping is shown in Figure 3. From this figure one can see the effect of the weighting in the tail ends of the distribution. The sample statistics are also well preserved. The final sample statistics as generated for all the parameters are shown in Table 4.

Table 4. Monte Carlo Sample Statistics

Parameter	Median	Beta Value	Bias
Structure Frequency	8.1	0.24	1.0
Structure Damping	0.07	0.33	1.0
Equipment Frequency			
5	4.6	0.18	0.92
8	7.8	0.22	0.98
14	14.4	0.21	1.03
24	23.6	0.21	0.98
Equipment Damping	0.05	0.30	1.0

[illegible]

[illegible]

[illegible]

[illegible]

Dynamic Analysis

A total number of 600 dynamic equipment time histories were made in generating the final response sample set. A modified version of SAP IV (MODSAP) was used for this purpose. The structural model was run 200 times (each time history was run 8 times). From each structural run, the amplified response (acceleration time histories) was saved at elevations 100 and 140 feet. These time histories were then used as input for the equipment models and the maximum accelerations of the equipment models were saved as the final response parameters.

For use in the SOV calculations floor response spectra were generated at both floors (100' and 140') for each time history using median structure and equipment properties. The resulting set of 25 floor spectra were then statistically analyzed to give median, 84% and upper bound curves at both locations. This was done for 3, 5, and 7% of critical damping.

Estimation of Response Parameters

Separation of Variables Approach

Estimation of the peak responses were made using a separation of variables (SOV) approach with spectra generated during the dynamic time history runs (Figure 4). From Equations 9 and 12 the following factors had to be accounted for:

Equipment:

1. F_m = Modeling Factor
2. F_δ = Equipment Damping Factor

[illegible]

一

[illegible]

Structure:

1. F_{mc} = Modal Combination Factor
2. F_{sa} = Spectral Shape Factor
3. F_{δ} = Structure Damping Factor

These factors account for the total variability in the equipment structure assemblage as run in the Monte Carlo simulation. The values obtained in the SOV approach are summarized in Table 5. All of the other factors present in Equations 9 and 12 were assigned values of unity with beta values of 0.0, since they were not introduced in the simulation.

The following paragraphs present the methodology used in calculating the factors. The methods used in this study are more analytical in nature than the general procedure; however, for purposes of comfirming the validity of the SOV approach they are appropriate.

EQUIPMENT

<u>Modeling Factor</u>

The modeling factor has traditionally been defined as accounting for the uncertainty in response due to modeling assumptions. One of the errors which could be made in modeling any item would be to inaccurately estimate the mass and stiffness characteristics. This would then lead to uncertainty on the fundamental frequencies of that item. This uncertainty on frequency should be accounted for in any response spectra type of analysis.

[illegible]

In a equipment-structure system the effect of miscalculating the frequencies would be compounded. The floor spectra, which peaks at the structures natural frequencies, would shift horizontally in accordance with the best estimate of the fundamental frequency of the structure. Likewise, for a subsystem which is responding primarily to motion filtered through the structure a shift in frequency would be translated into a shift along the median floor spectra curve (see Figure 5). In order to account for these shifts, the following procedure was followed:

1. Assume that the reported frequencies in the analysis are median centered.

2. Use the ratio of the response parameter used in design to the median value as the value of the modeling factor.

3. Assume that the distribution on the combined frequency shift has a lognormal standard deviation of about 0.32. This comes from the square root of the sum of the squares of the lognormal standard deviations due to structure frequency shift (0.25) and equipment frequency shift (0.20). This is the same as the β value for the modeling factor.

4. Use spectral response (acceleration) at different discrete frequency points along with the properties of the standard normal density function on frequency to arrive at a new distribution on response.

[illegible]

For example:

We are given the floor response spectrum in tabular form for a particular elevation on which a piece of equipment is mounted. The spectum has discrete values for response (r_i) corresponding to each frequency point ($freq_i$); however, the frequency points are generally evenly spaced on a logarithmic scale. The probability of response at a given frequency can be approximated as follows:

$$P_R(r_i) = \Phi(S_{i+1}) - \Phi(S_{i-1})$$

where: Φ is the Standard Normal Distribution Function

$$S_{i+1} = \ln\left[\frac{(freq_i + freq_{i+1})}{2x_m}\right] \cdot \frac{1}{\beta}$$

$$S_{i-1} = \ln\left[\frac{(freq_i + freq_{i-1})}{2x_m}\right] \cdot \frac{1}{\beta}$$

$freq_i$ is frequency at point i

x_m is the median value for equipment frequency

β is the lognormal standard deviation on combined frequency shift (0.32)

$P_R(r_i)$ is the probability mass function (PMF) on response; that is, the probability that R is equal to r_i for some i.

Once the resulting probability mass function on response has been determined the resulting statistics may be calculated through point estimates or through an examination of the cumulative distribution. In this study, the latter approach was used since the distribution on

[illegible]

[illegible]

[illegible]

[illegible]

response was not well defined by a common analytical function. The main descriptors of the distribution are reported as a median value and lognormal standard deviation (β) in accordance with the central limit theorem, and in following the development of the separation of variables approach. The value of response lying at a cumulative probability of 50% was reported as the median value, and the value lying at a cumulative probability of 84% was used in obtaining the lognormal standard deviation:

$$x_{.50} = \text{Median Value} = x_m$$

$$x_{.84} = 84\% \text{ Value}$$

and for lognormally distributed variables,

$$F_X(x_i) = \Phi\left\{\frac{\ln(x/x_m)}{\beta}\right\}$$

Therefore

$$F_X(x_{.84}) = \Phi\left\{\frac{\ln(x_{.84}/x_m)}{\beta}\right\}$$

$$\Phi^{-1}(.84) = \frac{\ln(x_{.84}/x_m)}{\beta}$$

noting that $\Phi^{-1}(.84) = 1.0$ yields

$$\beta = \ln\,(x_{.84}/x_m)$$

Damping Factor

The equipment damping factor represents the variability in response due to differences in actual damping and design damping. The factor is

[illegible]

[illegible]

[illegible]

[illegible]

calculated using the ratio between the response value at the design damping level to the median response value at 5% of critical at the frequency of interest. For calculating the uncertainty due to equipment damping, 5% of critical is considered median centered, and 3% of critical is judged to lie at a cumulative probability of 92.8% (1.46β):

$$F = \frac{\text{RESPONSE AT DESIGN DAMPING LEVEL}}{\text{RESPONSE AT 5\% OF CRITICAL DAMPING}}$$

$$\beta = \ln(R_{3/5}) / 1.46$$

where $R_{3/5}$ = ratio of 3% damped response to 5% damped response

STRUCTURE

Modal Combination

The modal combination factor for structures is defined as that factor which accounts for the variability in response due to the method used in combining dynamic modes of response. According to Newmark the SRSS of modes is judged to be median centered. The value of the factor is then taken as the value of the response used in design to that value obtained using the SRSS of modal responses.

$$F_{mc} = \text{Response from design / SRSS response}$$

In this study, the absolute sum of modal response was estimated to lie at a cumulative probability of +3B from the median (SRSS). Therefore, the variability due to modal combination may be estimated through the following equation:

$$\beta = (-1/3) \ln (\text{Absolute Sum Response / SRSS Response})$$

Spectral Shape

The spectral shape factor accounts for the variability in ground motion and the associated ground response spectra. In most fragility analysis performed using design spectra, this factor also accounts for any conservatism introduced due to smoothing and broadening of spectra. In this study, the ground spectra resulting from the 25 time histories run using median damping (7% for structures) were statistically analyzed. The resulting distribution on ground spectra was used as a basis for estimating the median and 84% ground spectra. With this information the distribution parameters for the spectral shape factor were calculated as follows:

$$F_{sa} = \text{design spectra response / median spectra response}$$

$$\beta_{sa} = \ln\,(Sa_{.84}/Sa_{.50})$$

where $Sa_{.84}$ = Spectral acceleration value lying at a cumulative probability of 84%

$Sa_{.50}$ = Spectral acceleration value lying at a cumulative probability of 50%.

Of course the beta value is dependent upon frequency along the ground spectra curve. In order to account for this variation, the average beta value in the frequency range 3 to 30 hertz is recommended or a β_R of about 0.7 on spectral shape (see for instance Figure 1). This is the value which was used in this study.

[illegible]
[illegible]
[illegible]
[illegible]
[illegible]

[illegible]

[illegible]
[illegible]
[illegible]
[illegible]
[illegible]
[illegible]

[illegible]

Damping

The structural damping factor, like the equipment damping factor, accounts for the variability in response due to differences in median and design damping. In practice this factor is usually estimated since the floor response spectra are obtained from dynamic analyses of the structural system made at a constant damping value. One method for estimating this factor is to use a ratio of spectra amplification factors at difference damping values [7]. The most correct method, however, would be a comparison of median response values obtained through dynamic analyses completed on the structural system at different damping values. In this study, the floor response spectra corresponding to structural damping at 3%, 5%, and 7% of critical were obtained for one time history. The response at 7% structure damping was considered median, while the responses at 3% and 5% were considered to lie at 0.96β and 2.42β from the median respectively. The distribution parameters on the structural damping factor were therefore calculated as:

F = Response at design spectrum / Response at spectrum generated using 7% structure damping

$$\beta = \ell n(R_{3/7}) / 2.42$$

where: $R_{3/7}$ is the ratio of response due to 3% structure damping to response due to 7% structure damping

Results

The values for the factors calculated in the SOV approach are summarized in Table 5. The resulting lognormal distribution parameters were obtained through Equations 9 and 12.

[illegible]

From the Monte Carlo simulation a sample of maximum response values at each item was obtained and a cumulative distribution function was plotted. The sample statistics were then calculated for each item and the results were compared to those obtained in the SOV approach. The resulting sample statistics are shown in Table 6.

Figures 6 through 13 show the cumulative distribution plots on response for each item at different elevations. The abscissa on each plot is one minus the standard normal variate corresponding to the paired value of acceleration at that point. From this value, one may calculate the exceedance value corresponding to the level of acceleration at that particular point. That is:

$$P(X \geq x_i) = 1 - \Phi(s_i) = \Phi(-s_i)$$

where: Φ is the standard normal distribution function (Tabulated in most texts on probability)

s is the standard normal variate, for lognormally distributed variables the transformation is:

$$s_i = [\ln(x_i/x_m)] / \beta$$

x_m is the median value of x

β is the lognormal standard deviation for X

Superimposed on these plots are the resulting lognormal distributions estimated through; (1) a statistical analysis of the Monte Carlo simulation sample set and 2) the analytical separation of variables approach.

Conclusions

Both the table on statistics (Table 6) and the plots (Figures 6-13) show that the method of separation of variables is accurate in the region examined (that is from x_m to 3β). This is good because this shows that approximate analytical techniques may justifiably be employed in arriving at final subsystem fragility estimates. The Monte Carlo method used in this study is very time consuming and involves extensive finite element analysis performed on a digital computer. With the number of trials needed to provide a reasonable data base the associated computer costs can become very high in a short period of time. The analytical approach, however, is easy to implement and takes relatively little time to complete. With practice, coupled with good design deocumentation, an items complete fragility description may be obtained in less than a day using the separation of variables approach.

Table 3. Earthquake Time Histories

EARTHQUAKE DATE	MAGNITUDE	RUPTURE MECHANISM	RECORDING STATION SITE CONDITONS DISTANCE	T. HISTORY NUMBER	COMP	ORIGINAL RECORD PEAK ACCEL. (G)	ORIGINAL RECORD PEAK VELOC. (CM/SEC)	ORIGINAL RECORD V/A CM/SEC G	MODIFIED RECORD PEAK ACCEL. (G)	MODIFIED RECORD PEAK VELOC. (CM/SEC)	MODIFIED RECORD V/A CM/SEC G	S_a|3-8.5 HZ (G)	SCALING FACTOR TO 2.0G (5-14HZ)
GAZLI,U.S.S.R. MAY 1976	MS=7.0 ML = 6.4	THRUST	KARAKYRPOINT ROCK/STIFF ALLUV. 4 KM	2 1	EAST NORT	0.70 0.66	47.2 44.4	68 68	0.70 0.66	47.2 44.4	68 68	1.33	1.38 1.41
TABAS, IRAN 16 SEP 1978	MS = 7.5 ML = 6.6	THRUST	TABAS STIFF ALLUV./ROCK 3 KM	4 3	TRAN LONG	0.70 0.81	105 91.5	150 113	0.70 0.81	105 91.5	150 113	2.33	1.11 1.08
SAN FERNANDO, CA 09 FEB 1971	MS = 6.6 ML = 6.4	THRUST	PACOIMA DAM ROCK 1 KM	5 6	S14W N76W	1.17 1.08	114 58.3	97 54	1.17 1.08	114 58.3	97 54	1.90	1.19 1.23
			LAKE HUGHES #12 ROCK 20 KM	7 8	N21E N69W	0.37 0.29	14.7 12.8	40 44	0.94 0.72	36.8 12.0	40 44	2.23	1.05 1.31
			CASTAIC STIFF ALLUVIUM 25 KM	9	N69W	0.29	27.8	96	0.92	89.0	96		1.51
IMPERIAL VALLEY, CA 13 OCT 1979	MS = 6.9 ML = 6.6	STRIKE- SLIP	DIFFERENTIAL ARRAY DEEP ALLUVIUM 5 KM	10 11	N00E N90W	0.49 0.35	42.5 67.8	87 192	0.37 0.51	31.7 40.2	56 78	1.45	1.81 1.45
			EL CENTRO #4 DEEP ALLUVIUM 4 KM	12 13	S50W S40E	0.37 0.49	77.6 37.1	210 76	0.37 0.33	34.8 31.0	94 58	0.92	3.25 2.08
PARKFIELD, CA 27 JUN 1966	MS = 6.4 ML = 5.6	STRIKE- SLIP	TEMBLOR ROCK 10 KM	14 15	N65W S25W	0.28 0.41	14.5 22.5	51 55	0.55 0.70	47.9 58.7	87 83	1.23	2.18 1.98
MORGAN HILL, CA 24 APR 1984	MS = 6.1 ML = 6.5	STRIKE- SLIP	COYOTE LAKE DAM ROCK 6 KM	16 17	N75W S15W	1.30 0.71	79.7 51.9	61 73	1.66 0.89	124 85.7	74 97	1.99	0.97 1.74
COALINGA, CA 02 MAY 1983	MS = 6.7 ML = 6.5	THRUST	PLEASANT VALLEY PUMP STATION (SWITCHYARD) STIFF ALLUV./ROCK 10 KM	18 19	N43E S45E	0.61 0.53	73.9 39.5	121 75	0.85 0.74	103 55.3	121 75	1.90	1.43 1.44
TABAS, IRAN 16 SEP 1978	MS = 7.5 ML = 6.6	THRUST	DAYHOOK (T) ROCK (L) 17 KM	20 21	N10E N80W	0.39 0.39	27.5 36.7	70 97	0.66 0.64	46.8 62.4	70 97	1.43	1.93 1.30
HOSGRI	MS = 7.0	STRIKE- SLIP BILATERAL	-	22 23	NORTH EAST								2.60 2.05
	MS = 7.0	STRIKE- SLIP UNILATERAL	-	24 25	NORTH EAST								2.55 2.04

1611-A

Table 5. Factors and Uncertainties from Separation of Variables Approach

COMPONENT AND LOCATION									
FACTOR	5HZ		8HZ		14HZ		24HZ		COMMENTS
	100'	140'	100'	140'	100'	140'	100'	140'	
EARTHQUAKE VARIABILITY (SPECTRAL SHAPE)	0.19	0.19	0.19	0.19	0.19	0.19	0.19	0.19	(1) MED=1.0
MODAL COMBIN.	0.18	0.07	0.18	0.07	0.18	0.07	0.18	0.07	(2) MED=1.0
SUM	0.26	0.20	0.26	0.20	0.26	0.20	0.20	0.20	SRSS (1,2)
MODELING	2.9	3.8	3.0	5.3	1.7	2.5	1.4	2.1	(MEDIAN)
FACTOR	0.16	0.48	0.25	0.41	0.18	0.53	0.10	0.13	(β)
STRUCTURE DAMPING	0.01	0.03	0.16	0.18	0.07	0.15	0.11	0.10	MEDIAN=1.0
EQUIPMENT DAMPING	0.05	0.08	0.11	0.18	0.03	0.03	0.00	0.00	MEDIAN=1.0
TOTAL β	0.31	0.53	0.41	0.52	0.32	0.59	0.30	0.26	
MEDIAN	2.9	3.8	3.0	5.3	1.7	2.5	1.4	2.1	
$\pm 2.4\beta$	6.1	13.6	8.0	18.6	3.7	10.2	2.9	3.9	

[illegible]

Table 6. Comparison of Distribution Parameters (Median, β)

METHOD	PARAM	COMPONENT AND LOCATION							
		5HZ		8HZ		14HZ		24HZ	
		100'	140'	100'	140'	100'	140'	100'	140'
APPROX S.O.V.	MEDIAN	2.9	4.0	3.2	6.2	1.7	3.0	1,4	2.2
	β	0.30	0.49	0.45	0.54	0.29	0.43	0.23	0.25
ANALYTICAL S.O.V.	MEDIAN	2.9	3.8	3.0	5.3	1.7	2.5	1.4	2.1
	β	0.31	0.53	0.41	0.52	0.32	0.59	0.30	0.26
DATA FIT	MEDIAN	2.8	3.8	2.9	5.7	1.7	3.0	1.3	2.3
	β	0.30	0.50	0.40	0.53	0.24	0.41	0.21	0.21

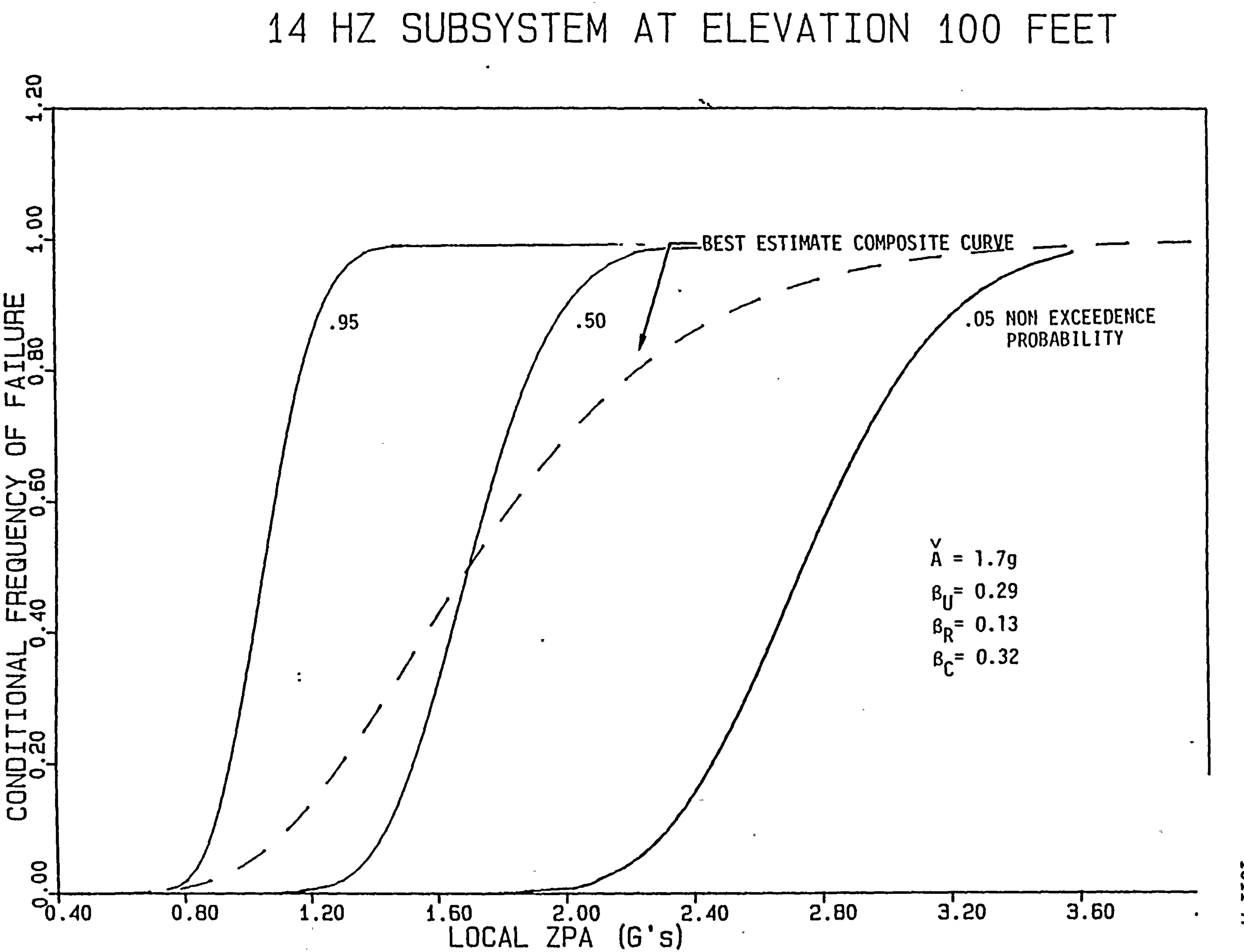

Figure 1. Typical Fragility Curve

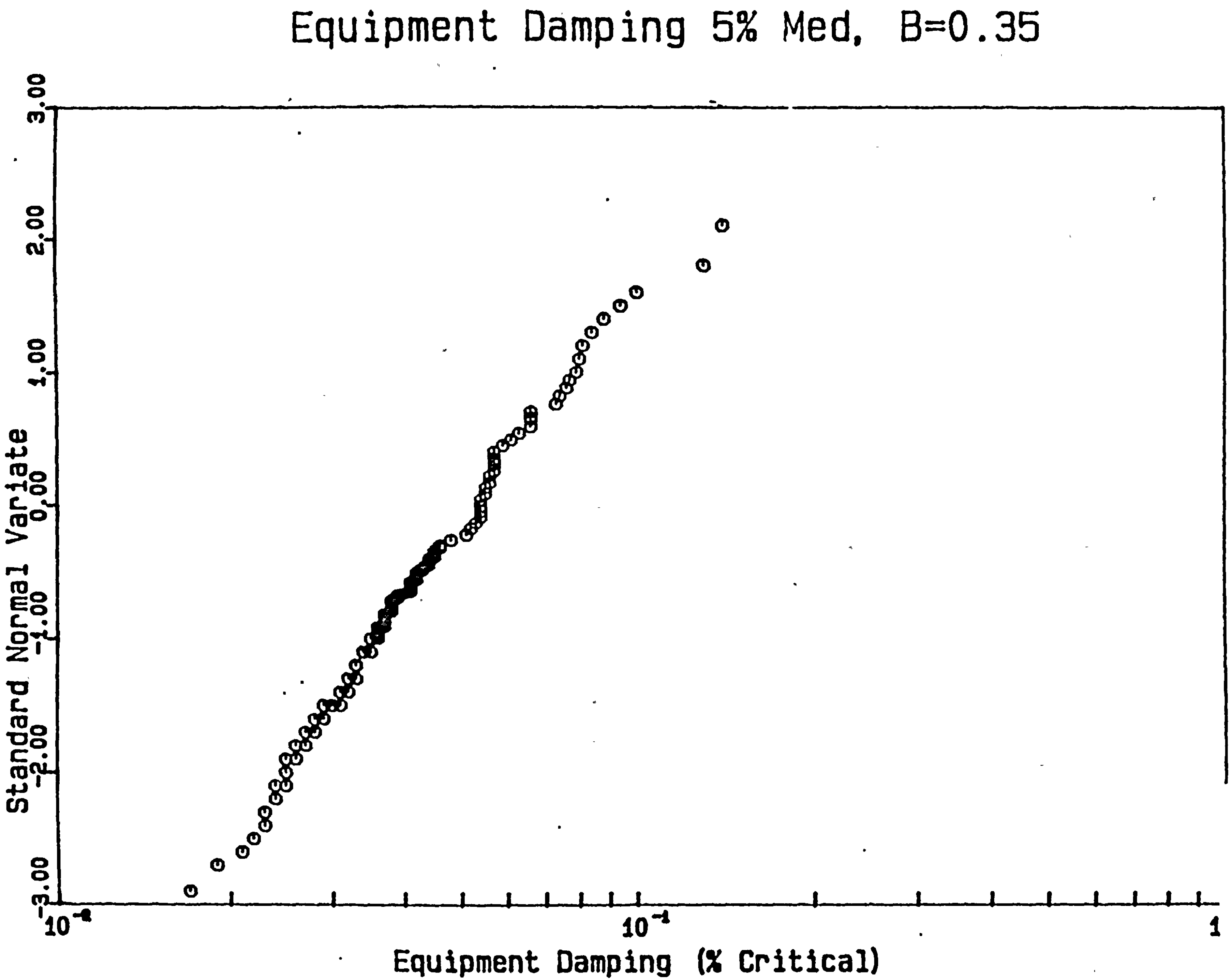

Figure 3. Monte Carlo Trials for Equipment Damping

1611-A

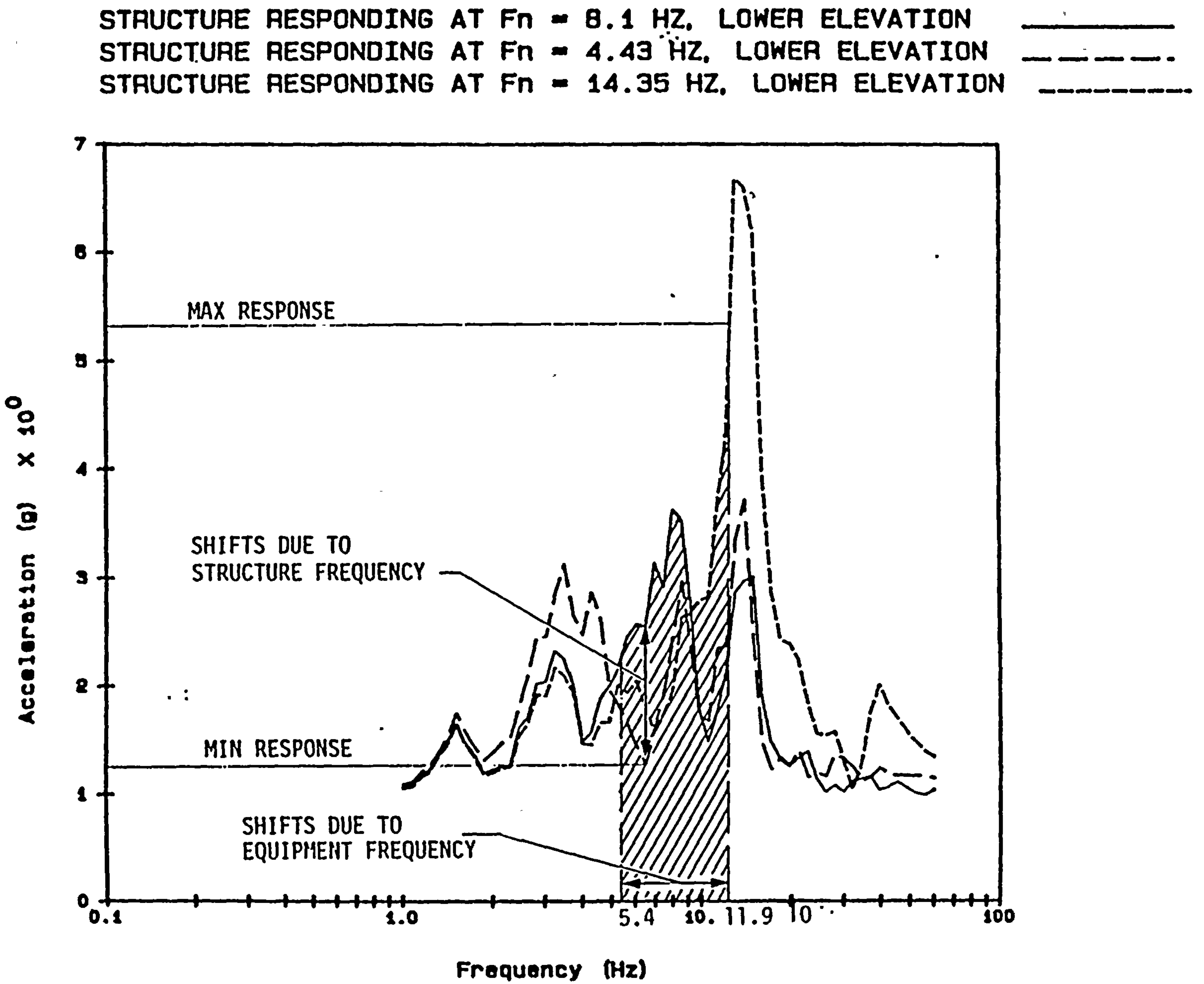

Figure 4. Shift in Response Due to Frequency Shift

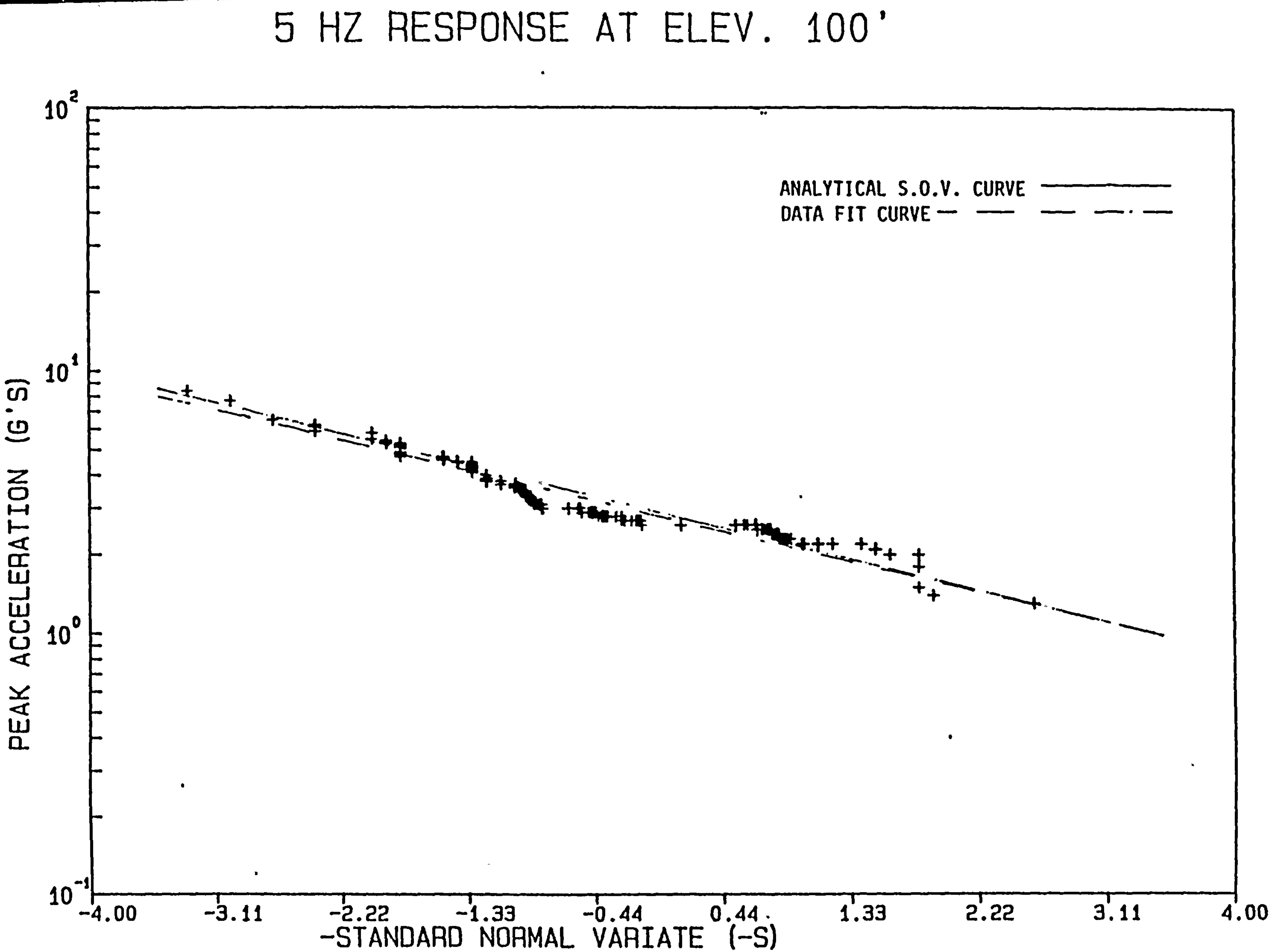

Figure 5. Equipment Response (5 hz item, Elevation 100')

B-33

1611-A

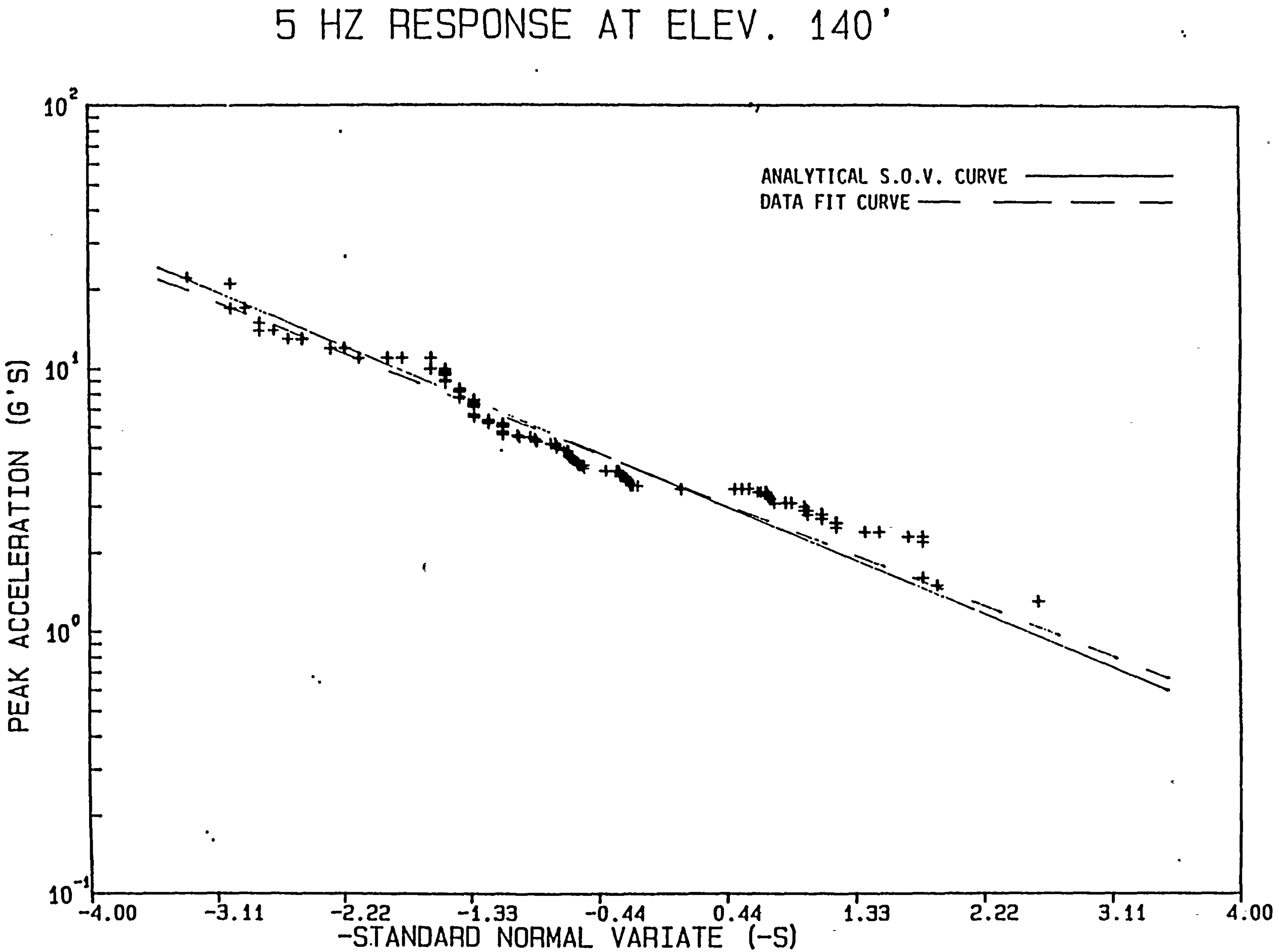

Figure 6. Equipment Response (5 hz item, Elevation 140')

1611-A

8 HZ RESPONSE AT ELEV. 100'

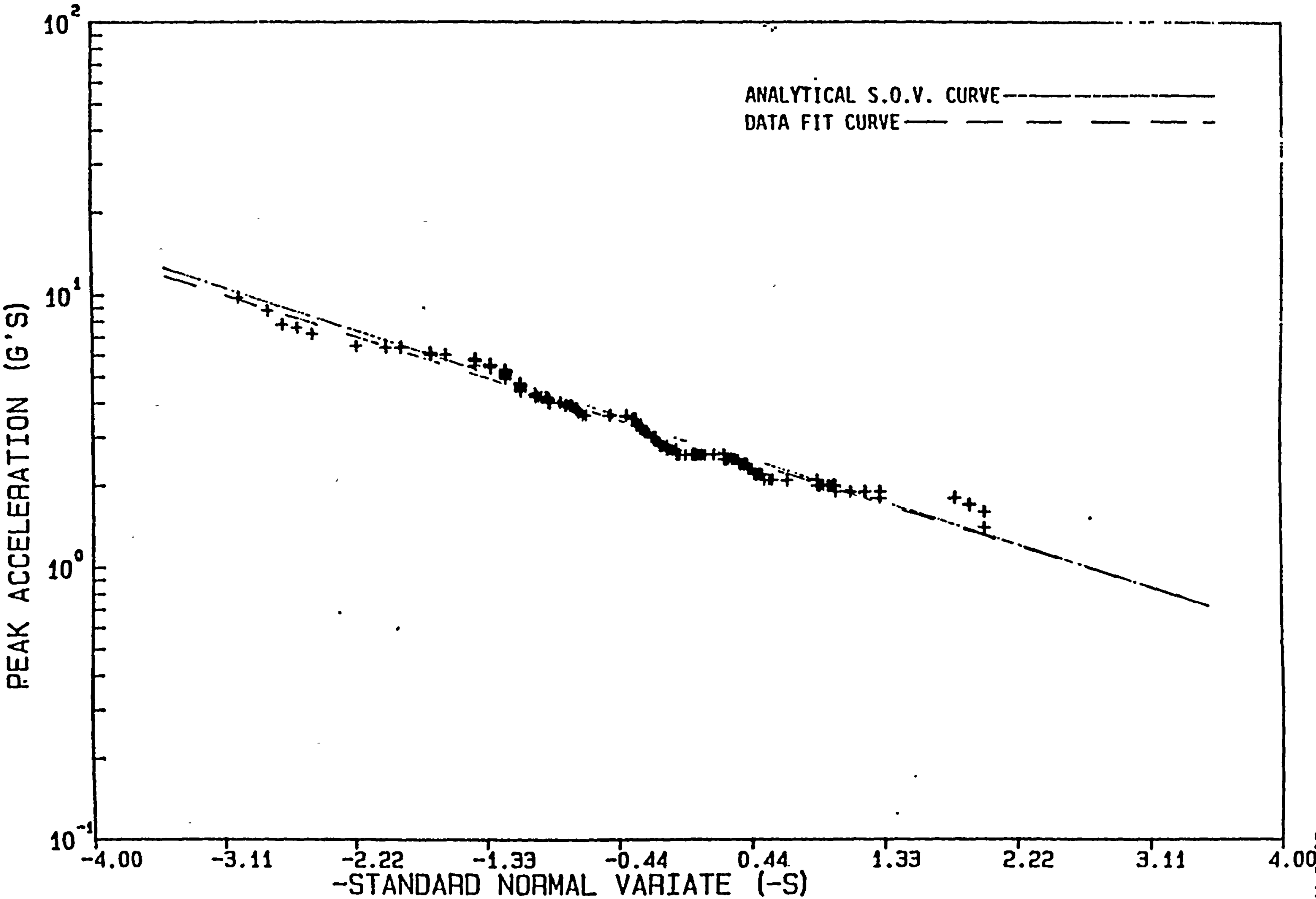

Figure 7. Equipment Response (8 hz item, Elevation 100')

B-35

1611-A

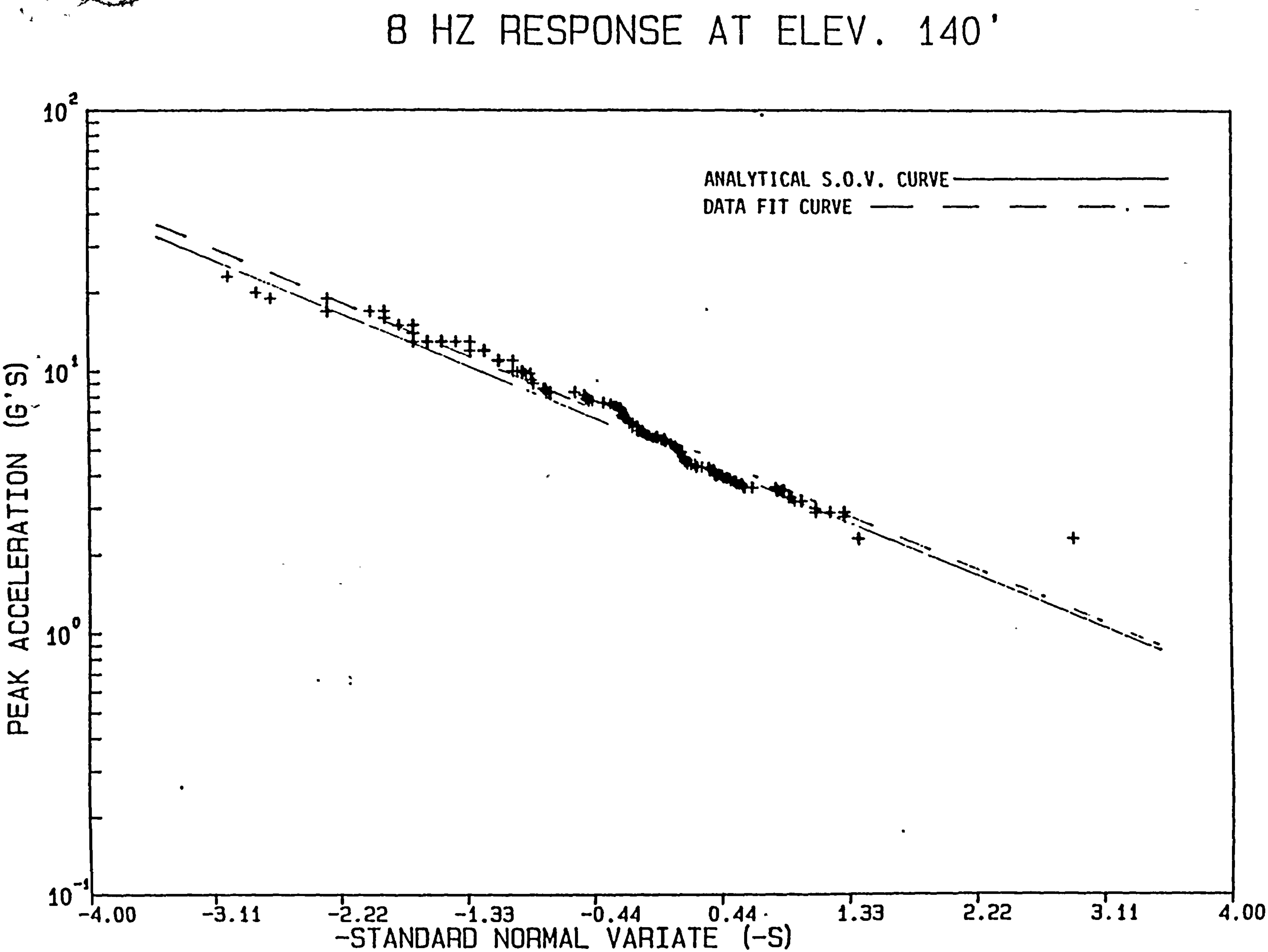

Figure 8. Equipment Response (8 hz item, Elevation 140')

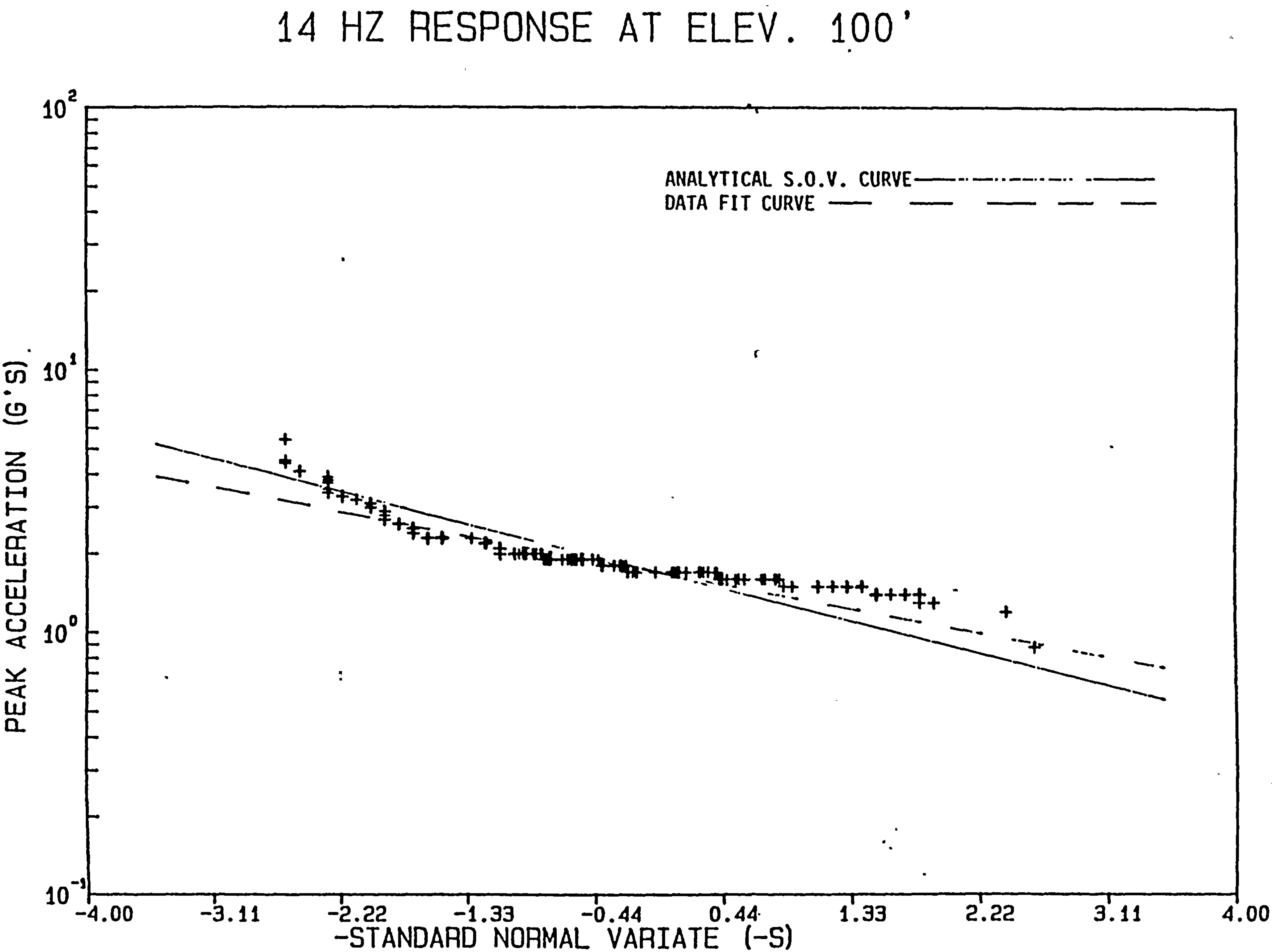

Figure 9. Equipment Response (14 hz item, Elevation 100')

1611-A

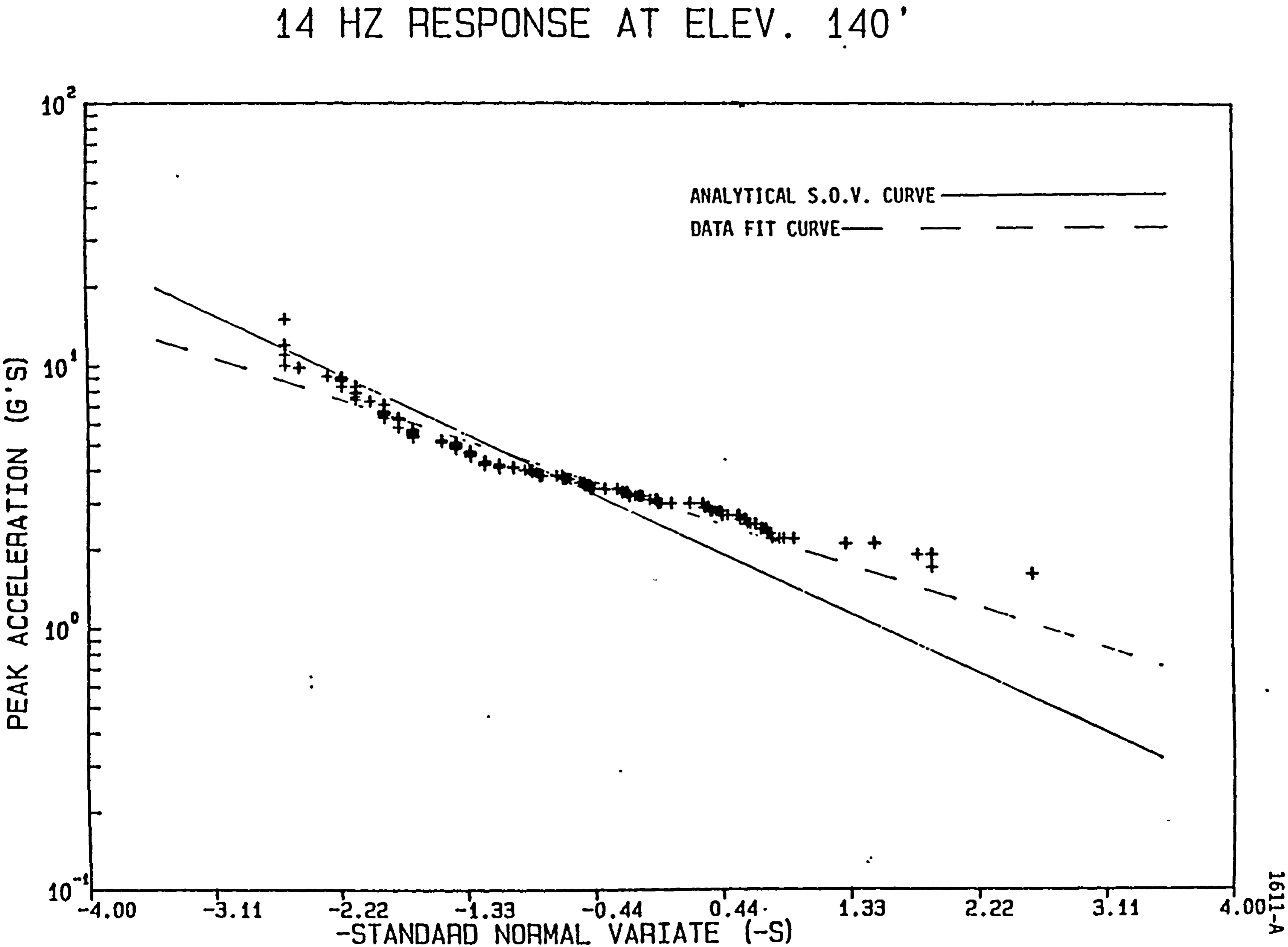

Figure 10. Equipment Response (14 hz item Elevation 140')

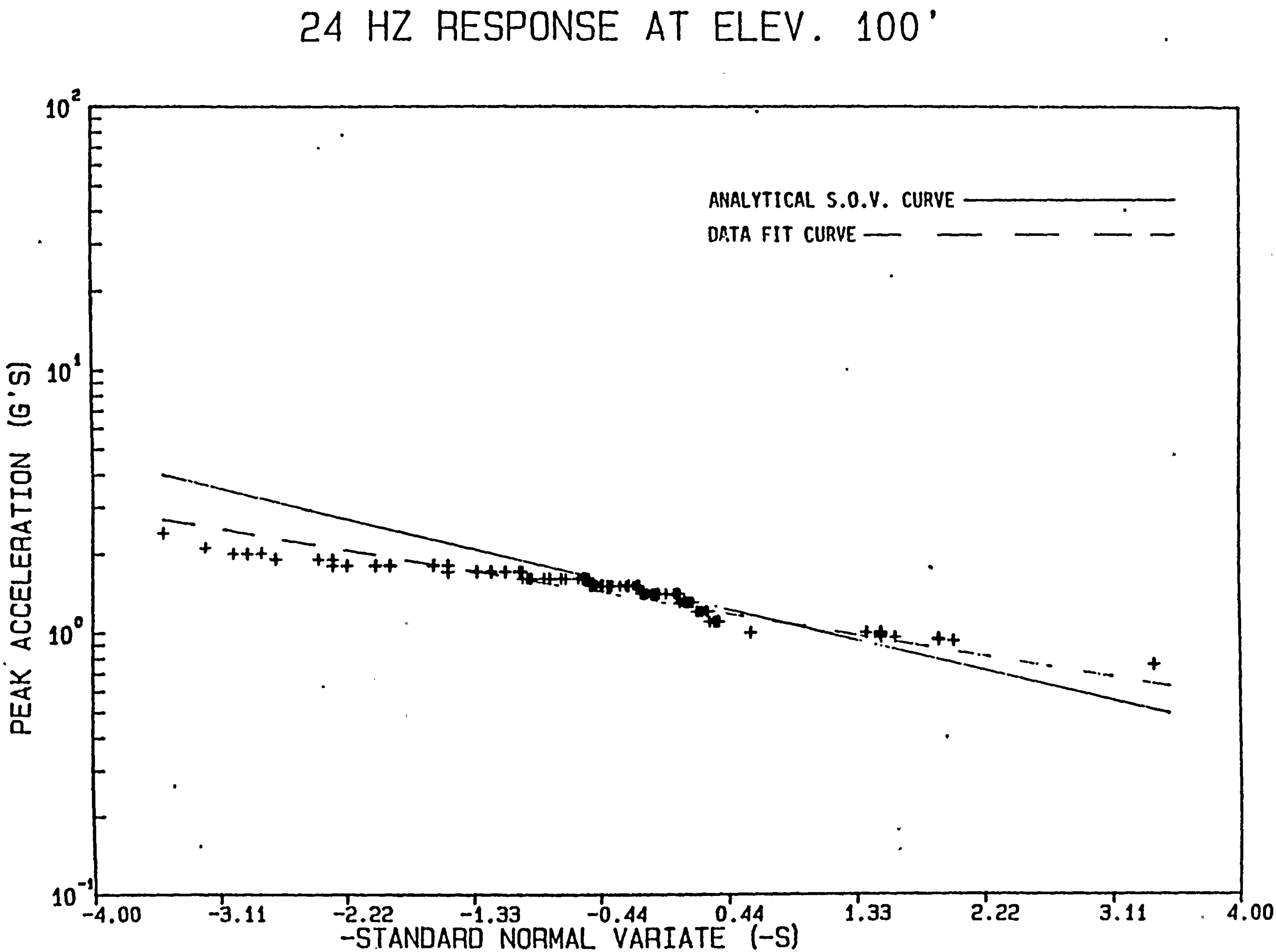

Figure 11. Equipment Response (24 hz item, Elevation 100')

1611-A

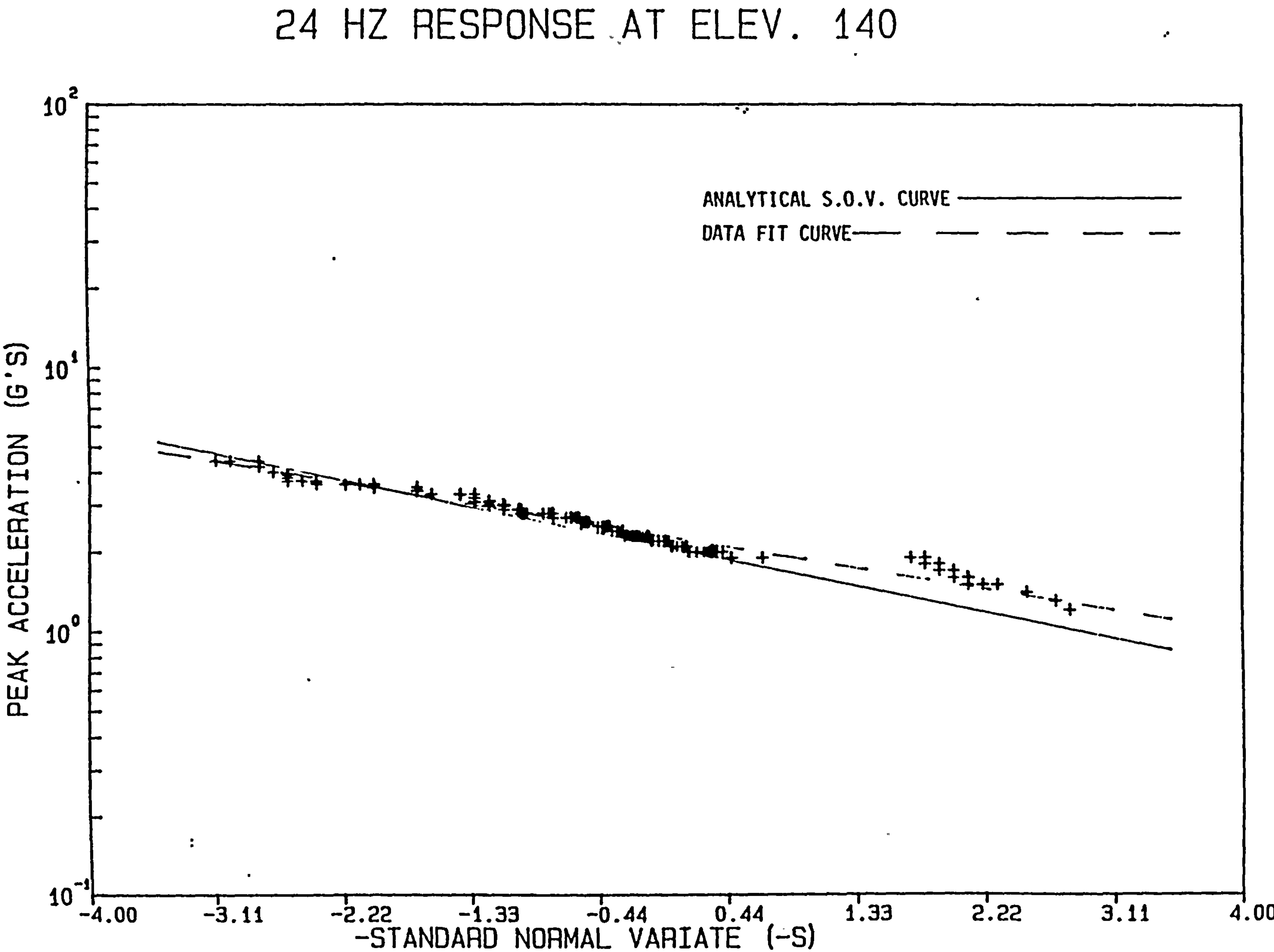

Figure 12. Equipment Response (24 hz item, Elevation 140')

1611-A

[illegible]

REFERENCES

1. Ang, Alfredo H-S., and Tang, Wilson H. 1975, Probability Concepts in Engineering Planning and Design. Vol I Basic Concepts, New York: John Wiley and Sons Inc.

2. Ang, Alfredo H-S., and Tang, Wilson H. 1984, Probability Concepts in Engineering Planning and Design. Vol II Decision, Risk, and Reliability. New York: John Wiley and Sons Inc.

3. Kennedy, R.P., and Ravindra, M.K. 1984, "Seismic Fragilities for Nuclear Power Plant Risk Studies", Nuclear Engineering and Design, Vol. 79, No. 1, May (I): pp. 47-68.

4. Kennedy, R.P., Cornell, C.A., Campbell, R.D., Kaplan, S., and Perla, H.F. 1980, "Probabilistic Seismic Safety Study of an Existing Nuclear Power Plant", Nuclear Engineering and Design, Vol. 59, No. 2, August: pp 315-338.

5. Kennedy, R.P., Campbell, R.D., Hardy, G., and Banon, H., 1982, "Subsystem Fragility, Seismic Safety Margins Research Program (Phase I)", NUREG/CR-2405, UCRL-15407. U.S. Nuclear Regulatory Commission, Washington, D.C.

6. Johnson, J.J., 1979, "Modsap. A Modified Version of the Structural Analysis Program SAP IV for the Static and Dynamic Response of Linear and Localized Nonlinear Structures", General Atomic Project 3273, June 1978. Document #GA-A14006 (Rev) UC-77.

7. Newmark, N.M., and Hall, W.J., 1977, "Development of Criteria for Seismic Review of Selected Nuclear Power Plants", NUREG/CR-0098, U.S. Nuclear Regulatory Commission, Washington, D.C.

8. Newmark, N.M., and Hall, W.J., 1982, "Earthquake Spectra and Design", Engineering Monographs on Earthquake Criteria, Structural Design, and Strong Motion Records, No. 3, Earthquake Engineering Research Institute, Berkeley, California.

9. Kenneally, R.M., and J.J. Burns, Jr., "Experimental Investigation Into the Seismic Behavior of Nuclear Power Plant Shear Wall Structures", Paper V-2, presented at the Symposium on Current Issues Related to Nuclear Power Plant Structures, Equipment and Piping, North Carolina State University, December 1012, 1986.

10. Thomson, W.T., 1981, Theory of Vibration with Applications, 2nd edition, Englewood Cliffs, New Jersey, Prentice-Hall Inc.

APPENDIX C
TURBINE BUILDING NONLINEAR ANALYSIS

C.1 Description of Problem

In Phase II of the Long Term Seismic Program (LTSP) for the Diablo Canyon Power Plant, the median seismic capacities of the civil structures were demonstrated to be quite high; above the 7g spectral acceleration cut-off except the turbine building. In addition, the Phase II fragility contained considerable uncertainty as a result of the unknown inelastic seismic load distribution between the major shear walls for seismic responses in the east-west direction.

Consequently, in Phase IIIA a simplified two dimensional inelastic model of the turbine building was developed to investigate the structure loads, load distributions and story drifts as well as develop in-structure response spectra for the structure at response levels close to failure. The model permitted inelastic response in the major E-W shear walls (Column Lines 19 and 31), the operating floor at EL 140', and the turbine pedestal, and allowed impact between the operating floor and the turbine pedestal. The computer code DRAIN-2D was used to perform the nonlinear time history analyses. A series of nonlinear analyses were performed with varying structure properties and earthquake ground motion in order to establish the turbine building median capacity and to obtain a better estimate on the uncertainty and randomness associated with the median capacity. The effects of uncertainty on important structure properties such as damping, stiffness and strength of the structural elements on the variability of the dynamic responses were considered by using the Monte Carlo technique. Randomness of the dynamic responses due to characteristics of earthquake ground motion was accounted for by using the 25 earthquake records which were used in the separation of variables (Appendix B) study. The median capacity of the turbine building was established using the shear story drift criteria which is an important indicator of structural damage of concrete shear walls.

[illegible]

C.2 Description of the Dynamic Model

The Unit 2 turbine building dynamic lumped mass model for the E-W response is presented in Figure C-1 and is superimposed on a schematic illustration of the turbine building in Figure C-2. This simplified two-dimensional model includes the two major E-W shear walls at column lines 19 and 31, the operating floor slabs at elevation 140', the turbine pedestal, and the gaps between the operating floor and the turbine pedestal represented by two gap elements. Floor and tributary wall mass was lumped at the floor elevations. Shear elements connecting the nodes were used to represent the properties of the shear walls at each story, the operating floor and the turbine pedestal. No soil-structure interaction effect was considered and a fixed base model was developed. Nodal coordinates of the model are given in Table C-1.

C.2.1 Mass Modeling

In developing the mathematical model, the mass of the structure was lumped at major floor elevations in accordance with conventional practice. The tributary wall mass was included. The effective mass of each of the beam-like portions of the operating floor diaphragm spanning from walls at lines 19 and 31, the slab between column lines 31 and 35, and the turbine pedestal was developed by the Diablo Canyon Project civil group (Reference C-1) for a single mass representation of each of these elements. The nodal masses of each lumped mass considered in the model are presented in Table C-2.

C.2.2 Stiffness Modeling

In computing the individual wall stiffnesses, the following median concrete properties were used:

$$E = 6.67 \times 10^5 \text{ ksf}$$
$$G = 2.85 \times 10^5 \text{ ksf}$$
$$\nu = 0.17$$

The uncracked flexural and shear stiffnesses of each story wall were computed by using the following equations:

$$\text{Flexural stiffness,} \quad K_f = \frac{12EI}{L^3}$$

$$\text{Shear stiffness,} \quad K_s = \frac{A_v G}{L}$$

where A_v and I are shear area and moment of inertia of the story wall and L is the height of the story. Effects of major cutouts in the wall such as door openings were considered in the stiffness calculations. No provisions were made for the additional stiffness of the embedded steel columns in the shear walls. This effect is expected to be small and tends to be offset by the stiffness decrease due to the displace concrete. The median effective wall stiffnesses accounting for cracking of the concrete and shear shape factor were estimated to be half of the uncracked stiffnesses. Table C-3 presents the effective wall stiffnesses of shear walls at lines 19 and 31.

For reinforced concrete shear walls which yield in shear under load reversals, pinching behavior is noted in the hysteresis loops due to opening and closing of the shear cracks. As shear cracks open wider and damage to the concrete increases, the concrete contribution to the shear

resistance decreases. A typical shear force-deformation diagram obtained during a structural wall test is shown in Figure C-3. This figure clearly illustrates the stiffness degradation and pinching of the hysteresis loops for a wall under the reverse cyclic loading. As a result, less hysteresis energy can be dissipated per cycle.

This pinching behavior of reinforced concrete shear walls failing in shear cannot be adequately modeled by either the bilinear or Takeda model. The inelastic shear element in the NTS version of the DRAIN code has a hysteretic behavior which realistically models the pinching behavior discussed above. The shear deformation hysteretic behavior of this inelastic shear element is defined by a set of 10 rules (Reference C-2) and is schematically shown in Figure C-4. Thus, each story of the walls at line 19 and line 31 was modeled by the DRAIN inelastic shear element in series with an element which has only flexural stiffness as shown in Figure C-1. This enables the separation of the shear deformation from the flexural deformation of the wall. The length of the inelastic shear element was limited to a very small fraction (0.01) of the story height in order to preserve the correct force-deflection properties of the flexural element.

The primary loading curve for the DRAIN inelastic shear element is shown in Figure C-5. The parameters used to define the primary loading curve are the effective shear stiffness, K_e, the second slope sK_e ($s = 0.03$) after yielding, and the yield shear force V_y. Other parameters used in the rules of the hysteretic behavior are:

Unloading stiffness parameter = 0.35
Strength degradation parameter = 0.95

For the operating floor and the turbine pedestal which were assumed to have flexural failure (Reference C-1) and the shear wall finite elements which have only flexural stiffness, the Takeda model with an unloading stiffness parameter, α, of 0.35 was used to represent the hysteretic behavior. The primary loading curves for the wall flexural elements are similar to that shown in Figure C-5. The effective flexural stiffnesses of these elements are given in Table C-3. The force-deformation curves for the operating floor diaphragm and the turbine pedestal were developed by the DCP civil group (Reference C-1) and are shown in Figures C-6 and C-7. The curves for the operating floor diaphragm account for different extent of concrete cracking at different load levels. Slightly different force-deformation curves were developed for east to west and west to east responses of the beam-like portions of the operating floor diaphragm due to nonuniform structural configurations. For the DRAIN input, the operating floor diaphragm force-deformation curve was approximated by a bilinear curve as shown in Figure C-6. Also, the same bilinear curve was used for both east to west and west to east responses of the diaphragm.

The impact between the operating diaphragm and the turbine pedestal was modeled by using the gap elements in DRAIN as shown in Figure C-1. At each time step, the gap element was checked for closing or opening and the stiffness was adjusted accordingly. The force-deformation curve of the gap element is shown in Figure C-8.

C.2.3 <u>Strength Modeling</u>

The yield shear force, V_y, in the primary loading curve of the shear wall element shown in Figure C-5 was defined as the shear force resisted by concrete only. Beyond V_y, additional shear is taken by the wall reinforcing steel. The concrete and wall reinforcing steel shear

capacities were evaluated by using the approach given in Section 4.1.1.3. Additional shear can be resisted by the embedded steel columns acting as dowels. One approach which converts the steel columns into equivalent concrete areas was considered to give median estimate of additional shear strength contributed by these columns.

The flexural capacities of the walls were evaluated by using Equation 4-10 with the effect of steel columns included. Contribution of the steel columns was limited by the column splices and anchor bolts. After the wall flexural capacities were evaluated, equivalent yield shear forces were estimated by using the elastic loads in the walls. These equivalent yield shear forces were used to define the primary loading curves for the the DRAIN wall elements which have flexural stiffness only. Table C-4 presents the yield shear forces of all the DRAIN elements for Walls 19 and 31.

C.3 Variability of Structure Properties

In order to study the dispersion in the response due to uncertainty in structure properties, a Monte Carlo technique was used in the turbine building nonlinear analysis. Important structure variables which would affect the structure response are: damping, stiffness, and strength. All three variables were assumed to have lognormal distributions with median and logarithmic standard deviations given below:

VARIABLE	MEDIAN	LOGARITHMIC STANDARD DEVIATION
DAMPING	7%	0.35
STIFFNESS FACTOR	1.0	0.50
STRENGTH FACTOR	1.0	0.25

[illegible]

Note that the stiffness and strength factors were used to scale the median stiffnesses and median strengths of the structural elements of the nonlinear model presented in Section C.2.

With the distributions defined, a value was then drawn at random from the distribution of each variable. For the turbine building nonlinear model, it was assumed that the stiffnesses and strengths of the two major shear walls cannot vary independently. However, among the walls, operating floor and the turbine pedestal the structure properties can vary independently. Table C-5 presents 50 sets of random variables for damping, stiffness factor and strength factor based on the above approach. Each set of these random numbers was used to adjust the median structure properties of the nonlinear model for a DRAIN analysis.

For the nonlinear time history analyses using DRAIN, the damping matrix is assumed to be of the following form:

$$[C] = \alpha[M] + \beta[K]$$

where

[C] = system damping matrix

[M] = system mass matrix

[K] = system stiffness matrix

α,β = damping parameters

For reinforced concrete structures at or just below the yield point, Reference C-3 recommends damping values between 7 and 10% of critical damping, the higher value being an average. However, energy dissipation when a structure goes into nonlinear response is primarily due to the hysteresis loops of the resistance function. To avoid possible double-counting of the hysteresis energy dissipation, the lower value, 7% was used for the median material damping in the study with potentially some resulting conservatism. For the material damping value generated for each Monte Carlo trial shown in Table C-5, a set of α and β damping parameters was selected by using the following equation:

λ = damping ratio at frequency f

$$= \frac{\alpha}{4\pi f} + \beta\pi f$$

The elastic natural frequencies of the turbine building DRAIN model for the given median structure properties are presented in Table C-6. For each Monte Carlo trial, the natural frequencies were estimated by scaling these median natural frequencies by the square roots of the appropriate stiffness factors.

C.4 Earthquake Ground Motion Input

The earthquake time history records used as input for the turbine building nonlinear analysis were the same 25 records used in the separation of variables check study (Appendix B). These records were representative of time histories which could be expected at the Diablo Canyon site for earthquakes with spectral accelerations of about 2 to 2.5g in the 3 to 8.5 Hz range. Use of these records in the time history analyses provided an estimate of variability of the structure response due to randomness of the input ground motion.

In preparing to input to DRAIN, the length of these earthquake records were reduced based on the 5-75% energy portions of the record which was recommended in Reference C-2. As a result, significant reductions in computation times were realized. The adequacy of the 5-75% energy fraction was demonstrated in Figures C-9 and C-10 where ground response spectra of the full length record and the truncated record of two earthquake time histories were compared.

C.5 Nonlinear Analyses

A series of DRAIN·nonlinear analyses were performed with the turbine building inelastic model in order to establish the median capacity and the variabilities. Variability in the structure response due to randomness in earthquake motion was included by using the 25 representative earthquake time histories as input ground motion. Three levels of input ground motion were considered for the nonlinear analyses. Each of the 25 records was scaled such that the 5% damped spectral acceleration averaged over the 3 to 8.5Hz frequency range was at 3g, 4g or 6g. For each specified level of input ground motion, a total of 50 Monte Carlo trials (DRAIN runs) were made. The 25 scaled records were used as input ground motion for trials 1 through 25 and were repeated for trials 26 through 50. For each of the 50 trials, structure properties were varied as discussed in Section C.3 in order to study the dispersion on the structure response due to variability of structure properties. Additional DRAIN runs with median structure properties were performed in order to separate variabilities on the repsonse due to uncertainty and randomness. The 25 scaled records were used as input such that variability due to earthquake randomness alone can be established. The following table summarizes all the DRAIN runs performed in the turbine building nonlinear study.

[illegible]

[illegible]

[illegible]

	SPECTRAL ACCELERATION LEVELS		
	3g	4g	6g
VARY EARTHQUAKE MOTION AND STRUCTURE PROPERTIES	50 RUNS	50 RUNS	50 RUNS
VARY EARTHQUAKE MOTION ONLY	25 RUNS	---	25 RUNS

For all nonlinear analyses, the direct integration of the equations of motion was performed using a technique which assumes constant acceleration within the time step. This method has the advantage of being stable for all frequencies and time steps and of not introducing damping into the system. The disadvantage of this method is that smaller integration time steps may be necessary than would be needed for more sophisticated integration methods. An integration time step of 0.005 seconds was utilized. This time step is generally expected to provide good accuracy for frequencies up to about 40 Hz. As a check on the accuracy of the selected time step, a sample analysis was performed using a time step of 0.0025 seconds. A comparison of structure response indicated that differences in quantities of interest were not significant so that the larger time step was judged to be adequate. At higher spectral acceleration levels, smaller time step size of 0.0025 seconds was used for some trials in order to achieve better convergence.

C.6 Structure Response

C.6.1 Story Drift Criteria

In doing a seismic fragility analysis, the factor of safety and the response levels have mainly been measured by stress or force

[illegible]

amplitudes. The seismic forces were generally estimated from the ductility modified response spectrum method and the structure strength was evaluated by using equations developed from test results such as the case for shear capacity of concrete shear walls. The estimated shear strength does not reflect the actual load level at which the wall collapses under the lateral force. Instead, this capacity predicts the load which damages the wall to the extent that equipment supported on the wall could lose its anchorage. For the turbine building walls at lines 19 and 31 where there is no safety-related equipment supported, the median capacity estimated by this approach tends to be conservative.

An alternative approach which is considered to be appropriate to use for estimating the turbine building shear wall median capacity is based on the shear story drift. The shear story drift is defined as the relative shear deformation of the wall between floors divided by the story height. Measurements in the laboratory and in the field have shown that damage to stiff low walls can be related to the story drift. Based on a large variety of studies summarized in References C-4 and C-5, the story drifts corresponding to shear failure of reinforced concrete shear walls varied from 0.5% to 1.0%. In consideration of the wall configuration and reinforcing steel, the effects of embedded steel columns, and the influence of axial load, a median shear story drift at failure of 0.7% was judged to be median centered for the turbine building shear walls at lines 19 and 31. It was also assumed that the shear story drift has a lognormal distribution. The turbine building median capacity was then estimated based on this median story drift at failure.

[illegible]

C.6.2 Median Capacity and Variability

The median capacity and the variability of the turbine building were estimated by using the shear story drift criteria in Section C.6.1 and the DRAIN nonlinear time history analysis results. As discussed in Section C.5, three sets of 50 DRAIN runs were made at spectral acceleration levels of 3, 4 and 6g in which both structure properties and earthquake ground motion were varied. As a result, dispersion in the structure response estimated from on these runs would represent a composite variability including both uncertainties in structure properties and randomness in the earthquake motion. From the two sets of 25 DRAIN runs at 3g and 6g levels, dispersion in the response due to earthquake randomness alone was estimated. The median capacity was estimated from all five sets of DRAIN analyses. At high response levels, DRAIN results indicated a significant shift in load from Wall 19 to Wall 31 such that at failure level, the lower story of Wall 31 was found to be the controlling element. Therefore, evaluation of the turbine building capacity was performed using the shear story drift of the lower story of Wall 31.

At each of the specified input spectral acceleration levels, an averaged probability of failure of Wall 31 was evaluated by averaging the probability of failure of each of the 50 Monte Carlo trials based on the story drift. The probability of failure for the 3g spectral acceleration case is given below as an example.

> At 0.7% story drift, the probability of failure of Wall 31 = 0.50
> At 0.5% story drift, the probability of failure is estimated at 0.16.

[illegible]

Thus, the composite logorithmic standard deviation ($(\beta_C)_\Delta$ value) of the story drift is estimated to be

$$(\beta_C)_\Delta = \frac{-1}{1.0}\ \ln\left(\frac{0.5}{0.7}\right) = 0.34$$

With the lower story drift of Wall 31, Δ_i, computed in each trial, the probability of failure can be found from the normal probability table with the variable u, where

$$u = \frac{1}{(\beta_C)_\Delta}\ \ln\left(\frac{\Delta_i}{0.7}\right)$$

For story drifts less than 0.25%, it is judged that there is essentially no probability of failure. The averaged probability of failure of all 50 trials was found to be 11% for the 3g case.

In a similar fashion, the average probabilities of failure for input ground motions at 4g and 6g spectral accelerations were found to be 34% and 75% respectively. The table below summarizes the probabilities of failure at the three spectral acceleration levels considered in this study

S_A (g)	PROBABILITY OF FAILURE
3	11%
4	34%
6	75%

Given these probabilities of failure corresponding to different spectral accelerations, a composite fragility curve for Wall 31 of the turbine building was defined and expressed by a median spectral acceleration capacity, $\check{S}_A$ and a composite variable, ϵ_C where ϵ_C is a

lognormal random variable with unity median and logarithmic standard deviation β_C given by:

$$\beta_C = \sqrt{\beta_R^2 + \beta_U^2}$$

The median spectral acceleration capacity and the composite logarithmic standard deviation for this failure mode were found to be:

$$\check{S}_A = 4.64g$$

$$\beta_C = 0.36$$

The β_R associated with the median capacity due to randomness in the earthquake motion was evaluated using the DRAIN results from the 25 runs in which only the ground motion was varied. No uncertainty in the structure properties was involved in these runs since median properties were used. Thus, β_U is equal to zero. The median story drift at failure remains unchanged at 0.7%. Variability associated with this median story drift includes both uncertainty and randomness. It was estimated that the 0.5% story drift is at about 2.24β from the median drift when only randomness was considered. Thus, $(\beta_R)_\Delta$ in the story drift was estimated to be 0.15.

Given the median story drift at failure and its logarithmic standard deviation $(\beta_R)_\Delta$, the averaged probabilities of failure of Wall 31 at different input levels accounting for randomness only were calculated as shown below:

S_A (g)	PROBABILITY OF FAILURE
3	3.1%
6	88%

[illegible]

Based on these data points the logarithmic standard deviation β_R associated with the median spectral acceleration capacity of Wall 31 was estimated to be 0.23. The β_U was found to be $\sqrt{0.36^2 - 0.23^2} = 0.28$.

It is to be noted that the β_R and β_U discussed above accounted for both randomness and uncertainty associated with the various factors considered in the fragility study such as strength, inelastic energy absorption, spectral shape, damping, modeling and modal combination. What were not included in the turbine building nonlinear analyses are the effects of combination of earthquake components and soil-structure interaction. For Wall 31, shear force due to ground motion in the north-south direction is not expected to be significant. Consequently, the median factor of safety on earthquake component combination considered in this study is unity and a nominal value of 0.05 was estimated for β_R. The factor of safety on the soil-structure interaction in consideration of the statistical incoherence from the ground motion wave was found to be 1.03 based on the discussion in Section 3.3.3. The coefficient of variation was found to be 0.05. Thus, the median capacity of the turbine building controlled by the wall at line 31 and its variability are:

$$S_A = 4.64 \underbrace{(1.03)}_{\text{SSI effect}} = 4.8g$$

$$\beta_R = (0.23^2 + \underbrace{0.05^2}_{\text{Earthquake components combination}})^{1/2} = 0.24$$

$$\beta_U = (0.28^2 + \underbrace{0.05^2}_{\text{SSI effect}})^{1/2} = 0.28$$

Table C-1. Turbine Building Nonlinear Model Nodal Coordinates

NODE NO.	X-COORDINATE (FT)	Y-COORDINATE (FT)
1	0.	0.
2	.19	0.
3	19.19	0.
4	19.38	0.
5	38.38	0.
6	38.55	0.
7	55.55	0.
8*	55.55	49.42
9*	55.55	-49.42
10	189.16	49.42
11	189.16	-49.42
12	189.16	0.
13**	322.77	49.42
14**	322.77	-49.42
15	244.16	0.
16	322.77	0.
17	343.77	0.
18	343.98	0.
19	355.98	0.
20	356.10	0.
21	378.10	0.
22	378.32	0.

* Slaved to Node 7

** Slaved to Node 16

Table C-2. Nodal Masses of Turbine Building Nonlinear Model

NODAL NO.	WEIGHT (KIPS)	COMMENT
3	1,573	WALL 19 AND FLOOR AT EL 104
5	832	WALL 19 AND FLOOR AT EL 123
7	4,219	WALL 19 AND OPERATING FLOOR*
10	2,250	OPERATING FLOOR*
11	2,250	OPERATING FLOOR*
12	25,000	TURBINE PEDESTAL*
16	6,331	WALL 31 AND OPERATING FLOOR*
18	2,130	WALL 31 AND FLOOR AT EL 119
20	2,460	WALL 31 AND FLOOR AT EL 107

*Reference C-1

Table C-3. Effective Shear and Flexural Stiffness of Shear Walls

CONCRETE SHEAR WALL	EFFECTIVE SHEAR STIFFNESS (KIPS/FT)	EFFECTIVE FLEXURAL STIFFNESS (KIPS/FT)
WALL 19		
EL 140 - EL 123	1.14×10^6	6.13×10^7
EL 123 - EL 104	1.22×10^6	7.55×10^7
EL 104 - EL 85	2.25×10^6	5.05×10^7
WALL 31		
EL 140 - EL 119	1.71×10^6	24.2×10^7
EL 119 - EL 107	3.10×10^6	99×10^7
EL 107 - EL 85	1.60×10^6	16×10^7

Table C-4. Yield Shear Forces (V_y) of Shear Wall Elements

CONCRETE SHEAR WALL	YIELD SHEAR FORCE (KIPS)	
	INELASTIC SHEAR ELEMENT	ELEMENT WITH FLEXURAL STIFFNESS ONLY
WALL 19		
EL 140 - EL 123	10600	13690
EL 123 - EL 104	11020	11220
EL 104 - EL 85	9230	14120
WALL 31		
EL 140 - EL 119	13230	30690
EL 119 - EL 107	17050	24770
EL 107 - EL 85	14890	22290

Table C-5. Variables of Model Structure Properties

TRIAL NO.	SYSTEM DAMPING VALUE	STIFFNESS FACTOR			STRENGTH FACTOR		
		SHEAR WALLS	OPERATING FLOOR	TURBINE PEDESTAL	SHEAR WALLS	OPERATING FLOOR	TURBINE PEDESTAL
1	.0601	.9343	.8421	1.4495	1.1481	.9319	1.1148
2	.0793	1.0607	.9839	.6679	1.0732	.9263	1.2484
3	.1155	.9275	1.0205	.4355	.9692	1.8888	1.0005
4	.1009	1.0914	1.7003	.7948	.8729	1.2734	1.0282
5	.1023	2.1317	1.5155	1.2248	1.4069	1.1721	1.1336
6	.0582	3.0935	.6578	1.3189	.6618	1.3248	1.4670
7	.0585	1.0504	1.1815	.5977	1.0734	.7686	1.4773
8	.0568	.9974	1.5550	1.0877	1.2396	.7181	.7032
9	.0684	1.5548	.5104	.8385	1.3007	1.2217	1.5525
10	.0698	1.1254	1.3876	2.2731	1.4946	.8750	.7939
11	.0704	.4634	1.1817	.4356	.7953	1.0006	1.1623
12	.1493	1.4327	1.3365	1.3245	.9122	1.0389	1.5407
13	.0572	.6004	1.3288	1.0898	.7238	.8229	1.1988
14	.0927	1.5996	.9293	2.1709	.9210	1.3397	1.3248
15	.1123	.4682	1.0784	.6464	.8982	.6652	.8286
16	.0652	1.2137	1.0849	1.1087	.7419	1.4439	.8299
17	.1053	1.1349	1.7651	2.0897	.6416	1.1718	.9177
18	.0609	2.1395	.9588	.5845	1.0878	.8770	.9039
19	.1096	1.2604	1.6396	2.5241	1.1662	1.6452	1.1995
20	.1074	1.6790	.8242	2.5171	.8942	.8675	1.0032
21	.0596	.6275	.7439	.6320	.8245	.7250	.7423
22	.0760	1.0896	1.0855	.5099	.8584	1.4128	1.0756
23	.1369	3.5920	.8568	1.3599	1.2019	.9804	1.1332
24	.0831	1.0797	.9291	.6403	1.5220	.5480	1.0474
25	.1240	1.0087	.9222	1.8344	.6911	.6206	1.0911
26	.0772	.5653	.8310	.8607	1.0071	.8561	.8499
27	.1136	1.3648	.5680	.6208	1.3277	.7726	1.3637
28	.0910	.6796	1.1320	1.4513	.9571	1.0147	.7058
29	.0496	2.2296	1.8930	1.1704	1.0630	1.1235	1.3609
30	.0486	.9323	3.7765	2.3605	1.4893	.6491	1.6148
31	.0538	.4250	.5502	2.0228	1.1503	.6496	.9712
32	.1009	1.1350	.5983	2.5905	.8772	.8909	.6511
33	.0949	.8769	2.0427	.9961	.7191	1.2164	.6773
34	.0365	1.1243	1.9010	.7875	1.5064	.7779	1.0995
35	.1507	1.6397	3.7699	1.4291	.9167	1.0773	1.2275
36	.0334	.8274	.9919	.5106	.9336	1.0267	.6908
37	.0523	.6222	1.4331	.9317	.9753	.8322	1.2863
38	.0357	.6568	1.4558	1.4051	.9462	1.0556	1.5023
39	.0603	1.0507	1.2858	1.2992	1.0741	.6953	.8159
40	.0753	.9401	1.7601	1.0112	.7298	.7261	1.5294
41	.0637	1.2690	.8582	.8481	.8885	.7238	.8793
42	.0391	.5772	.8199	.9413	.5133	.8863	1.2748
43	.1107	1.1182	1.3084	.4553	.9878	1.1935	1.1383
44	.1180	2.6135	.8649	1.0102	.7662	1.1832	.9608
45	.1142	3.3185	1.5687	.8905	1.1715	.9960	.9420
46	.1162	.8227	1.1102	.7581	.8490	1.6054	.7599
47	.0783	1.0485	3.6193	.9812	1.0399	1.2617	.8452
48	.0538	1.3066	.6226	.5341	.8526	1.0049	.9262
49	.0403	.6810	1.2759	.5473	1.1852	1.0856	1.2072
50	.0616	.3445	.4155	.8854	1.1008	1.1917	1.2165

1611-A

[illegible]

Table C-6. Elastic Modal Properties of the Turbine Building Model with Median Structure Properties

MODE	NATURAL FREQUENCY (HZ)	REMARKS
1	3.1	TURBINE PEDESTAL
2	4.0	OPERATING FLOOR
3	8.6	WALL AT LINE 31
4	9.5	WALL AT LINE 19

[illegible]

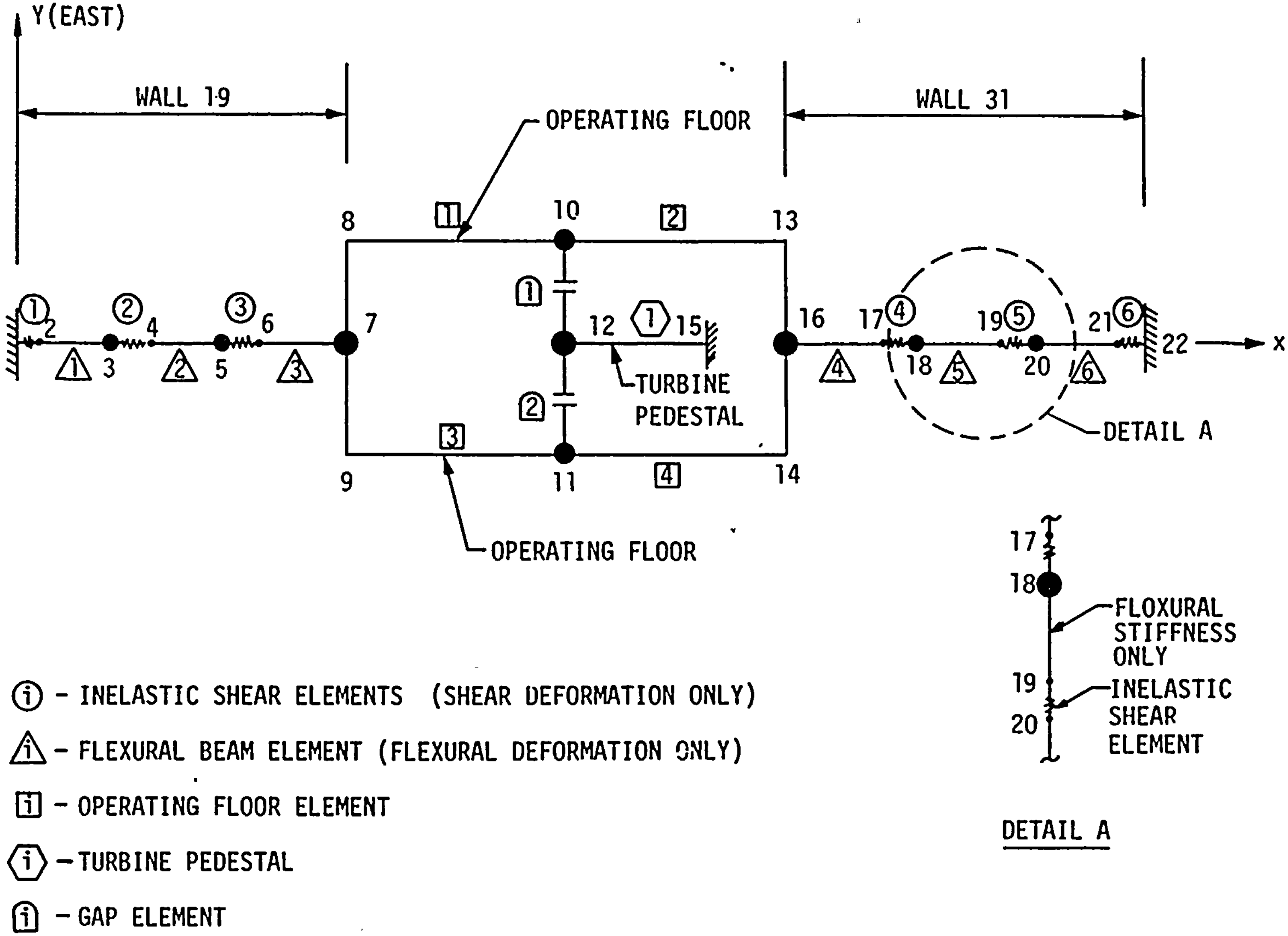

Figure C-1. Diablo Canyon Turbine Building DRAIN-2D Model

1611-A

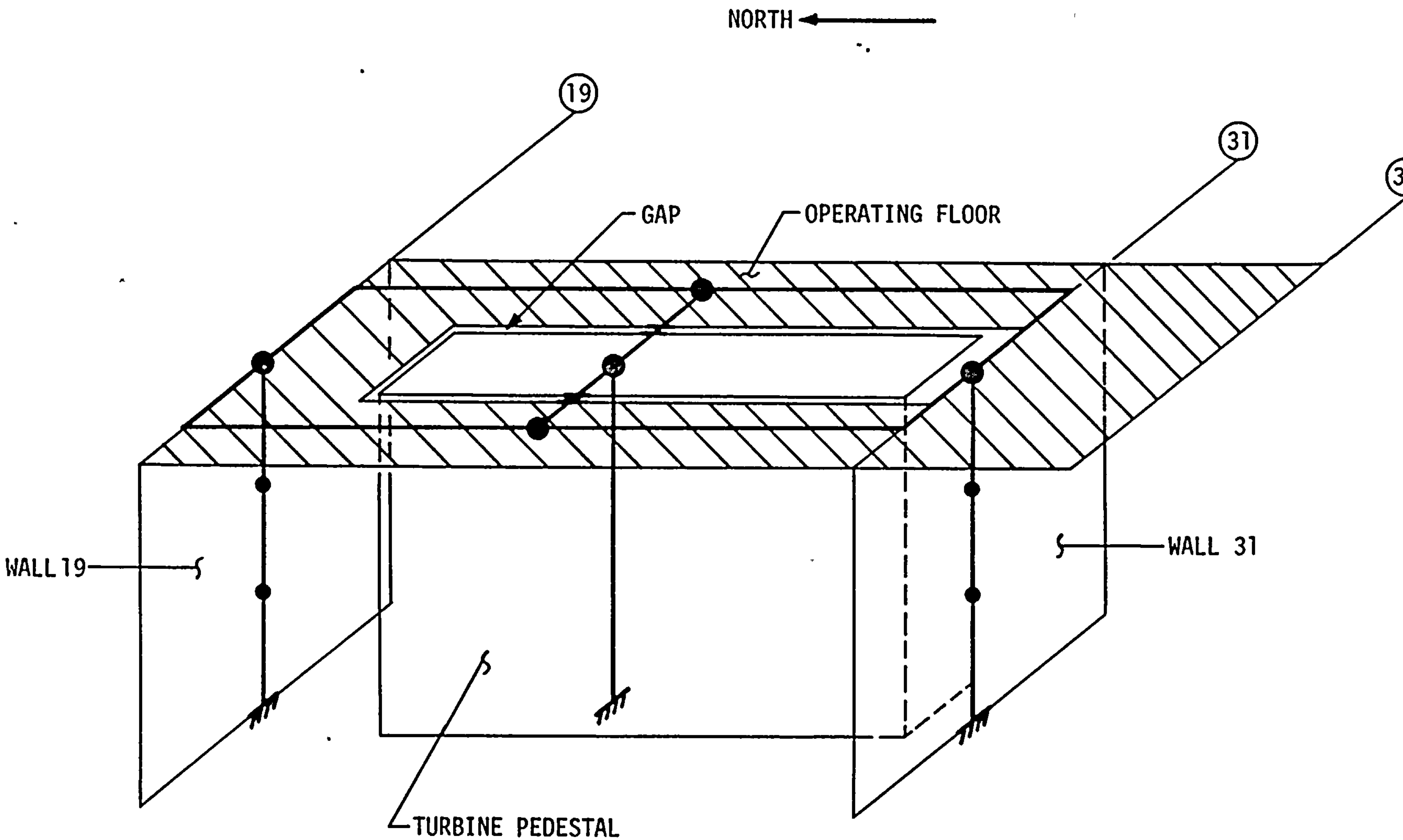

Figure C-2. Schematic Illustration of Turbine Building Nonlinear Model

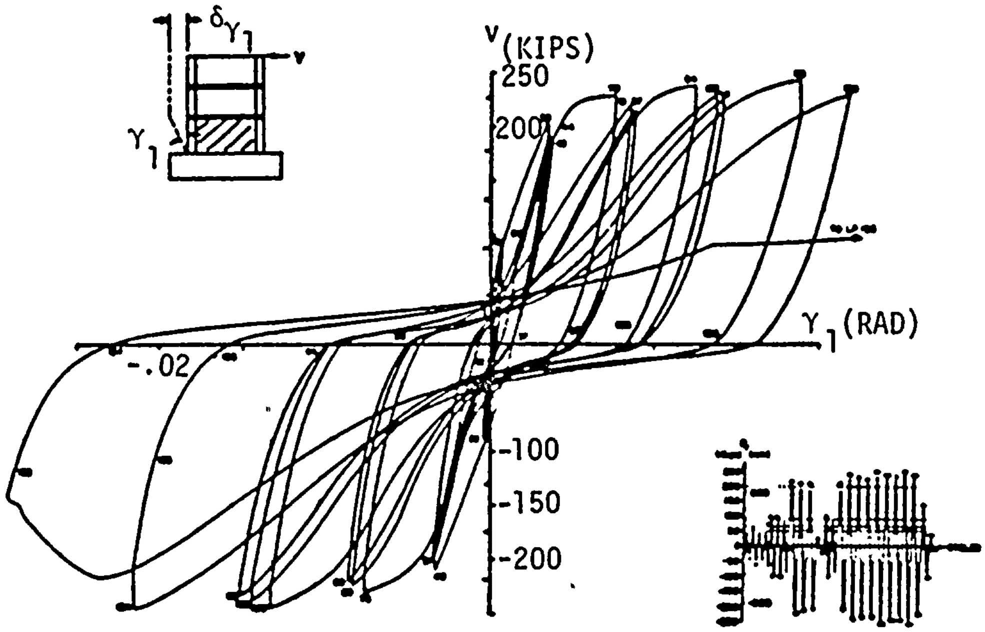

SHEAR FORCE-SHEAR DISTORTION DIAGRAM FOR STRUCTURAL CONCRETE WALL TEST (WANG, BERTERO, POPOV; 1975)

Figure C-3. Cyclic Load-Deflection Behavior of Concrete Shear Walls

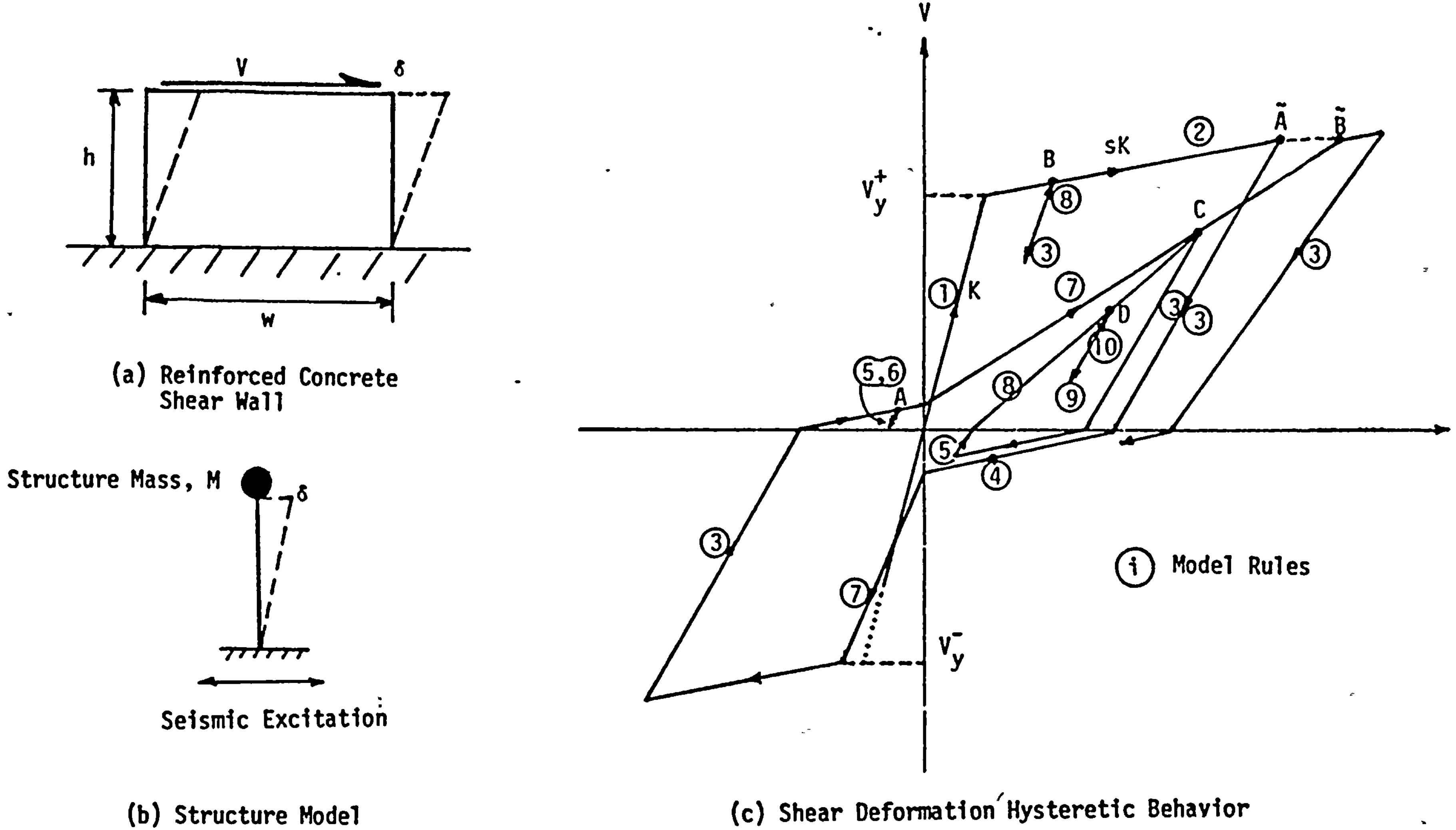

Figure C-4. Shear Wall Structure Model and Corresponding Hysteretic Deformation Behavior

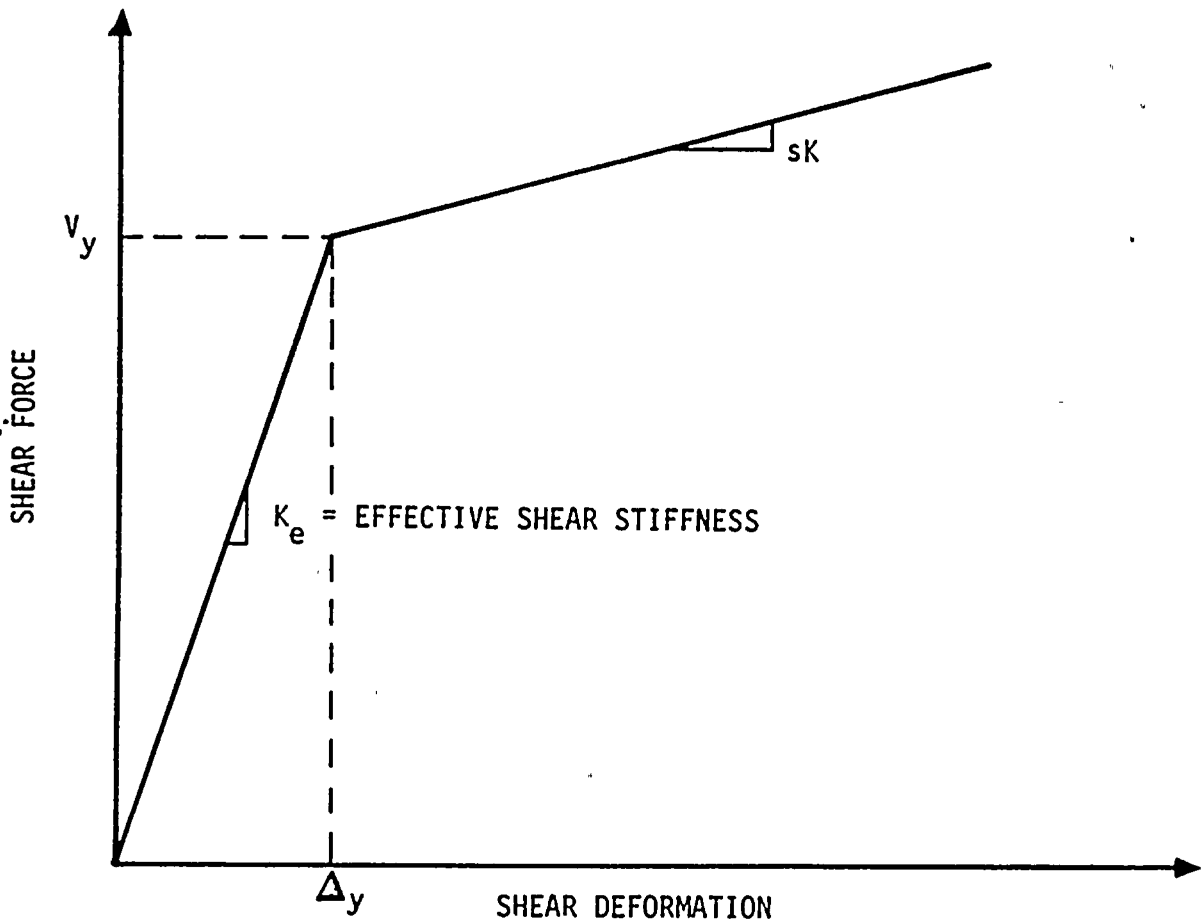

Figure C-5. Primary Loading Curve For DRAIN Inelastic Shear Element

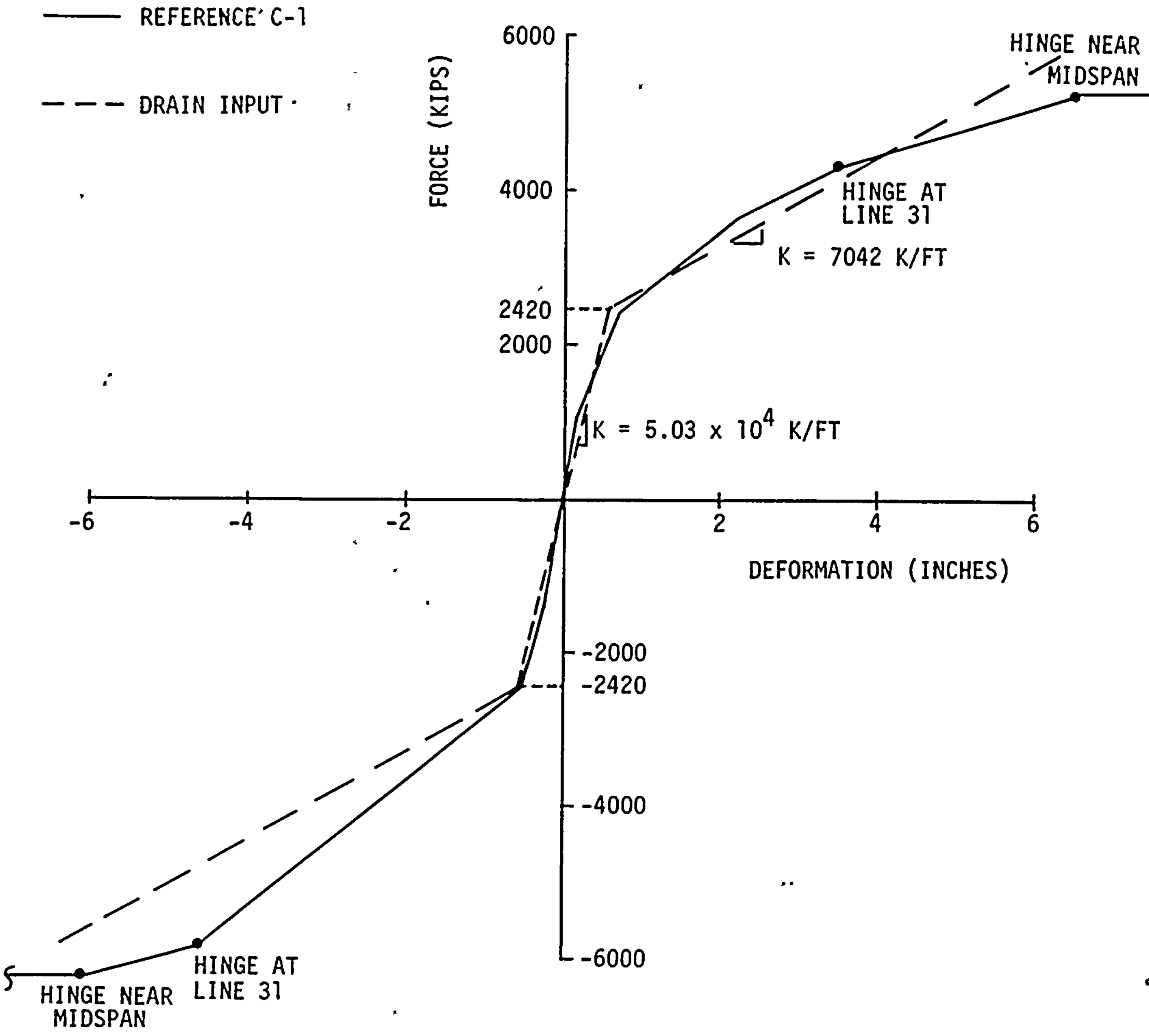

Figure C-6. Force-Deformation Curve of the Beam-Like Portion of the Operating Diaphragm at the Midspan (Reference C-1)

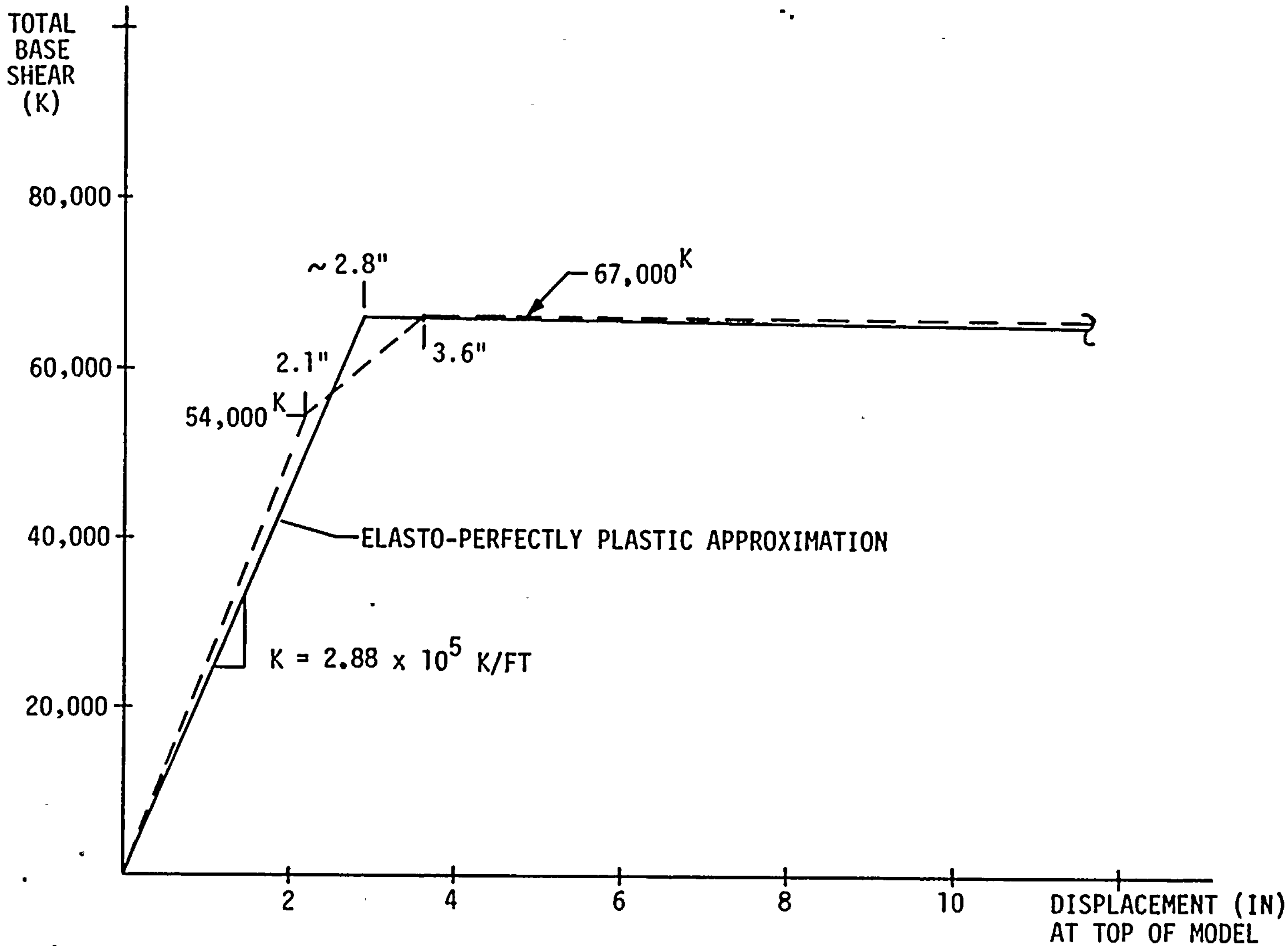

Figure C-7. Shear-Deformation Curve of the Turbine Pedestal (Reference C-1)

1611-A

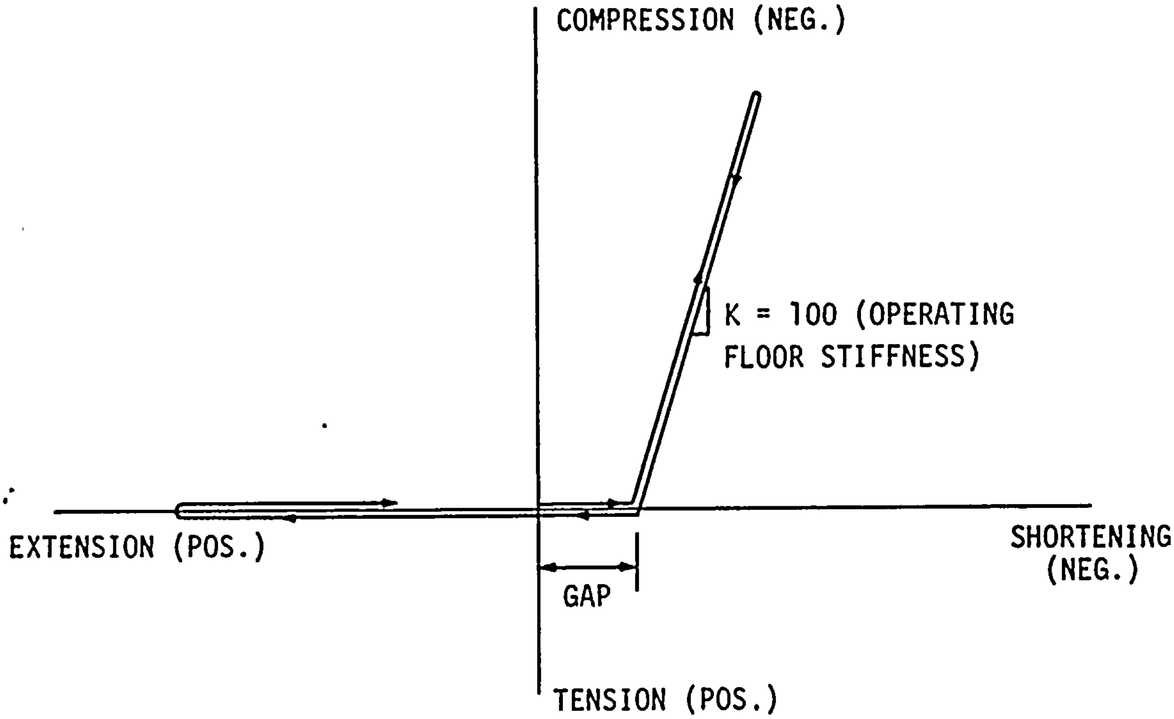

Figure C-8. Gap Element Force-Deformation Curve

BAZLI, U.S.S.R. 17 MAY 1976 KARAKYR POINT, COMP NORTH SCALED TO 3.08 5.0

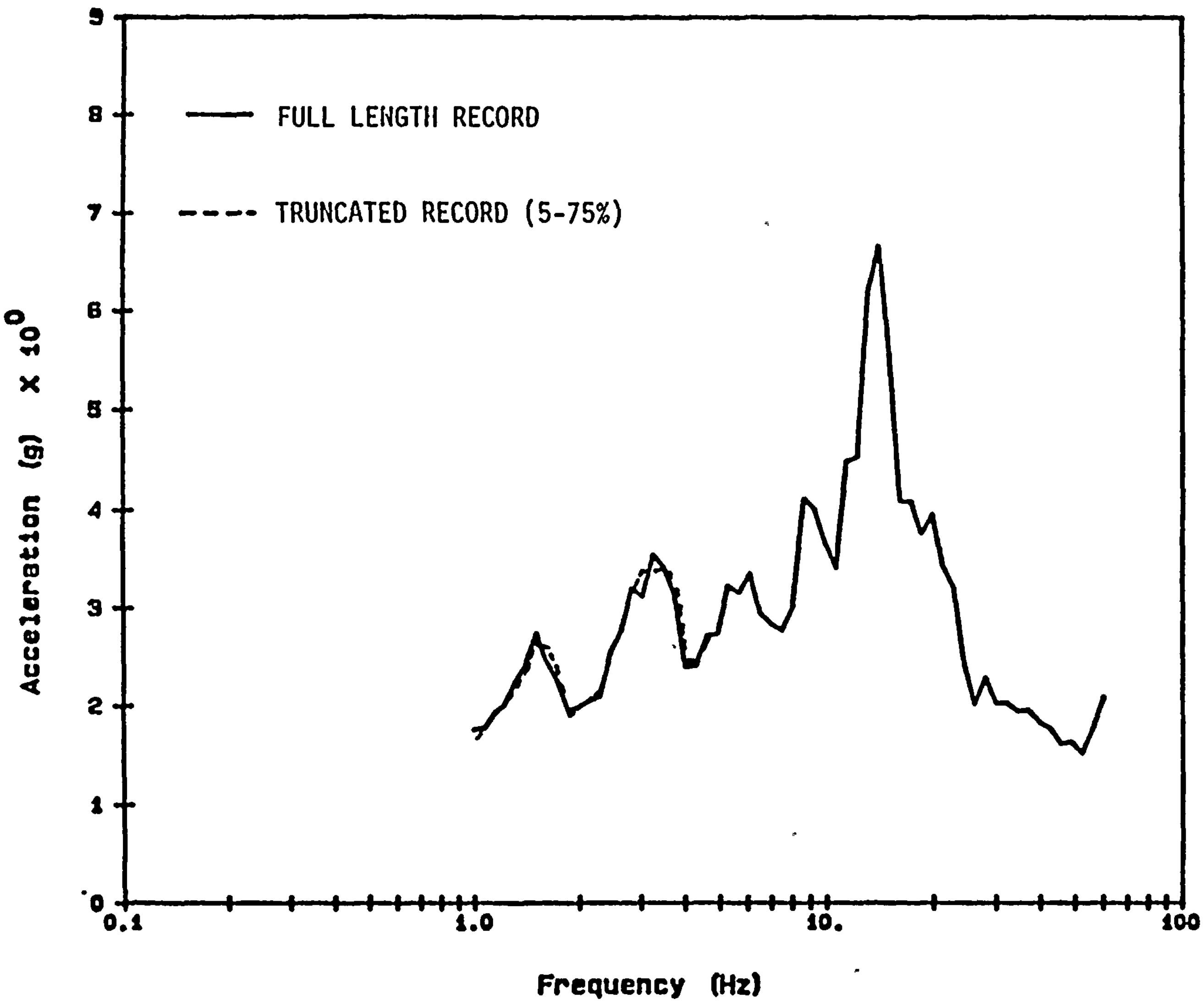

Figure C-9. Comparison of 5% Damped Ground Response Spectra of Scaled Earthquake Time History (Scale Factor = 2.288)

1611-A

SAN FERNANDO, CA. 09 FEB 1971. PACOIMA DAM, COMP S74W. SCALED TO 3.06 5.00 pct dampin

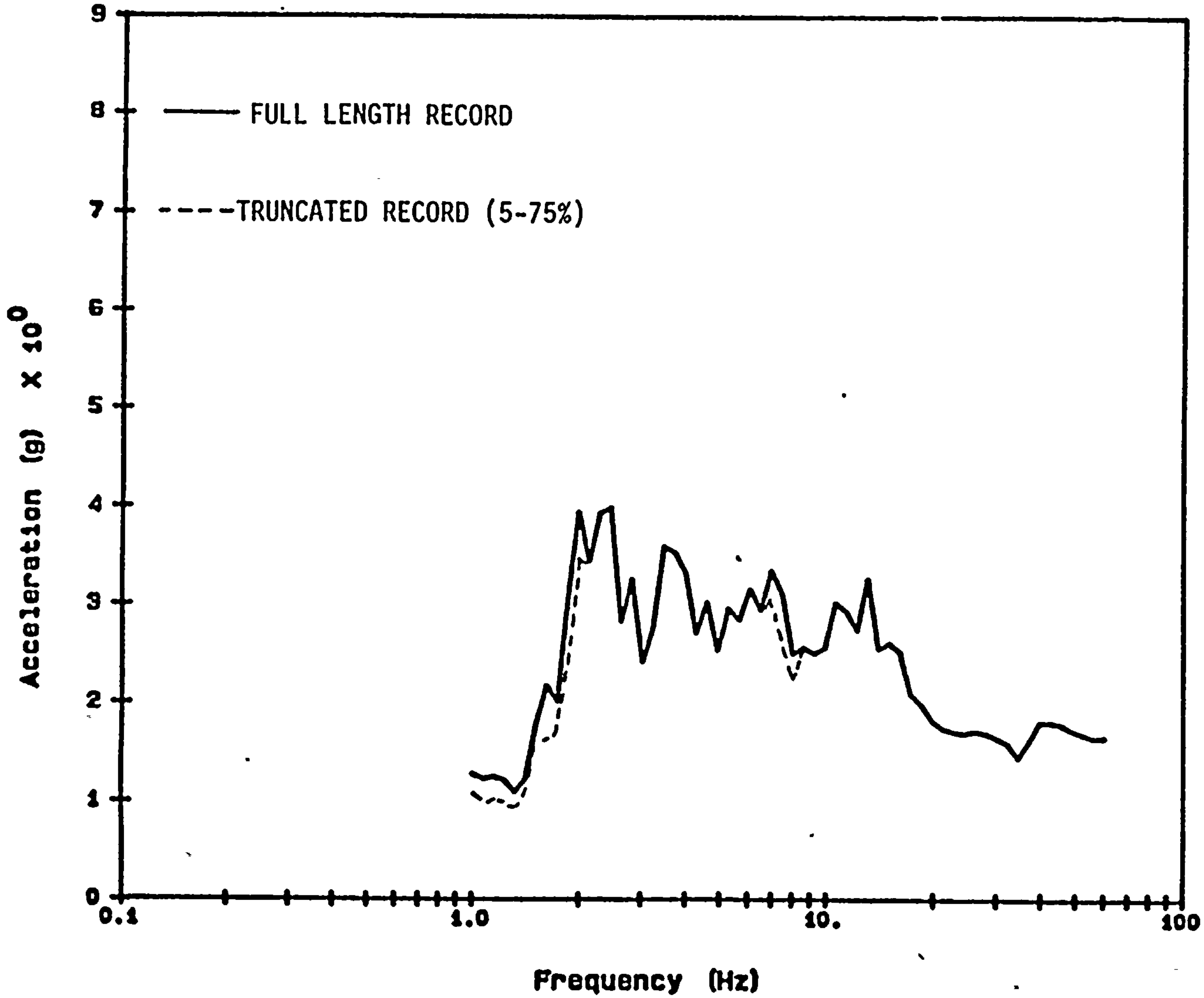

Figure C-10. Comparison of 5% Damped Ground Response Spectra of Scaled Earthquake Time History (Scale Factor = 1.584)

1611-A

[illegible]

REFERENCES

C-1 Letter from Bimal Sarkar to D.A. Wesley transmitting preliminary data for nonlinear analysis of turbine building dated October 31, 1986. QA Document Number 34001.01 M-437.

C-2 Kennedy, R.P. et al "Engineering Characterization of Ground Motion, Task I: Effects of Characteristics of Free-Field Motion on Structure Response," NUREG/CR-3805, May 1984.

C-3 Newmark, N.M., and W.J. Hall, "Development of Criteria for Seismic Review of Selected Nuclear Power Plants", NUREG/CR-0098, May 1978.

C-4 Algan, B.B., Drift and Damage Consideration in Earthquake - Resistant Design of R/C Buildings, Ph.D. Thesis, University of Illinois at Urbana-Champaign, 1982.

C-5 Gergely, P., "Seismic Fragility of Reinforced Concrete Structures and Components for Application to Nuclear Facilities", NUREG/CR-4123, December 1984.

C-6 Wesley, D.A., and P.S. Hashimoto, "Preliminary Evaluation of Nonlinear Seismic Response Effects for Nuclear Power Plant Shear Wall Structures", Report No. SMA 12205.02 prepared for Nuclear Test Engineering Division, Lawrence Livermore Laboratory by Structural Mechanics Associates, September 1980.

C-7 Cornell, C.A., "A Study of Factors Influencing Floor Response Spectra in Nonlinear Multi-Degree-of-Freedom Structures", prepared for Electric Power Research Institute, March 1986.

APPENDIX D

CORRELATION ANALYSIS

[illegible]

Introduction

The question of correlation between equipment failures has important ramifications on estimating system fragility frequencies, at least for dominant equipment items. In a "deterministic" computational procedure (i.e., one which ignores the uncertainty, p, on frequency of occurrence of a given ground acceleration, and the uncertainty, q, on the fragility frequencies, $f(c|a)$, for each component), it has been suggested (Kennedy, 1980) that for a system composed of components in parallel the fragility frequency $f(s|a)$ be estimated by:

$$f(s|a) \leq \min_{c \subset s} f(c|a) \qquad (1)$$

where: $f(c|a)$ is the component fragility for an item contained in the system s

and that for a chain of components in series the fragility frequency be given by:

$$f(s|a) \leq 1 - \prod_{c \subset s} [1-f(c|a)] \qquad (2)$$

These equations are, however, valid only for dependent (i.e., highly correlated) cases of component failure. For independent cases of component failure, the respective governing equations become:

series: $$f(s|a) = \prod_{c \subset s} [1-f(c|a)] \qquad (3)$$

parallel: $$f(s|a) = \prod_{c \subset s} f(c|a) \qquad (4)$$

[illegible]

Thus, for a series system a high degree of correlation between component failures reduces the system fragility {f(s|a)}. However, for a parallel series system, dependency between component failures results in an upper bound on system failure frequencies.

For different modes of failure in a given structure, or in similar structures, some degree of correlation between modes is expected. For instance, if the capacity of the lateral force resisting system (i.e., the shear walls) is actually higher or lower than the value used in the analysis, the acceleration capacities of all failure modes (including different structures) governed by the shear walls would be expected to be proportionately higher or lower. The actual capacity of the force resisting system may be different from that used in the evaluation due to differences in strength or modeling assumptions.

These effects are, of course, included in the variabilities associated with each mode of failure for a given structure or component. However, different degrees of correlation may exist from mode-to-mode. For instance, for a given structure with given concrete and reinforcing steel strengths, the variability on strength from mode-to-mode may be strongly correlated, while different modeling assumptions may result in little correlation for different failure modes.

This appendix presents the results of a correlation analysis performed on the response of components in a structural system subject to earthquake induced ground motion. The data base on elastic response used in this appendix was generated from the separation of variables check (Appendix B). The reader is referred to that appendix for a more thorough explanation of the structural system, the Monte Carlo simulation, and the reduction of the data.

[illegible]

Correlation Analysis

For random variables, say X and Y, the degree of linear interrelationship between the variates X and Y is measured by the covariance; that is,

$$\begin{aligned} COV\ (X, Y) &= E[(X - \mu_X)\ (Y - \mu_Y)] \\ &= E(XY) - E(X)\ E(Y) \end{aligned} \tag{1}$$

In most cases the normalized covariance, or the correlation coefficient is used in expressing the relationship between variates:

$$\rho = \frac{COV\ (X, Y)}{\sigma_X\ \sigma_Y} \tag{2}$$

The values of ρ range between -1 and +1; that is,

$$-1 \le \rho \le 1$$

The physical significance of the correlation coefficient can be inferred from Equations 1 and 2. If ρ is near unity and positive the values of X and Y tend to be both large or small relative to their respective means, whereas if ρ is near unity and negative, the values of X tend to be large when the values of Y are small, and vice versa, relative to their respective means. If ρ is small, or zero, there is little or no linear relationship between the values of X and Y.

With the response data generated in the Monte-Carlo simulation completed in the Separation of Variables study (Appendix B) it is possible to quantify the degree of correlation between the response of items of different frequencies subjected to earthquake motion located within the

[illegible]

same structure. A high degree of correlation would indicate a dependency between failure modes of these items -- provided the strength characteristics are similar. The correlation coefficients were computed between the following items:

1. Response between items of a different frequency located at the same elevation.

2. Response between items of a different frequency located on different elevations.

3. Response between items of the same frequency located on different floor elevations.

Results

The correlation coefficients as calculated are presented in Table 1. From this, it can be observed that there is a high degree of correlation between items of similar natural frequencies located on different floor elevations, However, this correlation decreases as one moves off of the amplified acceleration range (increasing frequencies above 14 hz).

The pragmatic results from this correlation analysis are obvious. For failure modes with little contribution to risk, consideration of correlation between modes is probably unimportant. However, consideration should be given to correlation between controlling seismically-induced failure modes for equipment items with similar frequencies in the same structure. Since the fundamental frequencies of the civil structures are quite widely separated, it is expected that the correlation between equipment items located in different structures will be low, even for equipment items with similar frequencies. The obvious

[illegible]

[illegible]

[illegible]

exception is equipment items with similar frequencies located on the base slabs of different structures since they will see similar input motions (neglecting SSI).

The effect of correlation on a system's failure frequency is, again, dependent on the type of system (series, parallel), see Equation 1-4. For a series system, correlation will increase the system's reliability, however, for a parallel system correlation will decrease the system's reliability.

For example, in a piping system responding wherein most components are responding at the same natural frequency (that of the system) the failure of any given pipe section is strongly correlated with the failure of any other section. Thus for a system composed of 1000 segments each with a probability of failure of .001 the system probability of failure is .001 for perfect correlation, whereas the system probability of failure is 1000 x .001 = 1 for no correlation (statistical independence). Consideration of some degree of correlation would put the system probability of failure somewhere between .001 and 1.

Table 1. Correlation Coefficients Between Component Response

RESPONSE	$R_{1,5}$	$R_{1,8}$	$R_{1,14}$	$R_{1,24}$	$R_{2,5}$	$R_{2,8}$	$R_{2,14}$	$R_{2,24}$
$R_{1,5}$	1.0	0.25	-0.02	0.04	0.91	0.30	-0.03	0.32
$R_{1,8}$		1.0	0.06	0.07	0.13	0.88	0.16	0.35
$R_{1,14}$			1.0	0.31	-0.01	0.02	0.87	0.31
$R_{1,24}$				1.0	-0.08	0.11	0.21	0.57
$R_{2,5}$					1.0	0.26	-0.06	0.38
$R_{2,8}$		SYMMETRIC				1.0	0.11	0.42
$R_{2,14}$							1.0	0.38
$R_{2,24}$								1.0

Where $R_{i,j}$ = response of "j" hz oscillator at floor "i".

Floor 1 = 100' elevation
Floor 2 = 140' elevation

[illegible]

REFERENCES

1. Ang, Alfredo H-S., and Tang, Wilson H. 1975, Probability Concepts in Engineering Planning and Design. Vol I Basic Concepts, New York: John Wiley and Sons Inc.

2. Ang, Alfredo H-S., and Tang, Wilson H. 1984, Probability Concepts in Engineering Planning and Design. Vol II Decision, Risk, and Reliability. New York: John Wiley and Sons Inc.

3. Kennedy, R.P., and Ravindra, M.K. 1984, "Seismic Fragilities for Nuclear Power Plant Risk Studies", Nuclear Engineering and Design, Vol. 79, No. 1, May (I): pp. 47-68.

4. Kennedy, R.P., Cornell, C.A., Campbell, R.D., Kaplan, S., and Perla, H.F. 1980, "Probabilistic Seismic Safety Study of an Existing Nuclear Power Plant", Nuclear Engineering and Design, Vol. 59, No. 2, August: pp 315-338.

5. Kennedy, R.P., Campbell, R.D., Hardy, G., and Banon, H., 1982, "Subsystem Fragility, Seismic Safety Margins Research Program (Phase I)", NUREG/CR-2405, UCRL-15407. U.S. Nuclear Regulatory Commission, Washington, D.C.

6. Johnson, J.J., 1979, "Modsap. A Modified Version of the Structural Analysis Program SAP IV for the Static and Dynamic Response of Linear and Localized Nonlinear Structures", General Atomic Project 3273, June 1978. Document #GA-A14006 (Rev) UC-77.

7. Newmark, N.M., and Hall, W.J., 1977, "Development of Criteria for Seismic Review of Selected Nuclear Power Plants", NUREG/CR-0098, U.S. Nuclear Regulatory Commission, Washington, D.C.

8. Newmark, N.M., and Hall, W.J., 1982, "Earthquake Spectra and Design", Engineering Monographs on Earthquake Criteria, Structural Design, and Strong Motion Records, No. 3, Earthquake Engineering Research Institute, Berkeley, California.

9. Kenneally, R.M., and J.J. Burns, Jr., "Experimental Investigation Into the Seismic Behavior of Nuclear Power Plant Shear Wall Structures", Paper V-2, presented at the Symposium on Current Issues Related to Nuclear Power Plant Structures, Equipment and Piping, North Carolina State University, December 1012, 1986.

10. Thomson, W.T., 1981, Theory of Vibration with Applications, 2nd edition, Englewood Cliffs, New Jersey, Prentice-Hall Inc.